NASA TT F-12,570

DEVELOPMENT OF EMITTERS AND COLLECTOR MULTI-LAYER SYSTEMS

H. Hubner, K. Janner and M. Peehs

Translation of "Entwicklung von Emittern und Kollektormehrschichtsystemen," Bundesministerium fur Wissenschaftliche Forchung, Forschungsbericht W 68-57, Aug. 1968, p. 118

NATIONAL AERONAUTICS AND SPACE ADMINISTRATION
WASHINGTON, D. C. 20546 OCTOBER 1969

TABLE OF CONTENTS

NASA TT F-12,570

DEVELOPMENT OF EMITTERS AND COLLECTOR MULTI-LAYER SYSTEMS

H. Hubner, K. Janner and M. Peehs

ABSTRACT. The described work is a part of an In-Core-Thermionic reactor development program. The system is proposed as an energy source for space vehicles. The thermionic element is built up of eight cells in a series. UO_2 pellets will be used as fuel. The fission of gas of each emitter is vented separately to avoid swelling due to fission gas pressure at the designed fuel burn up. Adequate methods to prevent plugging of the venting system were investigated. An instrumentative capsule for in-pile-testing emitters at nominal and higher heat rating was designed and is now under construction. Tungsten layers were deposited from the $W(CO)_6$. The interfacial diffusion of Mo-W was investigated. The joining technology for the designed development was developed. A method to build concentric collector systems ($Nb-Al_2O_3-Nb/1Zr$) was proved with good success.

0. Introduction

/*9

The works described in the present report are partial developments of an in-core-thermionic reactor (ITR) as a power source for space vehicles. This equipment consists chiefly of a suitable combination of thermionic convertor cells for the direct conversion of thermal energy into electrical energy on the one hand and of a nuclear reactor for releasing the necessary thermal energy on the other. As a study has shown [1, 2], such equipments offer favorable developmental prospects in the range of several kW_e up to several 100 kW_e.

It has been shown especially at a concept of a partial thermionic reactor [3] with Nb as a structural material as developed by us has a favorable power to weight ratio even with small output. The construction principle of a partial thermionic reactor provides for an inner zone consisting of thermionic combustion elements where the number of elements can be considerably changed according to the power requirements. This still sub-critical arrangement is amplified by thrust elements in such a way that the reactor possesses the desired reactivity with the utilization of the reflector.

We began in our plant about two years ago with the development of a combustion element to be used in the thermionic inner zone [4, 5]. Particular value was placed on the fact that the same type of combustion element could be used for all power ranges.

---

* Numbers in the margin indicate pagination of the foreign text.

Results which were achieved in the continuation of the work on the development of thermionic combustion elements from 1 April 1966 to 31 March 1967 are reported here.

1. Design and Method of Operation of the Combustion Element /10

1.1 The Emitter

1.1.1 Requirements for the Design for the Emitter

The design of the thermionic combustion elements and especially of the emitters containing the fuel must also be considered with the partial thermionic reactor in connection with the entire apparatus because the release of power by the emitter on the one hand depends on the quantity of fuel, the distribution of fuel, a material and geometry of the emitter and on the other hand the release of power is closely connected with the other parts of the reactor through neutron flow, neutron spectrum and lowering of flow.

Optimation calculations with respect to a minimum power to weight ratio with the given electrical power [6, 7] and neutron-physical considerations of a basic type have led to the following principles for the thermal or epithermal reactors consider here:

1) The proportion of UO_2 in the emitter should lie between 30 and 40% by volume for the basic construction at hand. A smaller proportion of fuel causes an increase of the entire mass and an increase of waste heat in the partial thermionic reactors; a larger proportion of fuel causes an increase of the mass of the fissionable material.

2) The fuel should be arranged in a thin layer and as far as possible far out in the emitter in order to keep the natural screening of the fuel and the screening by the cathode working material as small as possible.

3) The emitter should consist of a material with little neutron absorption. Molybdenum is a possibility, while natural tungsten can only be used in small amounts (layer thickness at the surface, e.g. about 0.2 mm).

In order to achieve a favorable operating behavior and a satisfactory longevity, the following requirements must also be fulfilled:

4) The emission surface of the emitter should permit achieving a high effective degree in the transformation of energy at the planned operating temperature of 2000°K. This can be attained in various ways, e.g. by high work of emission of the emitter in the vacuum, by orientation of the crystals and additives. /11

5) Temperature differences at the cathode should be small.

6) With the given emitter material, the electrical losses and at the

same time the material cost should kept small. These mutually exclusive requirements should be optimized taking neutron absorption into consideration.

7) The emitter must remain stable in form during its lifetime of at least one year and at an operating temperature of 2000°K because the minimum permissible convertor aperature and the effective degree along with it will be easily influenced. Expansion, evaporation and warping must also be kept small.

8) The emitter must be stable in function. For this it is necessary that the diffusion of uranium to the surface be held sufficiently small. In case W is used as an emission layer, the diffusion of molybdenum to the surface must also be presented.

The attempt has been made to observe this requirement in the designs described in the following.

1.1.2 Emitters with Separate Fission Gas Lines

Calculations have shown [5] that low-expansion emitters with a power density of 50 W_{th} per square centimeter of cathode surface for a lifetime of two years and at operating temperature of 2000°K without fission-gas exhaust line cannot be realized with the presently available fuels. For this reason, only emitters with fission-gas exhaust lines were first investigated in detail.

Figure 1 shows the cross section of a thermionic combustion element in which each emitter has its own fission-gas line. The emitter consists of a /12
molybdenum pipe in the thick walls of which axial borings have been made to receive the fuel (proportion of fuel by volume about 30%). The fuel is then housed in the form of cylindrical rods. Because of the relatively high UO_2 vapor pressure at the operating temperature, the latter evaporates at the surface of the rod and precipitates on the colder wall of the metal when feed play and fuel density are appropriately selected. In a case of the present design it is expected that in the stationary condition probably the fuel distribution as drawn would obtain. The distribution is characterized by the fact that the inner fuel surface is an isotherm. After a fairly long burn up and noticeable formation of fission gas, the latter can be diffused through short paths to the exhaust canals thus formed and from these flow outside through the collecting chamber and the fission-gas line. The port of the fission-gas pipe in the emitter is narrowed in order to avoid having an inadmissible large amount of fuel escape through the fission-gas line and which would then lead to a stoppage at the colder spots. A stoppage of this opening is prevented in the following manner:

a) A port of the fission-gas exhaust lines jut into the fission-gas collecting chamber in the form of a tube. After the stationary fuel distribution is adjusted, the tube is so strongly evaporated with UO_2 at the mantel surface that the heat created in the coaching increases the temperature of

the port of the tube to the temperature of the inner fuel surface when fuel is flowing through the tube.

b) Also with this solution, the port of the fission-gas tube juts into the interior of the fuel chamber. However, the port is additionally provided with a proportion of fission material (heating ring in Figure 3) which does not take part in the evaporation equilibrium. The amount of diffusionable material is measured so that even here the additionally created heat energy at least brings the port of the fission-gas ventilation to the temperature of the hot isotherm. The increased elimination of heat at the ends of the emitters through the series-connected bridges would lead to a clogging of the /13
fission-gas exhaust canals and to great temperature differences at the cathode. By widening the fuel canals at their ends, UO_2 can additionally condense and at least partially compensate for these heat losses. The reduction of the active emitter length also serves the same purpose by means of beveling the ends.

A tungsten cooling with the thickness of about 0.2 mm is provided for the entire emitter. This is to serve as a diffusion barrier against uranium, to improve the emission characteristics (higher work of emission in the vacuum than Mo) and to reduce the evaporation rate of the emitter. The relatively rapid diffusion between Mo and W requires special measures to maintain this layer, about which more will be reported in detail section 3 of this report.

The dimensions of the emitter were determined from optimation calculations which will be reported at another place [7]. Besides the neutron-physical effective values, these comprise the internal convertor properties, the design of the whole convertor and the properties of the entire equipment.

The testing of this emitter out-of-pile and the testing of a slightly transmuted form in-pile is planned for the reporting year 1967-1968. Preparations for reactor experiments in this connection are described in chapter 2.3.

1.1.3 Emitters With Central Fission-Gas Lines

The designs described in this section have been worked out for the purposes of study. The goal of the considerations was to replace the complicated construction of an element made up of emitters with separate fission-gas line by a rod with simple central ventilation, whereby even here value would be placed on an extremely small inactive emitter length. One possibility with /14
central fission-gas lines is presented in Figure 1.1. The emitter is similar to the one presented in Figure 1. Here, however, the fission gases from the ring-shaped collecting chambers in the emitters are first only led to the very next emitter in each case and are led to the outside by the emitters at the ends of the elements. Because of the potential difference between the emitters the metallic fission-gas line must be interrupted by insulating stretches. One possibility for this configuration has been presented enlarged in the cross section. The various expansion between collector and emitter can be absorbed by the bends in the fission-gas lines and the loop at the ends of the elements

without having large forces exerted on the bridges. The ends of the elements are of symmetrical design in the light of a series connection of many elements because otherwise two kinds of elements carrying fission gas and cesium would have to be built at various ends as a consequence of the load-dependent direction of flow.

Another possibility with central fission-gas exhaust line is shown in Figure 1.4. Here the fuel forms a pipe-shaped layer inside the emitter pipe casing carrying the current. The centering of the emitter in the collector system takes place at one end again above the bridge and at the other end above an insulating disk and a spring bellows through the bridge of the next emitter or at the end through a special bridge. The fission-gas electing chambers in the center of the emitters are connected with one another through the boring in the insulating disk. They are led to the outside by a central fission-gas line. Expansion differences between emitter and collector are absorbed by the low-power spring bellows. According to the dimension of the fission-gas canals between the emitters, a shifting of fuel from one emitter to another will either be permitted or completely prevented. A shifting of fuel is possible in the case of the large borings shown. In this case, an automatic reduction of the temperature difference at the emitter surface is therefore achieved not only inside an emitter but also between all the emitters of the element. In this way, depending upon the type of measures adopted for smoothing the power output, a small change in the reactivity of the reactors can occur. /15

The two designs carried out each leads to a Cs proof and gaseous metal-ceramic connection at the emitter temperature. An applicable solution of this problem is not known to the author. However, it can be recognized here that an improvement of existing technology would configure the entire construction of the thermionic combustion element in a far less complicated manner and thereby also less susceptible to disturbance.

1.2 The Whole Element

In the present concept of a partial thermionic reactor, partially [illegible]ter requirements which result from the operating conditions of the converto[illegible] reactor have to be weighed against one another in the construction of the thermal combustion elements. For example, the neutron-physical layout requires collectors having extremely thin walls, while in the electrical layout thick collectors are advantageous. Frayed-off calculations [7] and general considerations led to the following guidelines for the design of the collector system.

1.2.1 Requirements for the Design of Collector and Whole Combustion Element

1) The product of the specific electrical resistence and macroscopic neutron-absorption cross section should be as small as possible at the anodes, emitters and end pieces.

2) Voltage drop in collector and emitter must be coordinated with one another so that the operating conditions within a cell do not change too much.

/83

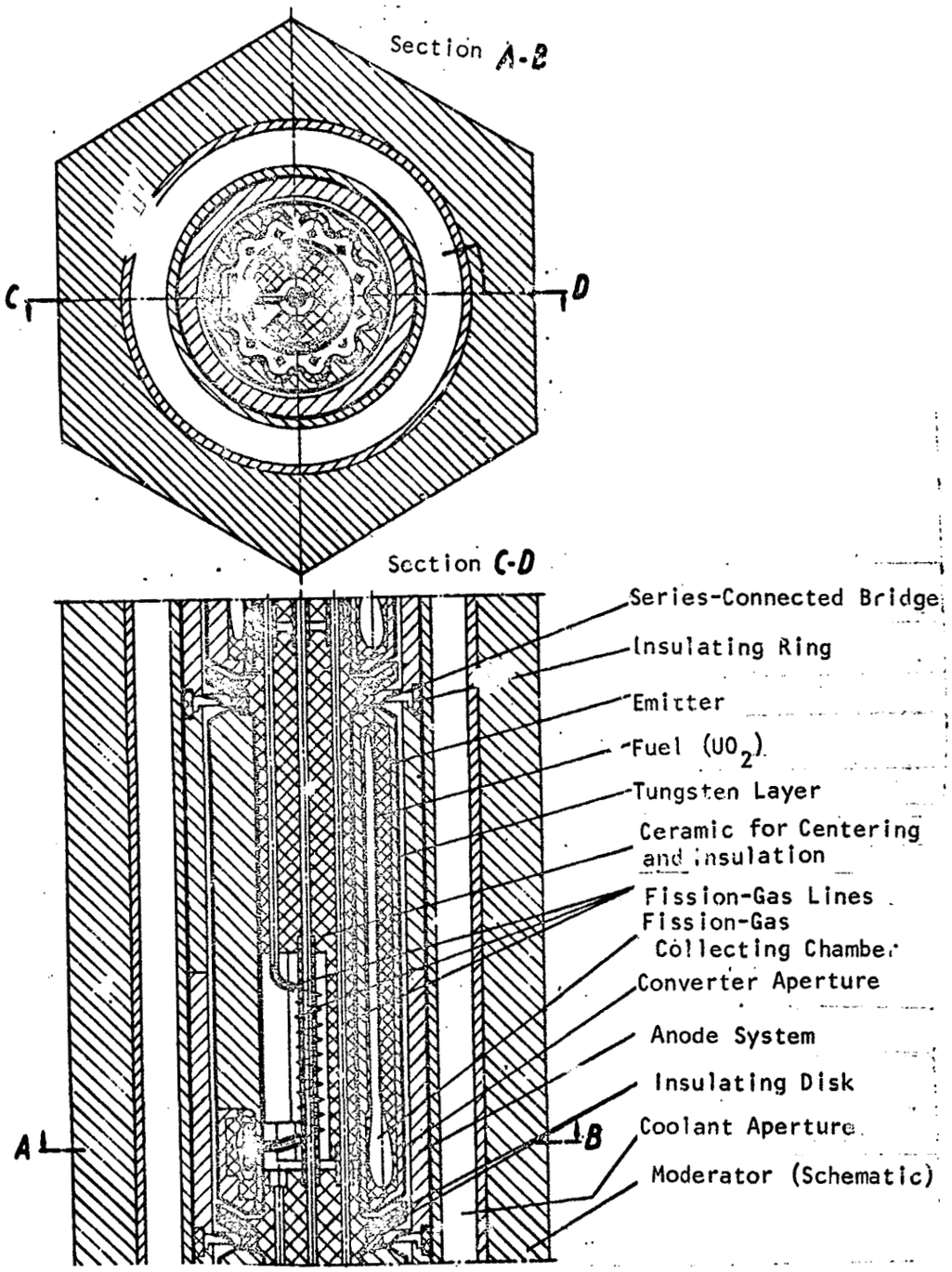

Figure 1.1. Cell of a Thermionic Reactor Combustion Element With Separate Fission-Gas Exhaust Lines.

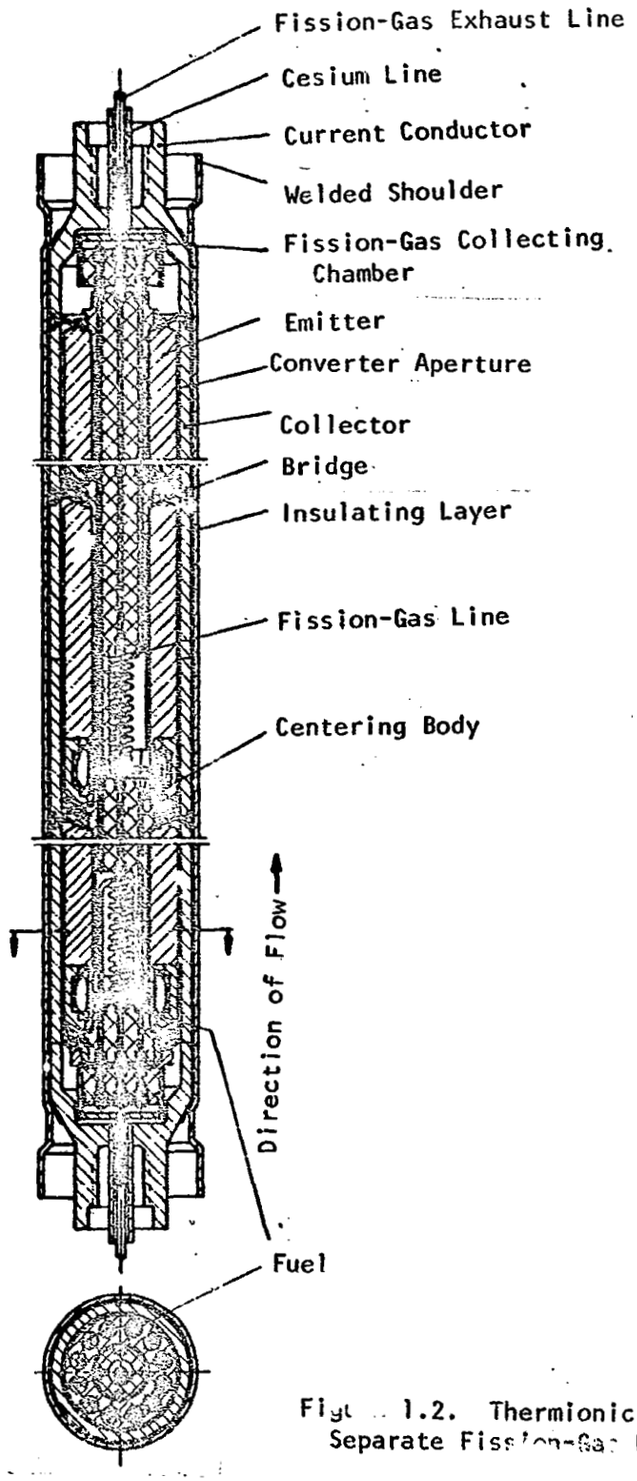

Figure 1.2. Thermionic Combustion Element with Separate Fission-Gas Exhaust Lines.

/85

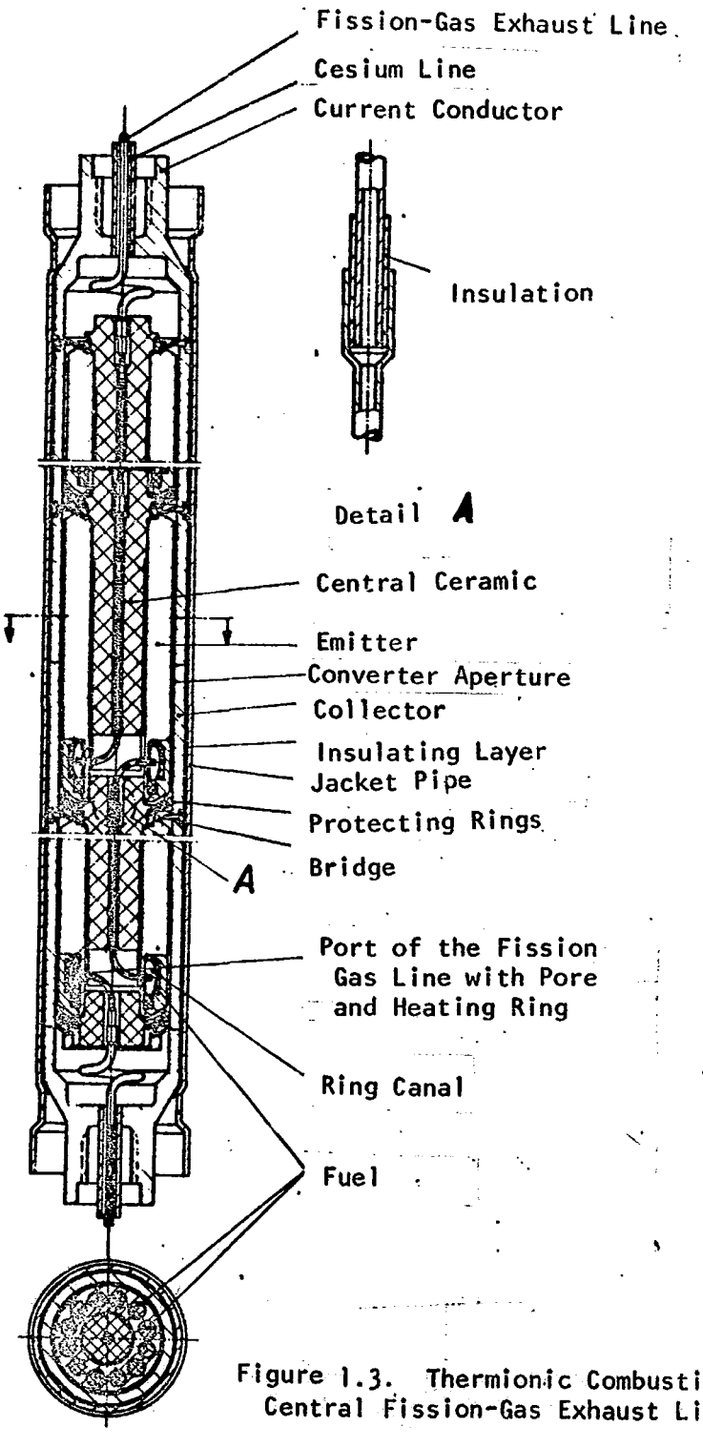

Figure 1.3. Thermionic Combustion Element with Central Fission-Gas Exhaust Line.

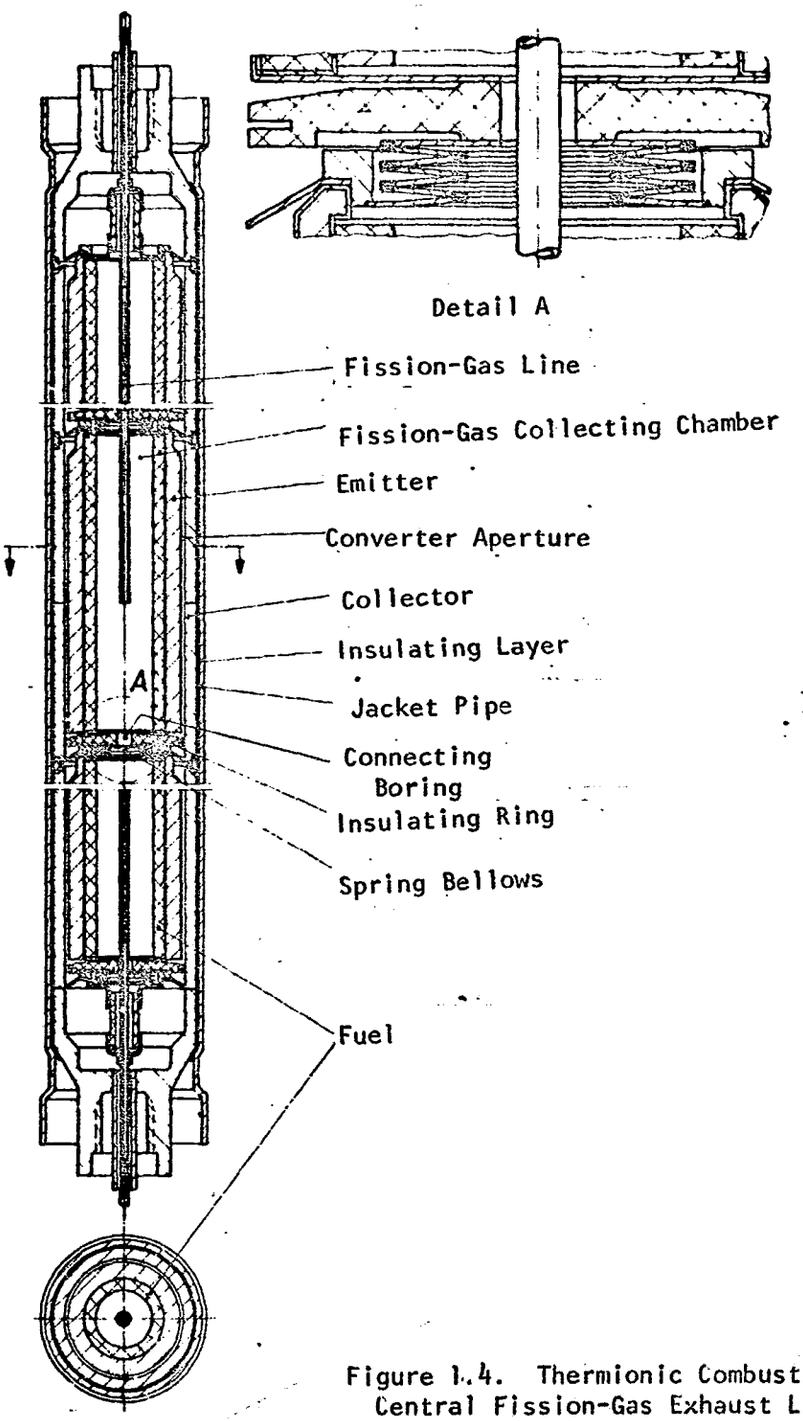

Figure 1.4. Thermionic Combustion Element with Central Fission-Gas Exhaust Line.

3) The radial temperature drop in the collector system should be smaller than 100°C at full power.

4) Axial temperature differences in the active range should remain smaller than 30°C (such differences could be created by the influx of heat over the bridge). /16

5) The electrical power losses over the insulation should be small. That is the case when

$$\rho_{(800°C)} \cdot d \geq 5 \text{ K } \Omega \text{ cm}^2,$$

where ρ is the specific electrical resistence and, d is the thickness of the insulating layer; creep currents at the ends of the layer can be neglected.

6) Centering and form stability of electrodes should permit a distance between electrodes as small as possible.

7) The inside of the collector system must be resistent to Cs vapor and the outside parts must be resistent to liquid metal and as far as possible also to hydrogen.

8) The following parameters should be optimum with respect to a minimum specific weight of the entire requirement with the given power output: cell length, bridge dimensions, interval of the active emitter ranges, collector and emitter temperature, temperature constant of the emitter surface, Cesium vapor pressure and load resistence.

9) The end pieces with ducts for current, cesium and fission gas must permit a sufficient uniformity of the power distribution and so should be built up symmetrically.

1.2.2 Description of Collector System and Whole Element

The design construction of the whole element in which the requirements given in section 1.2.1 are considered can be seen in Figures 1.1 and 1.2. In turn the convertor aperture (0.5 mm), collector system (Nb-Al_2O_3-NbZr1), coolant aperture,, outside jacket pipe (NbZr1) and a schematic diagram of the moderator (Yttrium or Zirkonium hydride) follow outside on the emitters described in section 1.1.2. The method of manufacture of the collector system is described under 5. It permits a very thin layer of insulation, which stands in good heat contact with the adjacent metal jackets and for that reason leads one to expect good characteristics of heat conductance. The individual collectors of the system are centered by means of insulating rings made of Al_2O_3 and connected so as to be gas tight. An overlapping projection /17 on the collector and the special position of the bridge prevent vapor deposits on the insulation ring by the emitter and the hot part of the bridge.

Centering the emitter in the collector system takes place on the one side directly through the series-connected bridge and on the other side through the central insulation bodies by the bridge of the next emitter. Insulating disks between the emitters should hinder the formation of a conducting layer and a gas discharge between adjacent emitters.

The central insulation body serves simultaneously in connection with sleeves to prevent a gas discharge between the fission-gas lines which are at different electrical potential. The spiraling of the fission-gas lines permits a deformation of the lines low in force. Forces in the fission-gas line will be caused by various thermal expansions of the structure materials. Simultaneously, the spiraling permits a reduction of the dissipation of heat to the ends of the elements. Each half of the fission-gas lines is insulated in the collecting chamber at the end of the element. From there the fissionable gas is led to the outside in a coaxial line through the cesium vapor line. A central line connects the two fission-gas collecting chambers. In order to make sure that the element can be installed in any situation for the purpose of series connection, the fission-gas and cesium line are led through both ends.

A thick and voltage-free connection of the element with the coolant line system is possible by means of a flange butt-welding joint at the ends of the pipe jacket. This also permits a relatively simple solution of the connection by grinding down the welding joint in the terrestrial prototype reactor.

The design presented was carried out in close coordination with the development of connecting technology described in chapter 4.

1.3 Installation of the Combustion Element /18

All the structural materials are degassed before use. An experimental program for determining the conditions for degassing has already been run in our plant. The installation of the combustion element takes place in a glove box under a protective gas.

1.3.1 Installation of the Emitter

1) Manufacture of the blanks
2) Tensionless annealing and degassing
3) Welding up the fission-gas tubes by means of e-rays

Leak Test of the Seam

4) Filling up with fuel
5) Shedding off the emitters

Leak Test of the Seams

6) W-layering
7) Polishing the emitter surface

8) Degassing the finished emitters

Mass Check

Test of the Emitter in the Convertor Operation at a Suitable Working Point of the Characteristic Line

1.3.2 Installation of the Combustion Element

1) Manufacture of an anode piece with tightened bridge and degassing of this part
2) Connection of the bridge with the emitter per diffusion bonding

El. Measurement of Resistence

3) Adding the second half of the anode by making a connection of the metal and ceramic for separating the anode in the series connection

Leak Test of the Metal-Ceramic Connection

4) Assembling the combustion elements and welding the individual anode halves below one another /19
5) Locking the combustion element

Leak Test of the Element

6) Attaching the layer of Al_2O_3 by means of plasma spraying and plain grinding of the ceramic layer
7) Shrink fitting of the outer pipe jacket by zones

Final Leak Test

Insulation Test

8) Evacuation and closing off the combustion element

2. Fuel Investigations /20

2.1 Non-Ventilated Fuels

2.1.1 Reduction of Expansion of Non-Ventilated Emitters by Reducing Temperature

2.1.1.1 Statement of the Problem

In using UO_2-Mo-Cermet as well as coated particles coated by Mo as fuel and cathode material in the thermionic reactor combustion element, an expansion effect of the cathode is to be expected at the high temperature of

utilization of 2,000°K and the required burn up, and this expansion leads to destruction of the convertor before reaching the end of its necessary lifespan [5].

Therefore, the prolonging of the lifetime expected as a consequence of expansion as a function of a reduction of temperature was therefore the subject of the following described investigations.

2.1.1.2 The Creep Law for Molybdenum

The general form of the creep law for metallic working materials is as following [8]:

$$\varepsilon = K(T)\,\sigma^{n(T)}\,t^{m(T)} \tag{2.1}$$

where ε is the change in length in %, σ is the stress in kp/mm^2, t is the time in hours, T is the absolute temperature in degrees (°K).

$$k(T)\left[\frac{\%\ mm^{2n}}{kp^{n}\ h^{m}}\right]$$

$k(K)$, $n(T)$ and $m(T)$ are characteristic functions for special metals, e.g. for Mo. A statement as to the connection of these functions is provided by the Larson-Miller equation: /21

$$T_1(C_1 - \ln \dot{\varepsilon}_1) = T_2(C_2 - \ln \dot{\varepsilon}_2) \tag{2.2}$$

If the creep data of Mo are evaluated, as they were published by General Electric [9] for the temperature range from 1,200°C-2,400°C, then it is found that $m(T)$ and $n(T)$ are functions which are only slightly dependent on temperature, while $k(T)$ is related as an exponential factor to T (Figure 5-Figure 6). The form of $k(T)$ derived from the experiment agrees well with the one derived from the Larson-Miller equation for the case where m = constant and n = constant. Therefore the out-of-pile creep law for Mo reads as follows:

$$\varepsilon = 8{,}0 \exp\left[1{,}2 \cdot 10^{-2} \cdot (T - 2073\,°K)\right] \cdot \sigma^{4{,}0}\, t^{(0{,}2 + 0{,}28\,T \cdot 10^{-3})} \tag{2.3}$$

for

$$1473\,°K \leq T \leq 2673\,°K$$

where $\varepsilon[\%],\ T[°K],\ \sigma[kp/mm^2]\ t[h]$ is to be used.

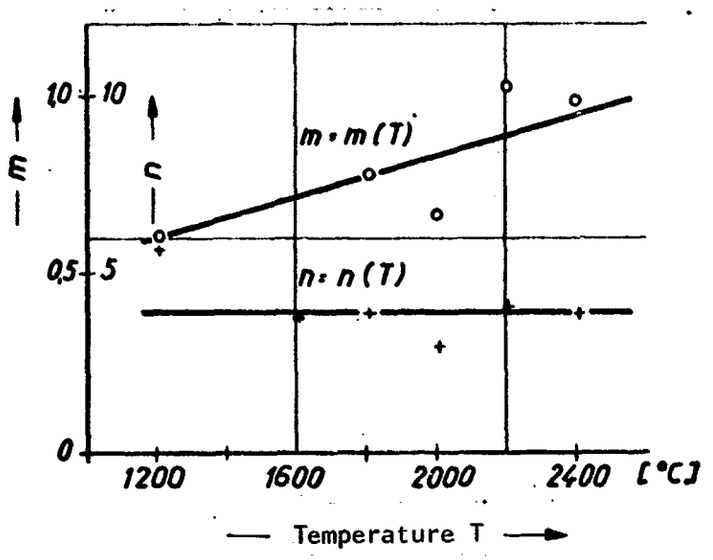

$n(T) \approx 4{,}0 =$ Constant

$m(T) \approx 0{,}2 + 0{,}28 \frac{T}{10^3}$ $\quad T\,[°K]$

Figure 2.1. Dependence of the Exponent of the Creep Law $\varepsilon(\delta,t,T)$ on the Temperature for Mo.

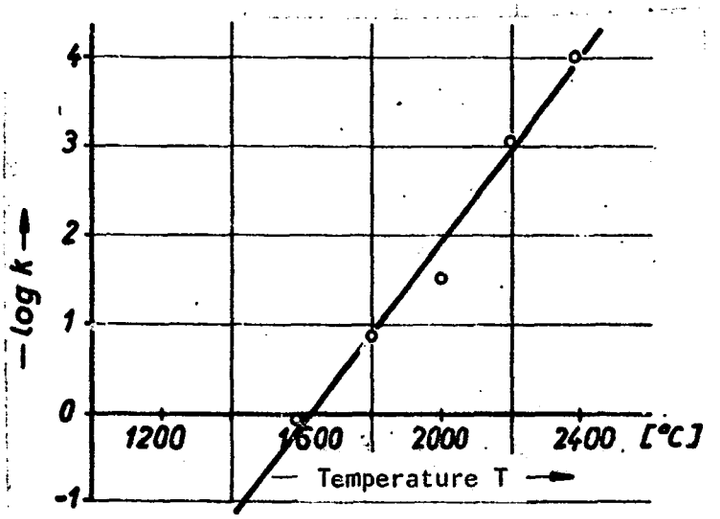

Figure 2.2. Dependence of the Proportionality Factor of the Creep Law $\varepsilon(\delta,t,T)$ on the Temperature for Mo.

2.1.1.3 The Change of the Longevity of a Thermionic Combustion Cathode as a Function of the Emitter Temperature with Optimum Convertor Operation

The expansion effect of a Cermet or a coated particle batch with the given internal structure has already been given by the author for the special application case T = 2,073°K [3]. By considering the equation (2.3), the relationship given there can be given in a form which is valid for the entire temperature range of interest as follows:

$$\eta(t) = \frac{m}{2(n+m)} \left(\frac{3}{2n}\right)^n \left[\left(\frac{u_0}{u}\right)^{1/n} - 1\right]^{-n} \cdot k(T) \left[\chi(T, W, U, V_p, r_i)\right]^n t^{n+m} \qquad (2.4)$$

$$1773^{\circ}K \leq T \leq 2673^{\circ}K \qquad /22$$

(%), U(%) (UO_2 concentration of the cathode) T(°K), W(kW/cm^3), r_i(cm) (particle radius), V_p(%) (proportion of pores in the UO_2), UO_2 = 74.1% (UO_2 space filling with hexagonal spherical packing) = (kp/mm^{2}h), k(T) ( ), t(h) or with n = 4.0 = 0.75:

$$\eta(T) = 1{,}25 \cdot 10^{-2} \left[\left(\frac{74{,}1}{u}\right)^{1/4} - 1\right]^{-4} \exp\left[1{,}2 \cdot 10^{-2} (T - 2073)\right] \chi^4 t^{4{,}75} \qquad (2.5)$$

The function χ is defined herein as follows:

$$\chi = \frac{\text{Increase of Stress in the Mo}}{\text{Unit of Time}} \qquad (2.6)$$

The limitation of equation (2.4) or (2.5) to the temperature range 1,500°-2,400°C compared to the basic equation (2.3) has the following reasons:

a) It must be taken into account that only above 1,500°C all fissionable gases arising are given off into the fission-gas pores and do not remain behind in the UO_2 [10].

b) Below 1,500°C, the toughness of UO_2 neglected in the derivation increases in such a way that the simplification of neglecting the toughness of the UO_2 is no longer permissible.

If the longevity τ of the cathode is defined as the time which transpires until an expansion effect of 1% has been achieved, then we obtain from (2.4) or (2.5)

$$\tau = \left\{\frac{2(n+m)}{m} \left(\frac{2n}{3}\right)^n \left[\left(\frac{u}{u_0}\right)^{1/n} - 1\right]^n k^{-1} \chi^{-n}\right\}^{\frac{1}{n+m}} \qquad (2.7)$$

If now a combustion cathode is operated with reduced power and temperature, then the expected change of longevity is obtained from the relationship: /23

$$\frac{\tau(T,\varkappa)}{\tau(T_0,\varkappa_0)} = \left\{\frac{k(T_0)[\varkappa(T_0)]^n}{k(T)[\varkappa(T)]^n}\right\}^{\frac{1}{n+m}} \tag{2.8}$$

The relationship $\varkappa_0/\varkappa$ can be represented as follows:

$$\frac{\varkappa_0(T_0)}{\varkappa(T)} = \frac{T_0\, W_{opt}(T_0)}{T\, W_{opt}(T)} \tag{2.9}$$

Since k/k_0 is likewise known from the creep experiments, equation (2.8) can be transposed into the following form:

$$\frac{\tau(T,\varkappa)}{\tau(T_0,\varkappa_0)} = \exp[0{,}25\cdot 10^{-2}(T_0 - T)]\left\{\frac{T_0\, W_{opt}(T_0)}{T\, W_{opt}(T)}\right\} \tag{2.10}$$

The thermal surface power of a convertor running at optimum as a function of emitter temperature was determined on the best W emitters investigated at that time in our plant and which were combined with a sprayed layer of plasma with a vapor plating top layer. From these measurements and on the basis of a geometric configuration of the fuel cathode, the necessary power density W_{opt} created by nuclear fission in the fuel was determined as a function of the working temperature of the convertor. In so doing, one χ is clearly allotted to each emitter temperature T and the relation τ/τ_0 is still only a function of T. That means that from:

$$W_{opt}(T) \sim \frac{T - 1{,}6\cdot 10^3}{T} \qquad \text{(with an approximately 0.5 mm electrode distance)} \tag{2.11}$$

It follows that:

$$\frac{\tau(T)}{\tau(T_0)} = \exp\left\{0{,}25\cdot 10^{-2}(T - T_0)\right\}\left\{\frac{T_0 - 1{,}6\cdot 10^3}{T - 1{,}6\cdot 10^3}\right\} \tag{2.12}$$

$$1773\,^\circ K \leq T \leq 2000\,^\circ K$$

Equation (2.12) represented the desired connection between the longevity of a Cermet and the operating temperature of an optimized thermionic convertor. Let equation (2.12) be evaluated finally for the following example: /24

$T_o = 2073^oK$ $T = 1800^oK$

$\frac{\tau(T)}{\tau(T_o)} = 4,1$

This means that a reduction of the emitter temperature from 2,073°K to 1,800°K with the same and still permissible expansion leads to an extension of the longevity by about the factor of 4.

2.1.2 Out-of-Pile Investigations of Coated Particles with Mo Shells

2.1.2.1 Statement of the Problem

In the 1965 annual report [5] ideas were developed by us how a nuclear heated thermionic emitter could be constructed from coated particles with a Mo coating. The ideal particle dimensions calculated there are, however, not commercially available. It is therefore being investigated to what extent the commercial coated particles are suitable for use in a thermionic convertor.

For this purpose, during the period of the report coated particles from the firm of NUKEM, GmbH were obtained:

Type	ø	Thickness
1.)	150 µ	5-6 µ
2.)	70-120 µ	5 µ
3.)	70-120 µ	2-3 µ

2.1.2.2 Heating Table Investigations

2.1.2.2.1 Experimental

The investigations are carried out in a commercial heating table under a vacuum of approximately 10^{-5} mm next Hg pressure using a Mo heating conductor. The coated particles to be investigated lie in a semicircular dish directly on the heating conductor. The temperature measurement takes place through pyrometers with consideration of the absorption losses on the covering glass of the heating table. The accuracy of measurement in this case is about ±70°C. Better reproducibility cannot be achieved since very quickly a covering layer of material vaporized from the coated particle forms on the glass. /25

The increase of absorption by the precipitation of vaporized substance is also applied in the estimation of the change of vaporization rates.

2.1.2.2.2 Program of Investigation

The experimental program carried out can be seen from Table 2.1. The goal of the investigations is to obtain information as to the sinter behavior of coated particles as well as to obtain information on the behaviour of vaporization.

2.1.2.2.3 Experimental Results

Type 1 coated particles have a smooth surface and a uniform coating thickness in the condition in which they are delivered, as investigations of polished sections showed. When they are heated at convertor temperatures, a roughening of the surface is observed within one hour. The surface then appears spotty as a consequence of the emission capability which varies from point to point.

In the investigation of Type 2 and 3 particles these phenomenon to some extent already occur after ten minutes. This may be caused by the facts that the coated particles already possess a fairly rough surface in the condition in which they are delivered. Hand in hand with this advancing roughening of the surface, bridge formations with adjacent particles can also be observed. Gradually the loose band of particles grows together to a batch. Finally, while still in the period of observation the roughening leads to a formation of cracks in the coating. The vaporizing UO_2 condenses--as subsequent investigations of polished sections show--on the upper layer of the coated particles as a consequence of the temperature being somewhat less there.

In the case of investigations with changing temperature (cycles between 2,000°K and room temperature) all these phenomena appear more often and more frequently. /26

It could be observed simultaneously in all cases that the rate of condensation of the particle surface decreases about 50% as the heating time increased.

2.1.2.3 Long-Term Heating Tests at 2,100°K

2.1.2.3.1 Experimental

The heating is carried out in a resistence furnace under vacuum. In this case, the vacuum during the first 24 hours is about 10^{-5} mm Hg pressure, and then it gradually reaches 10^{-6} mm Hg pressure. The temperatures are measured with a pyrometer, where the absorption at the glass observation port is corrected. The accuracy of measurement probably comes to ±30° at 2,000°K. Al_2O_3 was first used as crucible material, but this was later replaced by Mo.

2.1.2.3.2 Program of Investigation

The goal of the investigations is to repeat the results of the heating table investigations under definite conditions and to extend the experiments to longer times. The experiments carried out can be seen in Table 2.

2.1.2.3.3 Experimental Results

The final metallographic investigation for experiment number 1 according to Table 2 shows the same roughening as was found also in investigation of the heating table. Figures 3 and 4 show a comparison of the polished sections of the coated particles before and after heating. The same results are also found for experiments numbers 2-4/Table 2, even if in exaggerated form. In spite of the fact that the initial condition of the coated particles is different (cf. Figures 2.3 and 2.5), nevertheless the final condition after 239 hours heating is almost the same (Figures 2.6 and 2.7). The roughening of the surface has proceeded so far in this case that the shells have often broken open several times.

2.1.2.4 Chemical Investigations /27

2.1.2.4.1 Statement of the Problem

It was found for all heating tests that a considerable amount of substance was vaporized from the coated particles. The goal of the investigations is to determine the composition of this substance qualitatively as to the extent possible also quantitatively.

2.1.2.4.2 Experimental

For activation analysis, portions of the sample materials are irradiated in the FRM. Then the activated material is separated radiochemically and the individual fractions measured in a δ-spectrometer. The margin of error of the semi-quantitative analysis must be estimated at 20-50%.

2.1.2.4.3 Experimental Results

Precipitations were investigated which were created in heating Type 1 "coated particles" for 8 and 75 hours at 1,830°C and found on the Al_2O_3 crucible. The results of the analyses are compiled in Table 2.3.

2.1.2.5 Conclusion

Coated particles which still lay within the realm of the commercial capability of the manufacturer (NUKEM) were investigated; this applies both to the diameter of a minimum of 70-120/μ as well as for the minimum Mo layer thickness of 2-3/μ.

The configuration of coated particles in the purchased condition is quite various. While a fraction of 150/μ Ø possesses a smooth and uniform coating

of Mo on almost spherical-shaped UO_2 bodies, the fraction 70-120/μ Ø had an extraordinarily rough surface. This is caused by the bumpy and out-of-round configuration of the UO_2 body.

If the particles are heated at approximately 1,800°C, then a roughening of the surface takes place which already begins within one hour and inside 239 hours leads to a rupture of the Mo shell. Hand in hand with the roughening of the surface, it is also observed that the loose group of particles fuse together to form a batch.

An evaporation of the surfaces is noted during the heating. The rate /28
of evaporation decreases about 50% within one hour and then remains constant. As expected, Mo with over 99% by weight forms the chief proportion of the evaporating substance. Along with Mo, with 0.6% by weight there is a smaller proportion of tungsten, and in one case an additional 0.4% of uranium.

The existence of tungsten in the precipitation is surprising, for even when the Mo coating contained tungsten with 0.6% by weight as an impurity, the tungsten should be found only in a very small mass because of its much smaller vapor pressure if we are dealing here with the evaporation of pure metals. In any case, if the surface is eroded by evaporating oxides, the same types of attrition are to be expected in the same order of magnitude for Mo and W. Oxygen can diffuse to the surface from any possible over-stochiometrical UO_2 nucleus.

A proof of uranium in the precipitation only in the shorter heat test of 8 hours and not after 75 hours duration can be explained as follows:

The coated particles still have a slight surface impurity with UO_2 which stems from the manufacturing process. The UO_2 evaporates immediately after heating and precipitates on the collector and spreads out from there--since the latter is still found at almost the temperature of the sample--gradually throughout the whole furace.

Better results with coated particles for in-pile tests are reported by Winkenbach [10]. The coated particles, which are likewise manufactured by NUKEM, have, however, a thicker coating of Mo (10/μ) As subsequent investigations of the irradiated particles showed [11], these also show the same characteristic roughenings as we have found them also in the out-of-pile investigations. The facts that the particles nevertheless remain dense during the irradiation of 1,200 hours at 2,000°K is in the opinion of the author, however, merely to be understood by the thicker Mo shell and the temperature which was about 100° lower.

In summary it can be said that the coated particles with the Mo shells /29
available at the time are not suitable as nuclear fuel for thermionic convertors. In particular, the question of thermal roughening of the coated

particle surface at the convertor temperature, which under certain conditions is connected with the stoichiometry of UO_2 nuclei, must be investigated in more detail.

2.2 Ventilated Fuels

2.2.1 The Emitter

2.2.1.1 Stability of Shape

The construction of the emitter is represented in Figures 1.1 and 1.2 and described in chapter 1.1.2. The gaseous fission products arising diffuse at the high temperature and the short diffusion paths almost completely from the fuel from [10] and are taken off in the proper fashion. The remaining solid fission products cause a solid body expansion of the UO_2. However, as the following considerations will show, this only leads to a slight change in shape of the molybdenum, although both UO_2 as well as molybdenum can be considered almost completely plastic at 1,700-1,800°C. From the creep data available in technical literature [5, 9] it is found that--in case the stresses are sufficiently small--UO_2 creeps faster than Mo. Not until above a certain limiting stress does Mo creep faster than UO_2. Since possible stresses occurring are immediately compensated by creep, it is assumed that we remain in the area in which UO_2 creeps faster than Mo. It is therefore expected that the expansion of the uranium dioxide leads chiefly to an expansion in the direction of the inner cells and the molybdenum body of the emitter changes only very little.

2.2.1.2 Fuel Transport and Temperature Compensation Processes in the Emitter

It is well known that UO_2 at the operating temperature of the emitter of 2,000°K has a vapor pressure of 10^{-4} mm Hg pressure [13]. In starting and operating the emitter, the fuel relocations already described in chapter 1.1.2 occur and which lead to the formation of an empty space in the emitter. The latter is characterized by the fact that its surface forms an isotherm.

Since the free length of path is large compared to the distances of the surfaces standing engaged in the exchange of material, the evaporation values given by Rom [14] can be used in good approximation. Because the UO_2 rods are filled with a play of the order of magnitude of tenths of millimeters, it can be expected that the entire amount of fuel during the initial phase will evaporate and recondense on the Mo walls. The transport of material takes place relatively fast since the evaporating fuel columns--because of the poor heat transference to the Mo--constantly shows a higher temperature than the fuel condensed on the Mo. The vapor pressure of the condensed UO_2 can remain undisturbed in good approximation in estimating the rate of material transport because of the strong temperature dependence of the UO_2 vapor pressure

/30

[13]. An exact consideration of these effects is practically not possible since the resistence to heat transfer between evaporating UO_2 column and condensed film is undefined and difficult to obtain by calculation. One estimation of the relocation time carried out under the limitations described comes to

$$t_{ü} \approx 200 - 300 \text{ h}$$

Temperature inhomogeneity in the emitter is compensated for by the fact that a UO_2 transport takes place through the gas phase from the hot to the cold place. The UO_2 which additionally condenses at the colder places is likewise burned off and provides the additional heat energy which is still necessary for temperature compensation. For example, such a transport rate of UO_2 is to be expected at an emitter temperature of 2,000°K and with a temperature difference of 20° so that this inhomogeneity of 1% of the rated value should be compensated for by the relocation of fuel in approximately in

$$t_{ü} \approx 100 \text{ h}$$

As the above, rough estimations have shown, the time necessary for leveling the temperature is smaller than the transition time of the emitter from the initial condition to the condition of fuel equilibrium distribution. It can therefore be expected that a quite uniform temperature distribution will be established on the emitter surface at the end of this first burn out phase. More exact calculations for the problem of UO_2 transport in the emitter during operation are planned in the future reporting period. /31

Attention must be paid to a corresponding U/O ratio because of the expected relocation processes extending over the evaporation phase. Only approximately stoichiometrical UO_2 evaporates congruently [15]. If the stoichiometry is not present, then UO or UO_3 occurs in the gas phase along with UO_2. UO and UO_3 can cause an oxygen corrosion of the emitter or lead to a penetration of U into the Mo.

2.3 Preparation of Radiation Tests of Emitters

2.3.1 Extrapolation of the Expansion Effect Occurring at Time Swept Radiation Experiments of Thermionic Emitters

2.3.1.1 Statement of the Problem

The expansion of the fuel cathode conceived by us is in any case controlled by the creep law of Mo at an operating temperature of 2,000°K. As a

consequence, the expansion cannot accelerate corresponding to the burn out sweep if the creep of the Mo is not also accelerated by a corresponding increase in temperature. From this we have the first task.

a) Finding the temperature increase ΔT as a function of the burn out sweep p. In paragraph 2.1.1.2 the author pointed out that the expansion of the fuel follows an exponential law of time with a high exponent. So long as the expansion effect remains under the indicated limit of the measuring process, it cannot be determined in a trivial manner. The result of this is an "incubation period" of the expansion depending upon the measuring process. Here we find the second task.

b) Judgment of the stated value of a time extrapolation of the expansion effect from the available experimental results.

2.3.1.2 Determination of the Temperature Increase ΔT as a Function of the Burn Out Sweep p /32

If the experimental results of a genuine timed sweep should correspond to the burn out sweep factor p, then the following condition must apply to the deformation as a consequence of expansion:

$$\varepsilon\{t_p, T_2\} = \varepsilon\{t, T_1\} \qquad (2.13)$$

For simple burn out For p-multiple burn out

T = Temperature, t = Operating Time, and p = Sweep Factor of the Burn Out.

A deformation of the emitter surface can only take place as a consequence of molybdenum creep in the present cathode types. As a consequence, the creep law for molybdenum must be made a basis in the determination of the temperature increase ΔT.

$$\varepsilon = K(T)\sigma^{N(T)} t^{M(t)}$$
$$\varepsilon = k(T)\sigma^{n(T)} t^{m(t)} \qquad (2.14)$$

A linear setup is permissible if the fissionable gases are not ventilated for the temporal behavior of the stress with time during the burn out.

$$\sigma = apt \qquad (2.15)$$

a ≤ Proportional factor, which also simultaneously contains all the necessary geometric factors.

When equation (2.15) is now introduced into (2.14) and integrated taking into consideration the boundary condition $\varepsilon(0,T) = 0$ we obtain:

$$\varepsilon(t,T) = \frac{k(T)\{ap\}^{N(T)}}{M(T)+N(T)+1}\, t^{M(T)+N(T)+1} \tag{2.16}$$

If now equation (2.16) is used for both cases p = 1 and p > 1 in (2.13), it follows that: /33

$$\frac{K(T_1)\alpha^{N(T_1)}}{M(T_1)+N(T_1)+1}\, t^{M(T_1)+N(T_1)+1} = \frac{K(T_2)\{ap\}^{N(T_2)}}{M(T_2)+N T_2+1}\, t^{M(T_2)+N(T_2)+1} \tag{2.17}$$

In order to evaluate the equation (2.17), it can be assumed in a limited temperature range that

$$\begin{aligned} M(T) &= M_0 + \sum_{v+0} M_v(T) \\ N(T) &= N_0 + \sum_{v+0} N_v(T) \end{aligned} \tag{2.18}$$

The simplification is sofar not too incisive since M and N only slightly depend upon temperature. If equation (2.18) is introduced into equation (2.17), then we obtain

$$p^{M_0+1} = \frac{K(T_2)}{K(T_1)} \tag{2.19}$$

If the Larson-Miller relation is now evaluated for the temperature relationship of the creep rate using the simplifying assumption of equation (2.18) and for a small temperature range, then we find:

$$\frac{K(T_2)}{K(T_1)} = \exp\{C(T_2-T_1)\} \tag{2.20}$$

C = Constant

From the experimental results of General Electric [9], the behavior of k(T) was obtained. If the results are corelated, then we obtain:

$$\Delta T = 70 \ln p \qquad (2.21)$$

Therefore, a temperature increase ΔT can now be clearly allotted to a burn out sweep p in a temperature range of the operating temperature of thermionic convertors of 2,000°K, in case a time sweep corresponding to the burn out sweep is desired in the study of the expansion effect. /34

2.3.1.3 Evaluation of the Stated Value of a Time Extrapolation of the Expansion Effect from the Experimental Results at Hand

After the end of the radiation, the diameter of the cathode can be measured with a measuring process having the accuracy g. In this, two cases may obtain: a) there is an expansion effect which is measurable; b) there is no expansion effect which is measurable.

a) In this case, an extrapolation to fairly long utilization times is simple if one starts according to equation (2.14) from a simplified form of the time and behavior of the expansion.

$$\varepsilon = \bar{K} t^{M} \qquad (2.22)$$

With a known M, K can be determined from the experimental time and the expansion effect.

b) In this case, an extrapolation is very unsure, since two other possibilities must yet be discussed: no expansion has taken place; an expansion has taken place, but the effect is smaller than the accuracy of measurement g.

A decision between the two possibilities cannot be made. One can merely offer a maximum estimation. For this case it must be assumed that the expansion effect would have been measurable if the experiment had only been continued on for a short period of time. Then it follows:

$$g = \bar{K} t_0^{M} \rightarrow \bar{K} = g/t_0^{M} \qquad (2.23)$$

t_0 = Expansion time; g = Stated Limitation of the Measuring Process.

In this way we have an upper evaluation of the expansion effect as a function of time. /35

$$\varepsilon \leq g \left(\frac{t}{t_0}\right)^{M} \qquad (2.24)$$

Thus the value of the extrapolation is closely connected to the accuracy of measurement g and the in-pile experimental time t_0.

Example. A total expansion of 1% with a cathode diameter of approximately 20 mm in two years is still not permissible. A time sweep about the factor of 2 appears possible. With an experimental time of say six months, the measuring process must permit measurement of an increase in diameter of the cathode according to (2.23) of 10/μ. With an experimental time of three months, a resolution capacity of 1.5/μ is required. A natural limitation of the experimental time limit therefore represents just the possible resolution capacity of the diameter measuring process.

2.3.1.4 Conclusion

A temperature increase belonging to a particular burn out sweep can clearly be calculated. The latter is relatively small. The reason for this can be sought in the strong relationship of creep rates to temperature. From this results the still higher requirements for accuracy of the temperature regulation during the radiation.

Extrapolations of the expansion effect for longer utilization times from shorter and possibly time-swept radiation experiments are very uncertain. For proof that the permissible expansion rate of 1% in two years is not exceeded for one of the cathode types suggested, minimum experimental times of 4 to 6 months are necessary.

2.3.2 Radiation Experiments

2.3.2.1 Statement of the Problem

The preparation of radiation experiments with fuel emitters was begun. The experiments were to be carried out in the second isotope canal of the Federal Republic in Karlsruhe. The goal of these radiation experiments is to /36
obtain data on the long term behavior, i.e., to answer the question whether the proposed emitters operate satisfactorily during the planned long term time of about two years under the operating conditions of thermionic cells (temperature, heat output, expansion and creep limits).

For this reason, the emitters which in their essential characteristics correspond to the ones to be used later in the thermionic convertor combustion element are irradiated. The emitters are filled with the planned amount of fuel and provided with a tungsten layer, the series-connected bridge and (depending on type) with a fission-gas line and a collecting chamber. Only under these experimental conditions are results to be expected on the thermal loading of fuel, the mechanical stress of the structural materials, the behavior of the tungsten layer at operating temperature and under reactor radiation and the functioning of the fission-gas ventilation.

In order to shorten the radiation time, the experiments are arranged in such a way that the fuel developes double the specific heat output as in the

nominal operation in the thermionic convertor combustion element (heating surface load at the cathode surface is 100W/cm^2 instead of 50W/cm^2). In this way, the doubled burn out is achieved in the given experimental time or the time in order to sweep the time by factor of 2. For a time acceleration of temperature controlled processes such as creep or diffusion, the temperature during radiation must be raised by about 50°C (see paragraph 2.3.1). One radiation test each is planned with three, six and nine months radiation time so that burn out conditions are achieved such as would be present after six, twelve and eighteen months operating time under nominal conditions.

Since the creep rate of molybdenum, depends strongly on temperature, the cathode's temperature must be measured exactly and carefully controlled during /37
the radiation experiments. Therefore a radiation capsule should be constructed which fulfills the following functions:

a) A high surface loading of the emitter surface of 100W/cm^2 (rod output 628W/cm) must be led away, where the temperature distribution over the entire length of the emitter must be similar to that of the emitter in the convertor cell.

b) The emitter must be maintained force free so that changes in form which develope as a consequence of expansion of the fuel and different thermal expansion can take place unhindered.

c) The radiation capsule must be provided with an instrumentation to measure the emitter temperature.

d) Changes of emitter power which occur owing to neutron flow fluctuations and increasing burn out must be compensated by an electrical auxiliary heater so that cathode's temperature is regulated constant with respect to time.

2.3.2.2 Construction of the High Output Radiation Capsule

In order to carry out the tasks named, an experimental insert is laid out and calculated which can be inserted into the Federal Republic's number 2 isotope canal. Its construction in principle can be seen in Figure 2.8.

The experimental insert contains two emitters and two fission gas containers one over the other. It is filled with helium and welded shut. On the upper side it tapers to a support which fits into a carrier pipe in the immersion tube of the FR 2.

The amount of heat produced in the emitter is given off through radial /38
heat radiation and conduction to a niobium pipe arranged concentrically around the emitter. The aperture between emitter surface and niobium pipe is filled with inert helium (30 mm Hg pressure). The width of the aperture comes to 0.6 to 0.8 mm; its exact value is determined in heat-technical free tests. The proportion of heat radiation in the entire output comes to only 20%.

/88

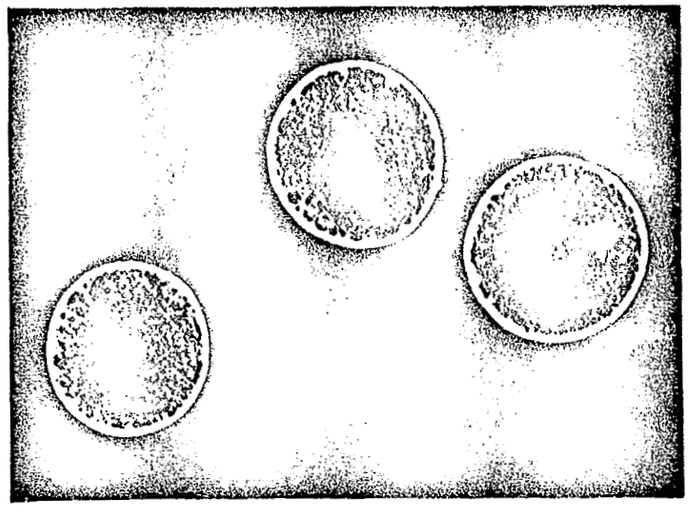

Figure 2.3. Coated Particles in the Condition Delivered: Diameter of the UO_2 = 150/μ, Coating Thickness 5/μ, Enlarged 200 Times.

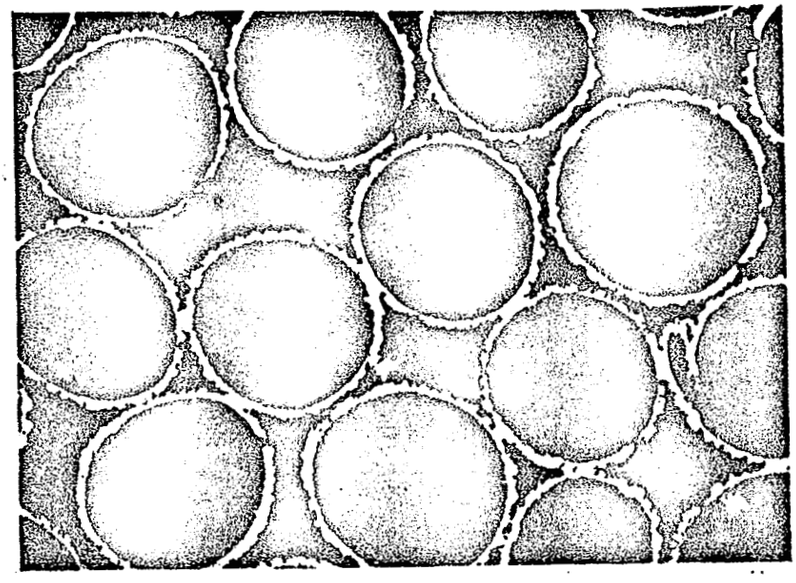

Figure 2.4. Coated Particles as in Figure 2.3, However Shown After 75 Hours Heating at 2,000°K, Enlarged 200 Times.

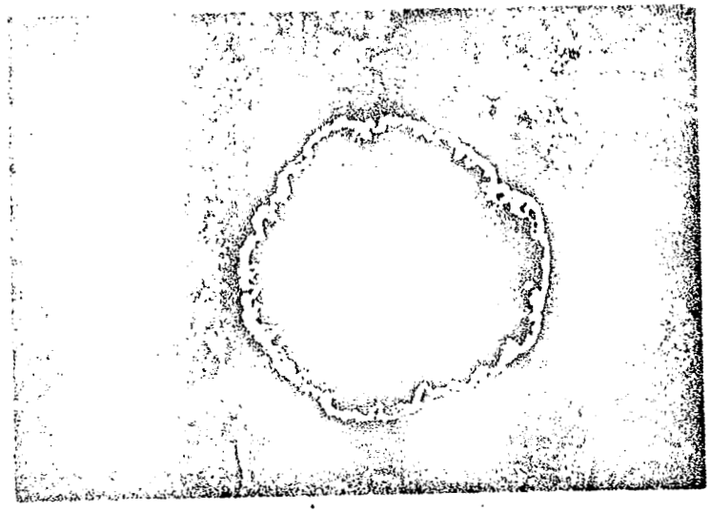

Figure 2.5. Coated Particles in the Condition in Which They Are Delivered, Diameter of the UO_2 = 70-120/μ, Coating Thickness 2-3/μ, Enlarged 500 Times.

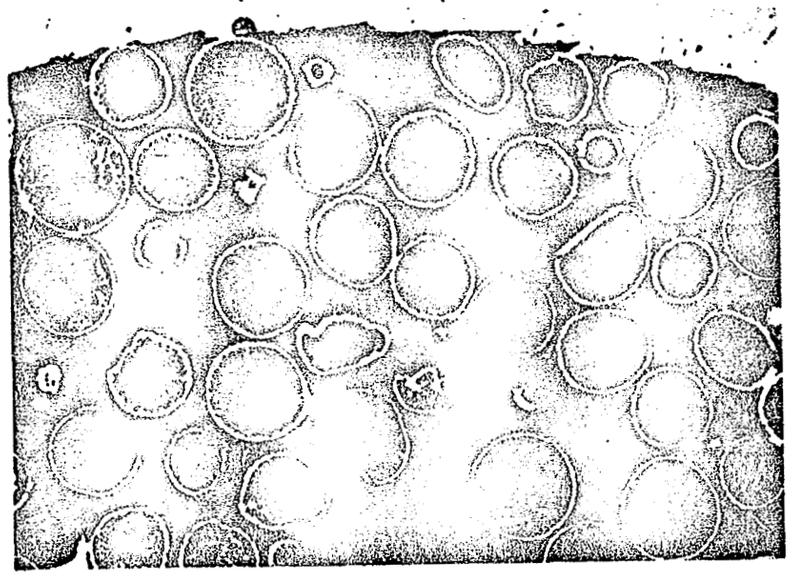

Figure 2.6. Coated Particles as in Figure 2.3, However After 239 Hours Heating at 2,000°K, Enlarged 100 Times.

/90

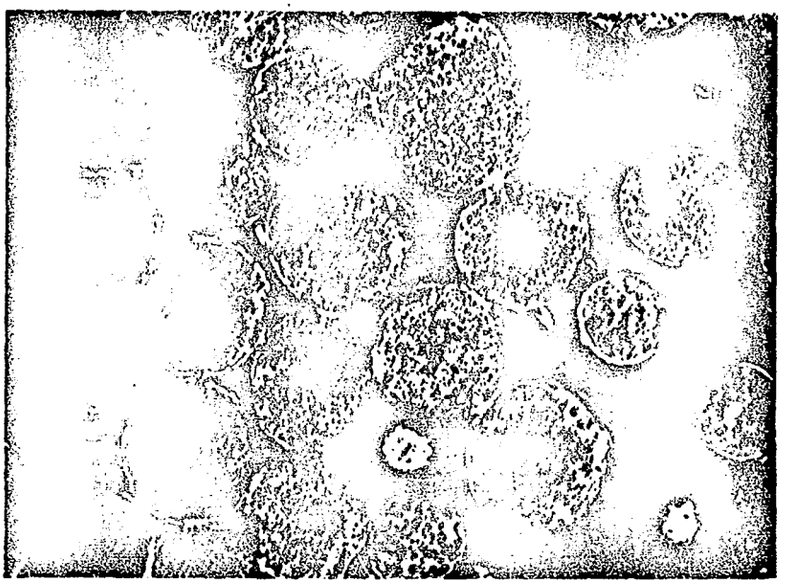

Figure 2.7. Coated Particles as in Figure 2.5, However After 239 Hours Heating Time at 2,000°K, Enlarged 200 Times.

/38

The cathode hangs in the niobium tube on the cathode-anode bridge provided in the convertor cell conceived. Its lower end moves freely at the axis in order to pick up various heat extensions and centers over a second bridge to the niobium tube. The temperature of the niobium tube lies between 450°C and 750°C according to the power of the auxiliary heater which is wound electrically around the tube with which the surface temperature of the emitter of 1,780°C is kept constant with fluctuations of flow.

The filament winding is surrounded by a steel pipe. Intermediate spaces between steel pipe, niobium tube and heating conductor are filled up with copper to make a good heat-conducting transition. Steel ribs radiating around the outside are fastened on the outside of the steel pipe in the axial direction and lie on the inner wall of another steel pipe. Its thickness is measured in such a way that the temperature of the niobium pipe makes possible a satisfactory regulating width of the electrical heater.

The outer steel pipe forms the housing of the experimental insert. Between the latter and the inside of the immersion tube in the FR 2 there is an aperture of 2.5 mm widths through which D_2O flows for cooling the experimental insert. The experimental insert is led into the immersion tube by means of spheres which press on the outside by springs.

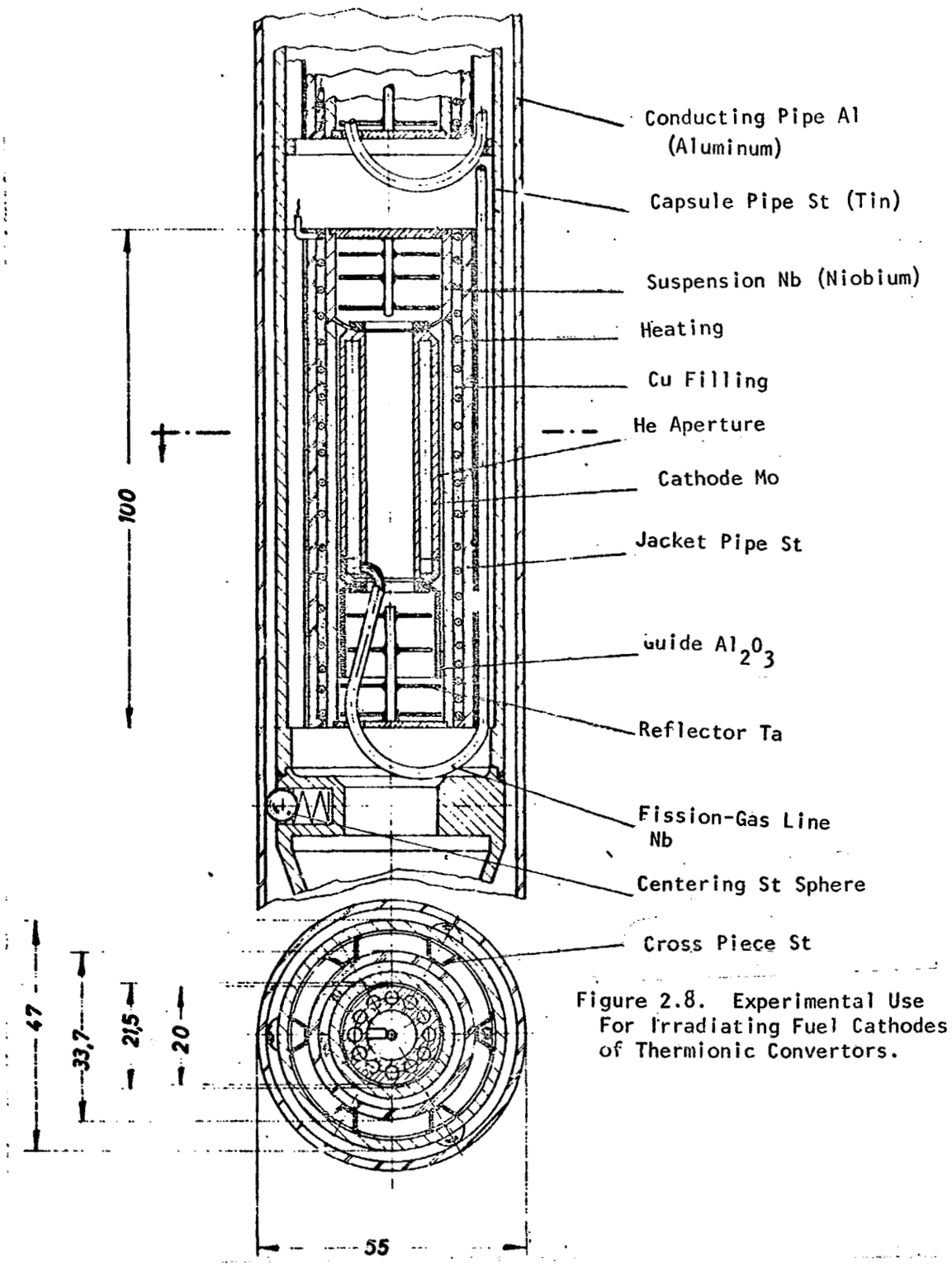

Figure 2.8. Experimental Use For Irradiating Fuel Cathodes of Thermionic Convertors.

Ten closely welded or soldered sleeve thermocouples rise up from the experimental insert along with two coaxial lines of the neutron flow acceptor and four connections for the electrical heater. /38

The calculated radial temperature behavior in the experimental insert is represented in Figure 2.9. /39

2.3.2.3 Instrumentation

The emitter temperature is measured with each of two thermocouples WRe 5%--WRe 26%. At the same height as the emitters, the temperatures of the steel pipe are measured with three thermocouples made of NiCr-Ni placed around 120° and the neutron flow is measured with a flow detector which gives off a direct current proportional to the flow. These measuring data are registered with dot printers during the entire time of radiation.

During the first few days of radiation, a correlation must be found between the emitter output (or neutron flow), electrical output and temperature of the steel pipe at constant emitter temperature. This correlation must permit the emitter temperature to be held constant even with a breakdown of both high temperature thermocouples. Therefore, suitable measuring instruments are provided for the measurement of the electrical heat output.

2.3.2.4 Regulating the Emitter Temperature

The emitter temperature can deviate at the beginning of the radiation experiment from its calculated value. Reasons for this are the uncertainty of the neutron-physical layout (±30%), deviations in the degree of richness of the fuel, measuring errors in the determination of flow in the IK positions and tolerances in installation. Compensation for these errors as well as the increase of the neutron flow (about 10%) required with increasing burn out takes place by resetting the experimental insert to other isotope-canal positions by making use of the radial flow gradients.

After compensation of the large temperature deviations at the beginning of the radiation time, small changes of emitter temperature are compensated by the electrical auxiliary heater.

With a rated heat production of the emitter of 3,140 watts, the heater is operated at half maximum heater output. The maximum heater output comes to 3,770 watts per emitter section. From this and from the temperatures of the niobium tube, there is a regulating range of ±13%, i.e. with fluctuations of the emitter output between ±13% the emitter temperature remains constant. With the measuring value of one of the two tungsten-rhenium thermocouples, there is an approach to an electronic regulation which changes the time average value of the heating potential over a phase section through thyristors. A maximum heating potential comes to $220V_{eff}$. /40

/92

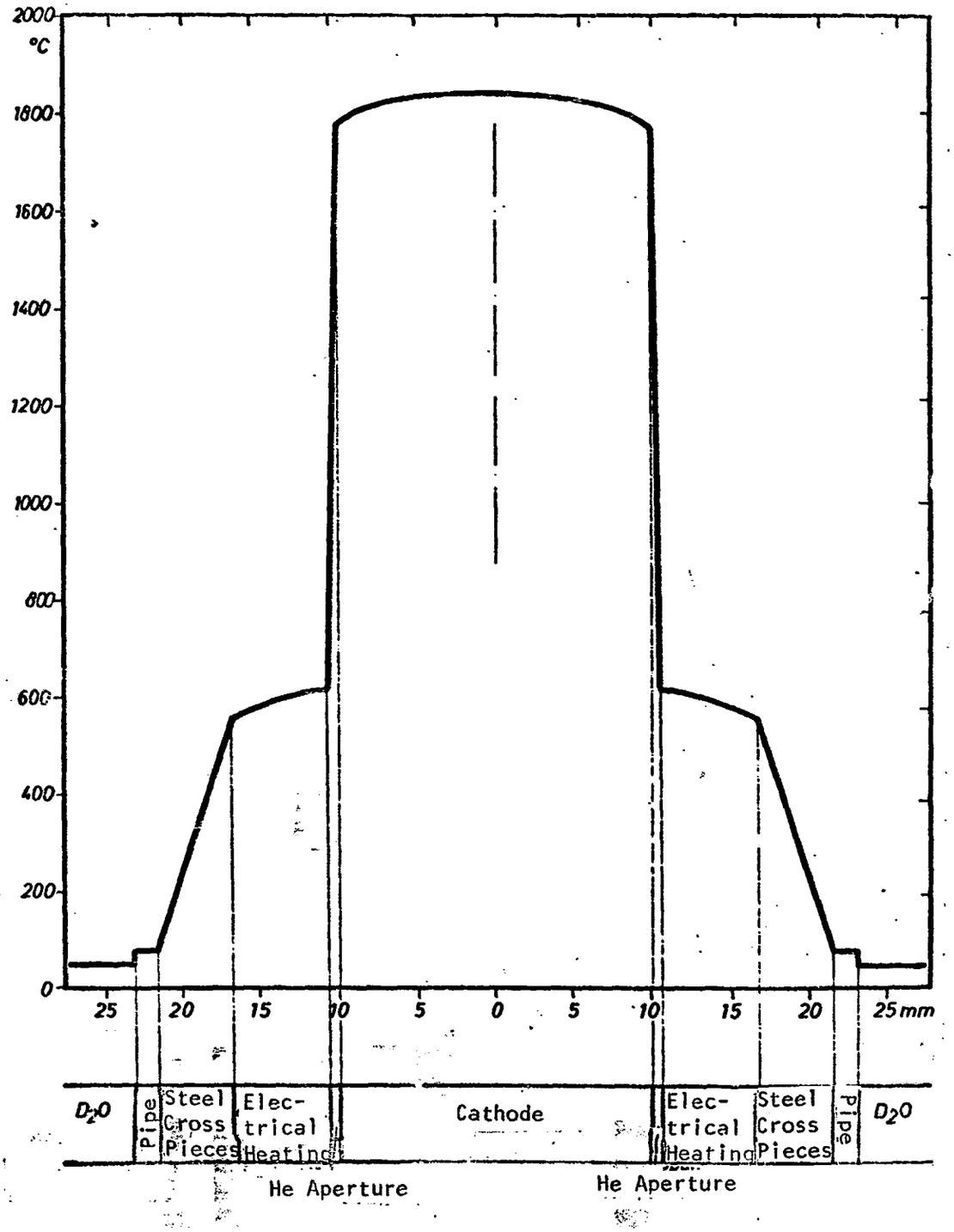

Figure 2.9. Radial Temperature Curve in the Radiation Capsule (Calculated).

With the breakdown of one of the two WRe thermocouples, the element still functioning is connected to the regulator. With the breakdown of both WRe thermocouples, the regulator is controlled by one of the three NiCr-Ni elements in the steel pipe or operated by hand.

2.3.3 Heat-Technical Experiments

The layout data for the high-output radiation capsules must be tested before using in the reactor. For this purpose, the part of the radiation capsule which contains the emitters and which is shown in Figure 2.8 is built and operated in a test band, where the power producing emitters are tested as a resistence heated niobium tube of the same temperature and heat-surface loading.

Goal of the heat-technical experiments are the exact determination of the size of the helium-filled aperture between the cathode surface and the niobium tube, assuring the functional capability of the experimental insert by maintaining the upper temperature limits, testing of the temperature regulation, testing of the technological production methods of components of the experimental insert and the temperature measurement at reference points in case of breakdown of the high temperature thermocouples in the reactor.

2.3.3.1 Test Stand

The test stand for the heat-technical testing of the radiation capsule can be seen in Figures 2.10 and 2.11. The high power supply of the resistance heated niobium tube, the pump stand, the vacuum recipients which contain the radiation capsule balance network, the helium supply and the helium after cleaning stretch can be seen. /41

In order to avoid oxidation of the odd parts, the vacuum recipient and later the radiation capsule are evaculated to a high vacuum and then filled with helium at about 30 mm Hg pressure. The flask helium has to be led beforehand through an after cleaning stretch in which it drops off impurities of oxygen, steam and carbohydrates to a molecular sieve at the temperature of liquid nitrogen. The concentration of steam of the purified helium comes to about 1 ppm, and that of the flask helium about 7 to 8 ppm.

Figure 2.12 shows a cross section through the experimental arrangement and the balance network of the radiation capsule as it is to be mounted in the experimental arrangement. The resistance heated niobium tube (6), whose lower tapered end of 60 mm length simulates the emitter, hangs in a water-cooled vacuum container (1), through whose window (2) its temperature is determined by pyrometer at the water-cooled flow inlets (3), pole choose (4) and contact jaws (5). The radiation capsule--water-cooled sleeve (8) and electrical auxiliary heater (9)--is set up through the centralizers (7) and (10) on the heating pipe, is fastened to a support leg (12) through a sprung receiver (11) and provided with thermocouple and water contacts (13, 14). Helium inlet and vacuum connector are found at (15) and (16).

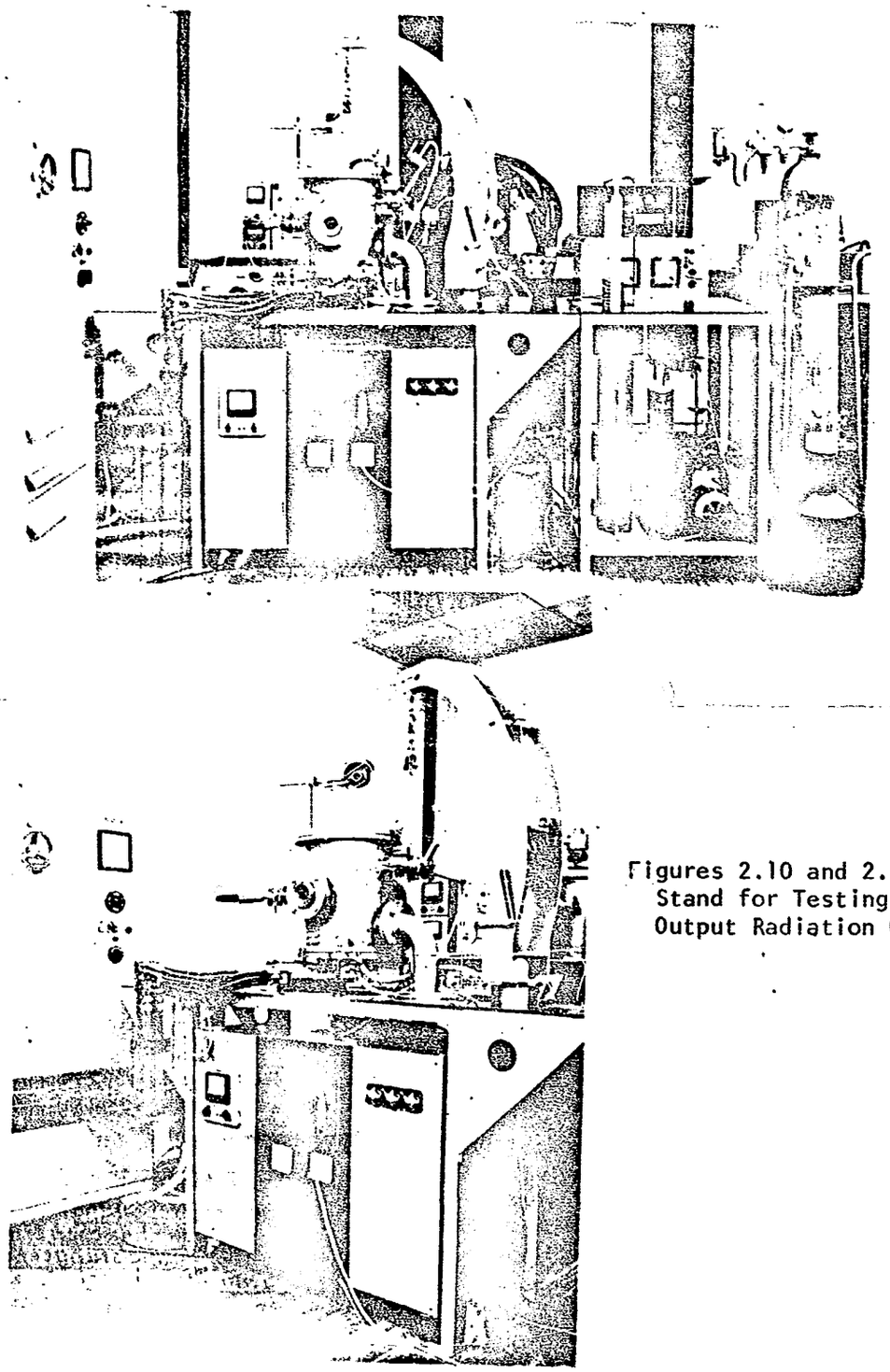

Figures 2.10 and 2.11. Test Stand for Testing the High Output Radiation Capsule.

/94

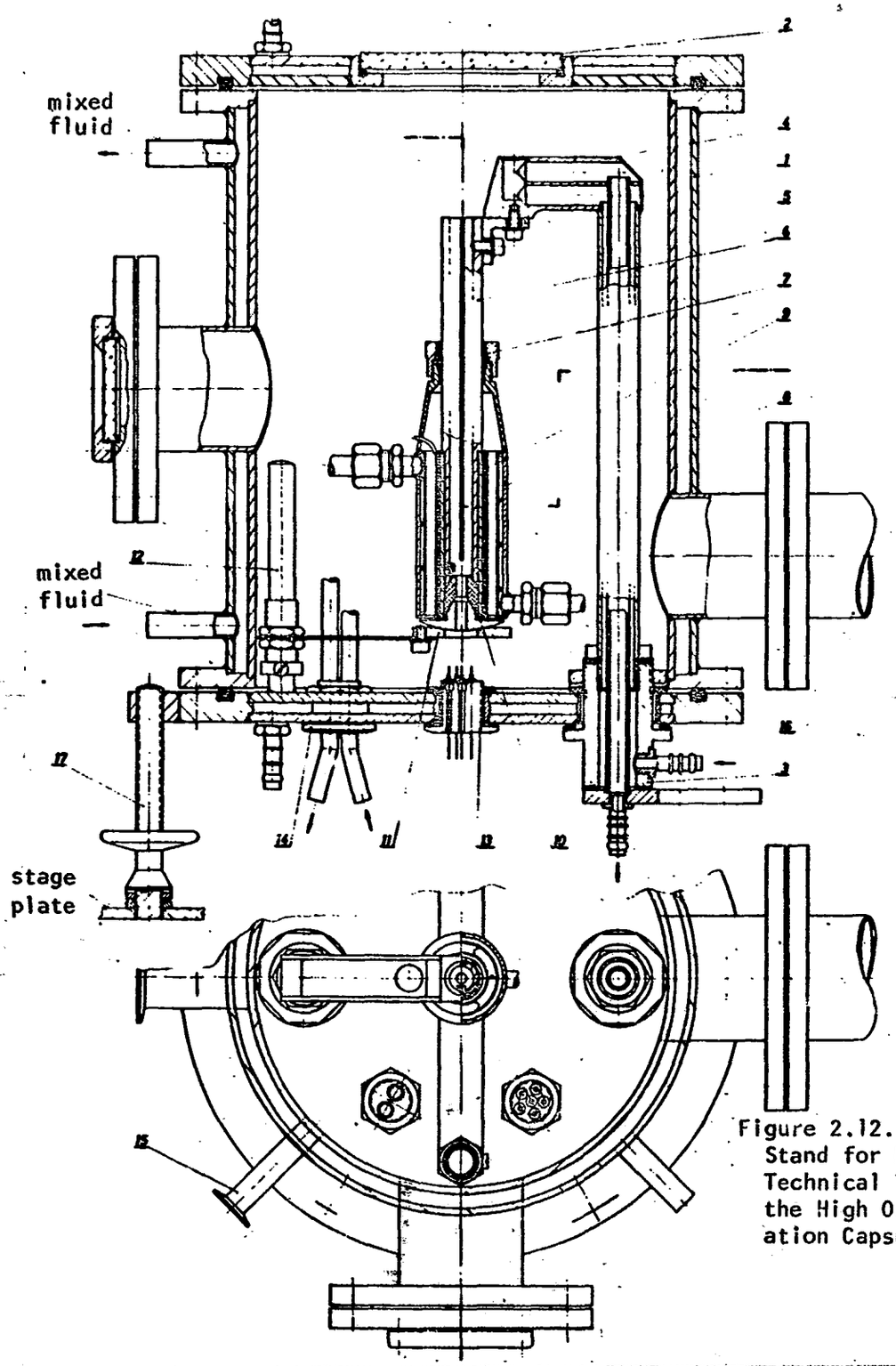

Figure 2.12. Test Stand for Heat-Technical Testing of the High Output Radiation Capsule.

2.3.3.2 Measurements /41

After the balanced network of the radiation-capsule is finished, temperature measurements are carried out which should verify the temperature profile calculated and shown in Figure 2.9. At first, the resistance heated niobium tube (6 in Figure 2.12) is put into operation and the temperature behavior is determined along the axis of the tube in a vacuum and at a helium pressure of 50 mm Hg by means of a pyrometer. The measurements are represented in Figure 2.13. In operating the heating pipe in the balance network of the experimental insert, therefore when cooling over a helium aperture about 0.5 mm thick, the temperature curve will continue to be smoothed out. /42

After conclusion of the temperature measurements of the heat-conducting components, the construction of the first experimental insert is begun.

2.3.4 Neutron-Physical Calculations

The flow thickness of thermal neutrons in the FR 2 isotope canal at Karlsruhe was calculated as is necessary for carrying out the radiation experiments in the above described experimental insert and with the required output density in the fuel.

A fuel enrichment of 93% U-235 in the uranium is provided for the cathode used in the thermionic reactor. In order to reduce costs and because of the essentially easier determinations of safety for less enriched fuel, only fuel enriched to 20% U-235 is used for the radiation experiments. In order to achieve the same heat release, a correspondingly higher neutron flow in the experimental reactor must be present.

The thermal neutron flow in the interior of a D_2O-filled FR 2 isotope canal, thus the undisturbed flow, is well known. The neutron flow distribution in the environment of the canal is changed by bringing in so strong an absorber as the experimental insert with the thermionic fuel cathode. With the help of the diffusion theory, first the flow curve in this outside range is calculated. The latter is represented along with the undisturbed flow in Figure 7.7. The flow at r = 8 cm was used as a limiting value for the flow reduction calculations.

The calculation which was carried out according to the collision probability method (Amouyal-Benoist-Mueller) (Figure 2.15) shows the flow curve in the experimental insert according to this method (curve 3) along with the flow curve according to the diffusion theory from Figure 2.14 (curve 2).

An average thermal flow in fuel of $\phi_B = 1.8 \cdot 10^{13}$ cm^{-2} s^{-1} is required /43 for a thermal output of 3,140 W per cathode corresponding to $100 W/cm^2$ cathode surface. In consideration of the calculated flow reduction there is the possibility of $\phi_0 = 7.0 \cdot 10^{13}$ cm^{-2} s^{-1} for the selection of a radiation canal in the D_2O-filled canal.

/95

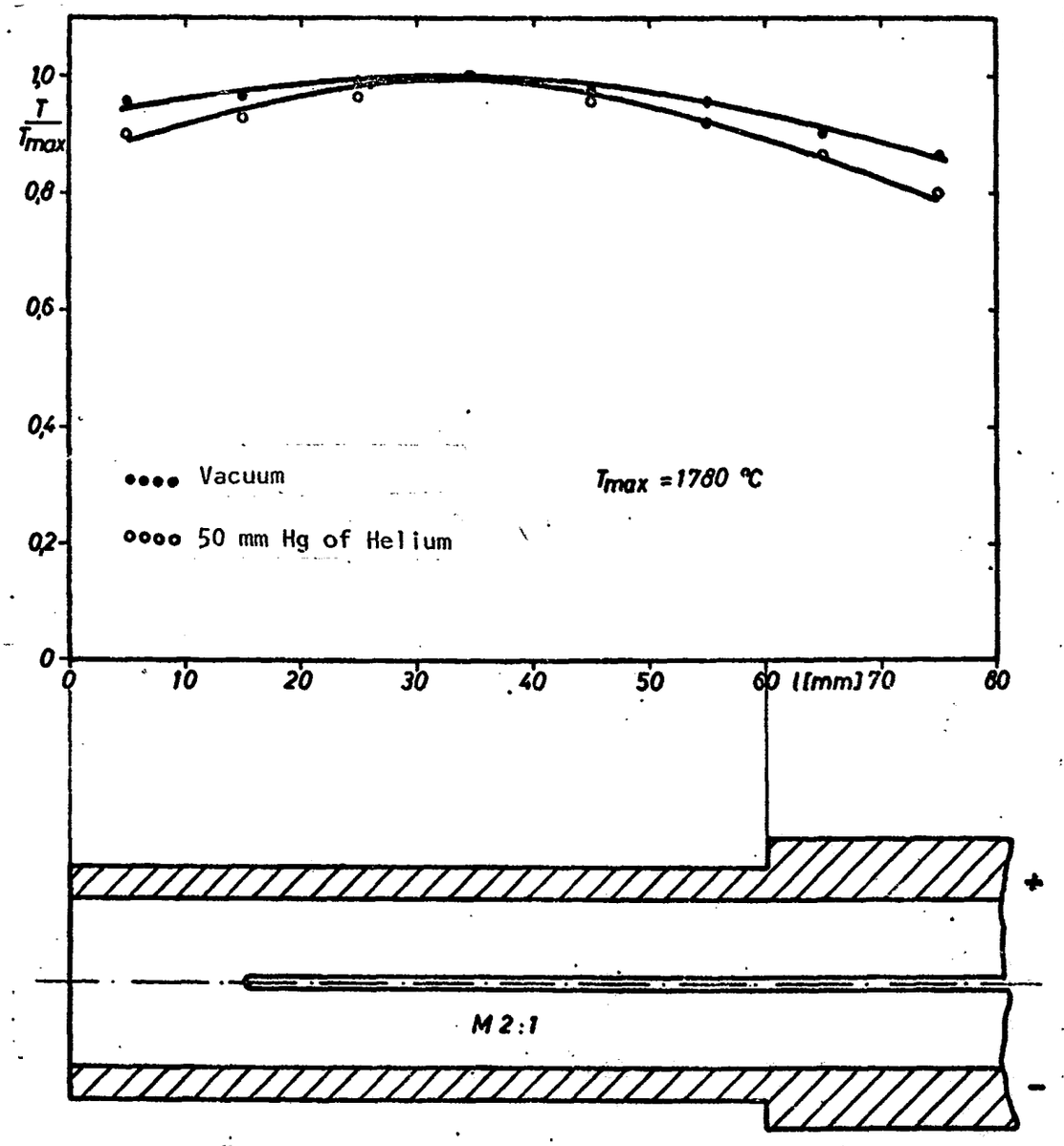

Figure 2.13. Measured Temperature Curve at the Surface of the Heating Pipe in a Vacuum and in Helium.

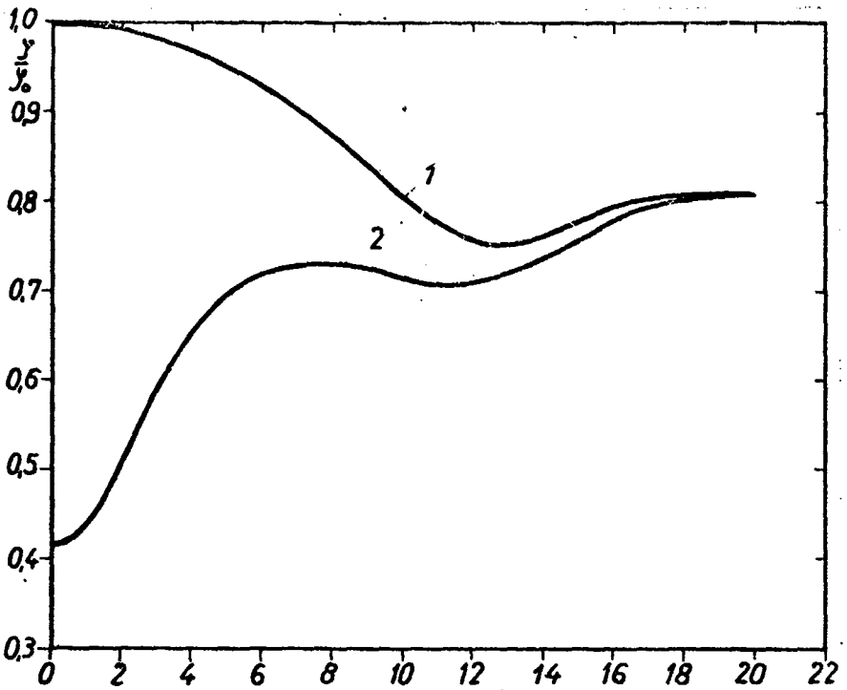

Figure 2.14. Flow Curve in Undisturbed Isotope Canal (1) and in the Environment of the Experimental Use (2) According to the Diffusion Theory.

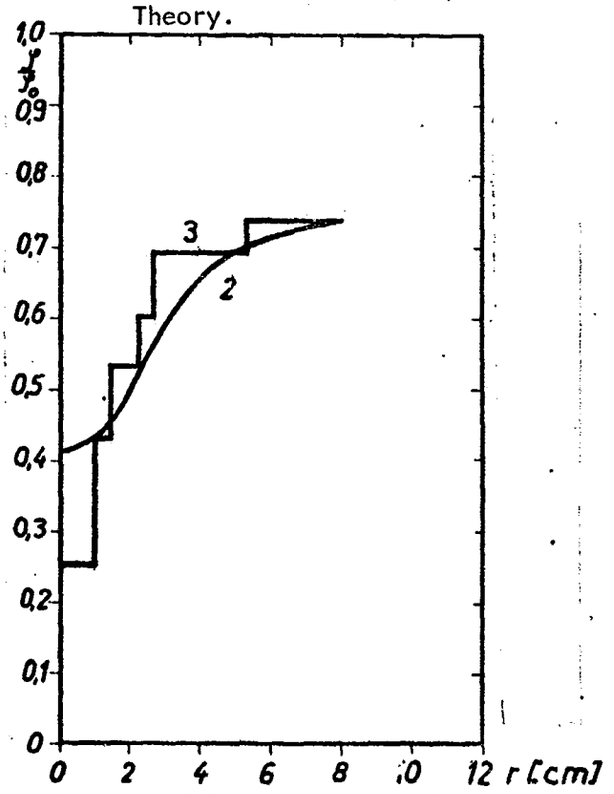

Figure 2.15. Flow Curve in the Experimental Use According to the Diffusion Theory (2) and According to the Transport Theory (3).

In order to avoid flow bellying, absorbers 25 mm in length and of the macroscopic effective cross section as the fuel zone are attached to the ends of the cathodes. /43

2.3.5 Production Experiments

The dimensions of the experimental insert and its upper connecting piece were discussed in connection with the Department for Reactor Operation of the Society for Nuclear Research at Karlsruhe, where work on reactor inserts (immersion tube, screen plugs) in which the experimental inserts are to be housed during radiation is to be carried out.

We began with production experiments for making the electrically heated cooling and heating body (in Figure 7.1 designated with hanging heating pipe--pipe jacket), where filling up the intervals between the heating conductors with copper with inductive heating and in the radiation furnace was tested.

Along with the cooling of the emitter containing fuel in the experimental insert along the helium filled aperture, another cooling method was investigated. It consists in leading off the heat output over metal cooling sheets by heat conduction and heat radiation. The cooling plates consist of niobium and are welded along the sleeve lines with the electron radiation on the cathode. Figure 2.16 shows a cross section through a cathode with 20 welded /44
cooling plates. The plates become so hot at operating temperature on the emitter side that they do not prevent changes in shape of the cathode in the reactor (expansion). The plates on the outside are soldered in a slotted pipe. Between cathode and pipe there is a vacuum which under certain conditions can be of advantage with respect to a helium filling.

3. Investigations for Producing W-Emitter Layers /45

3.1 Production of W Layers by Pyrolysis of $W(CO)_6$

3.1.1 Statement of the Problem

It has been stated a number of times in technical literature [16-18] that the method of vapor plating is the best suited for the production of tungsten layers. There are fundamentally two different methods to choose from:

The reduction of tungsten halogenized with hydrogen permits achieving a high layering rate [19]. Serious disadvantages of this method are, 1) the columnar structure caused by the high layering rate and, 2) the hydrogen-halogen compounds which are formed at high temperature and which react very strongly. By using hydrogen, all the problems of gas purification occur simultaneously if tungsten layers of high purity are desired.

All these disadvantages are aborted by the tungsten hexacarbonyl method. Sofar, only a small to average layering rate could be achieved. Details of the method have already been reported by the author [5].

/97

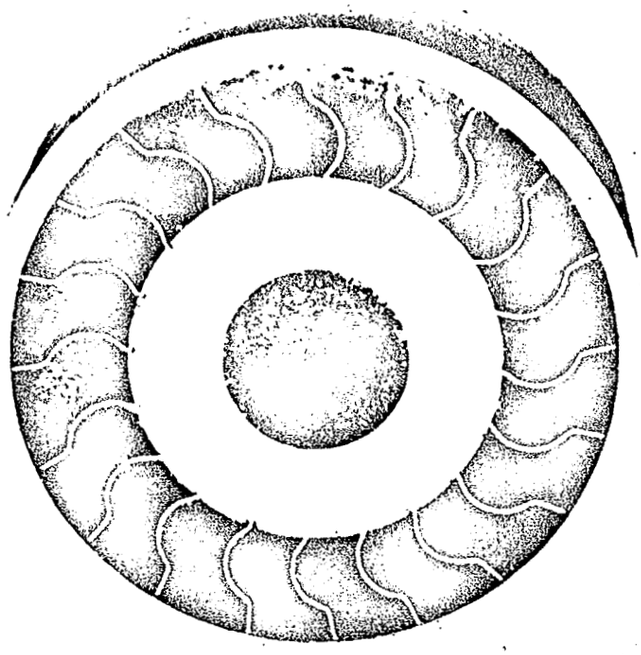

Figure 2.16. Cathode with Cooling Sheets of Niobium (Cross Section) (Enlargement 2.5 Times)

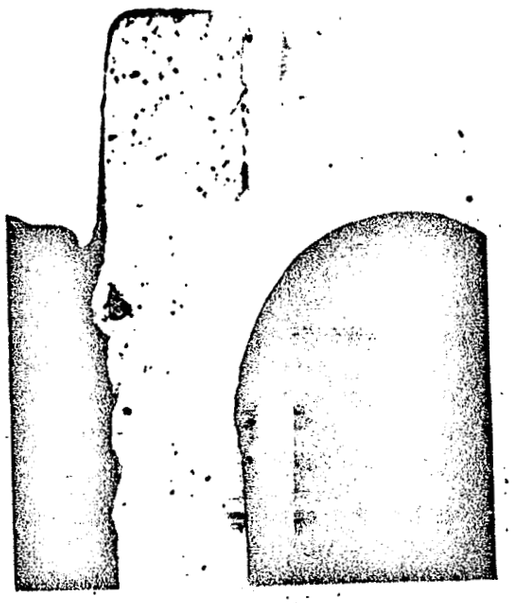

Figure 2.17. Niobium Cooling Sheet Welded to Cathode Enlarged 100 Times.

There is also the attempt to create tungsten layers of a certain structure for reasons of mechanical toughness and properties of thermionic emission and diffusion behavior. Therefore, a combination of plasma spraying and vapor plating is suggested by the author [5]. /45

Accordingly, two problems are to be solved in order to improve the vapor plating method: 1) increasing the rate of layer; 2) controlling the layer structure during layering. The experiments necessary to do this are described in the following and the results are discussed. /46

3.1.2 The Layering Rate

Two different methods for coating the sample surface with tungsten hexacarbonyl were applied for investigating the factors influencing the layering rate:

1) Indirect Coating. The tungsten hexacarbonyl is located in a tank of suitable cross section in the layering container. The initial cross section is sized corresponding to the output of the pump so that the pressure in the container can be dropped about two orders of magnitude below the vapor pressure of the tungsten hexacarbonyl at room temperature. After separating the pump from the container, the pressure gradually increases and the container is slowly filled with tungsten hexacarbonyl gas. All the tungsten hexacarbonyl molecules which owing to thermal movement come into contact with the hot surface of the sample, which has a temperature of over 1,200°C or more, are split pyrolytically.

2) Direct Coating. The tungsten hexacarbonyl is located in a tank of large initial cross section. The opening of the carbonyl reservoir is in this case large enough so that the amount of tungsten hexacarbonyl flowing out approximately corresponds to the output of the pump under working pressure.

Simultaneously, care is taken so that the sample to be coated hangs directly in the exiting streams of tungsten hexacarbonyl gas. In so doing, essentially more tungsten hexacarbonyl molecules touch the surface than in process 1).

3.1.2.1 The Effect of the Base /47

During the course of the experiments it has been shown that the base has an important influence on the rate of layering. The effect is particularly strong when layering using method 1). Figure 3.1 shows the layer thickness as a function of the layering time. It is recognized that if layering is begun on a polished molybdenum surface, the thickness of the layer increases rapidly and then slows down. Conversely, if one begins with a molybdenum suface which has first been plasma-sprayed with tungsten, then the growth rate is at first slower, remains then for constant for a fairly long time and then finally exceeds the rate which can be expected from a polished surface.

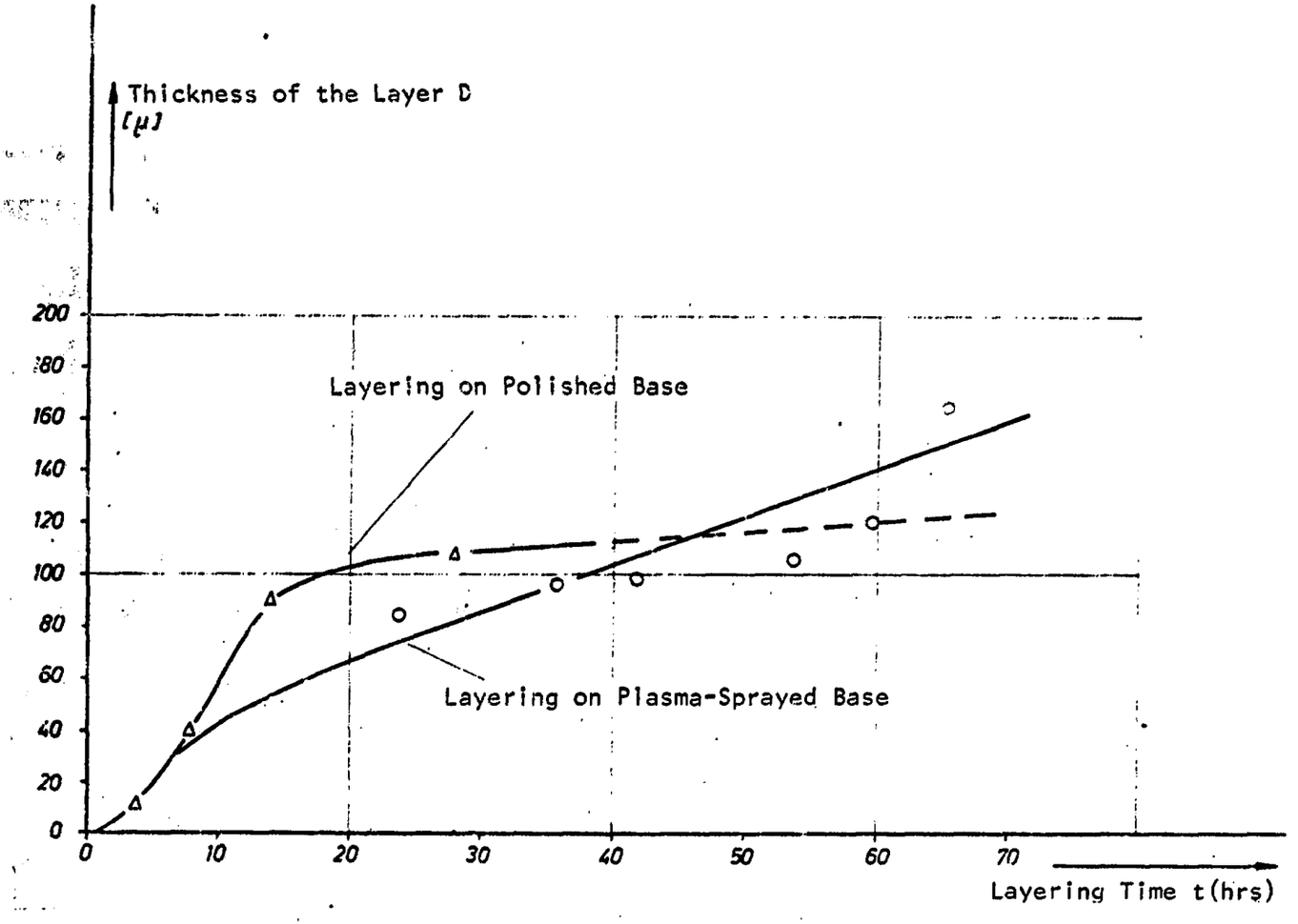

Figure 3.1. Effect of Base on the Rate of Layering-Layering Temperature Approximately 1,200°C.

3.1.2.2 The Effect of the Supply of Tungsten Hexacarbonyl

Figure 3.2 compares the thickness of the layer as a function of time in methods 1) and 2). The essentially faster layering rate in process 2) is noticeable. Both cases began with a polished molybdenum surface. In process 1) with about 140/μ thickness, a clear increase in the layering rate is to be observed. Conversely, with process 2) even at 200/μ, an almost constant growth in thickness can be noted. /47

3.1.2.3 The Effect of Temperature

In the temperature range of 1,200°C-1,500°C, no dependence of the layering rate on the temperature could be clearly observed in our experiments.

3.1.3 The Formation of the Inner Structure

It can be seen immediately that the methods of layering described in the preceding section have a considerable effect on the formation of the inner layer structure. The surface orientation in the goniometer method and the grain size were measured as a characteristic magnitude of the tungsten layer structure.

3.1.3.1 The Effect of the Molybdenum Base /48

In a case of the indirect spraying of the molybdenum surface with tungsten hexacarbonyl and the small growth rate connected with it, the tungsten grows epitactically on the molybdenum surface, i.e. the tungsten crystals take over the crystal structure of the molybdenum base.

The intensities of the (100), (200) and (211) tungsten crystallites oriented with parallel faces to the surface were measured on an approximately 40/μ molybdenum sample layered with tungsten (Table 3.1). Approximately the same distribution of intensity is found for the corresponding lines at the surface of the tungsten and--after its attrition--in pure molybdenum. By comparing the intensity with ASTM normal values, conclusions can be drawn as to the distribution of frequency. That means that in the molybdenum and in the tungsten there is about the same frequency of orientation for the individual orientations.

For a more exact check of the existing state of affairs, the orientation frequency was measured for two molybdenum samples after different heating periods at the temperature of layering. Then both samples were layered from measuring to measuring with about 10/μ of tungsten each. The measured intensities are listed in Figure 3.3. It is recognized even here that almost all the measured orientations of the molybdenum were then taken over with the same frequency by the tungsten. Proceeding further it is even found that the change, which was different from sample to sample, of the surface orientation frequency of the molybdenum can be observed during the heating and also during the later layer growth of the tungsten.

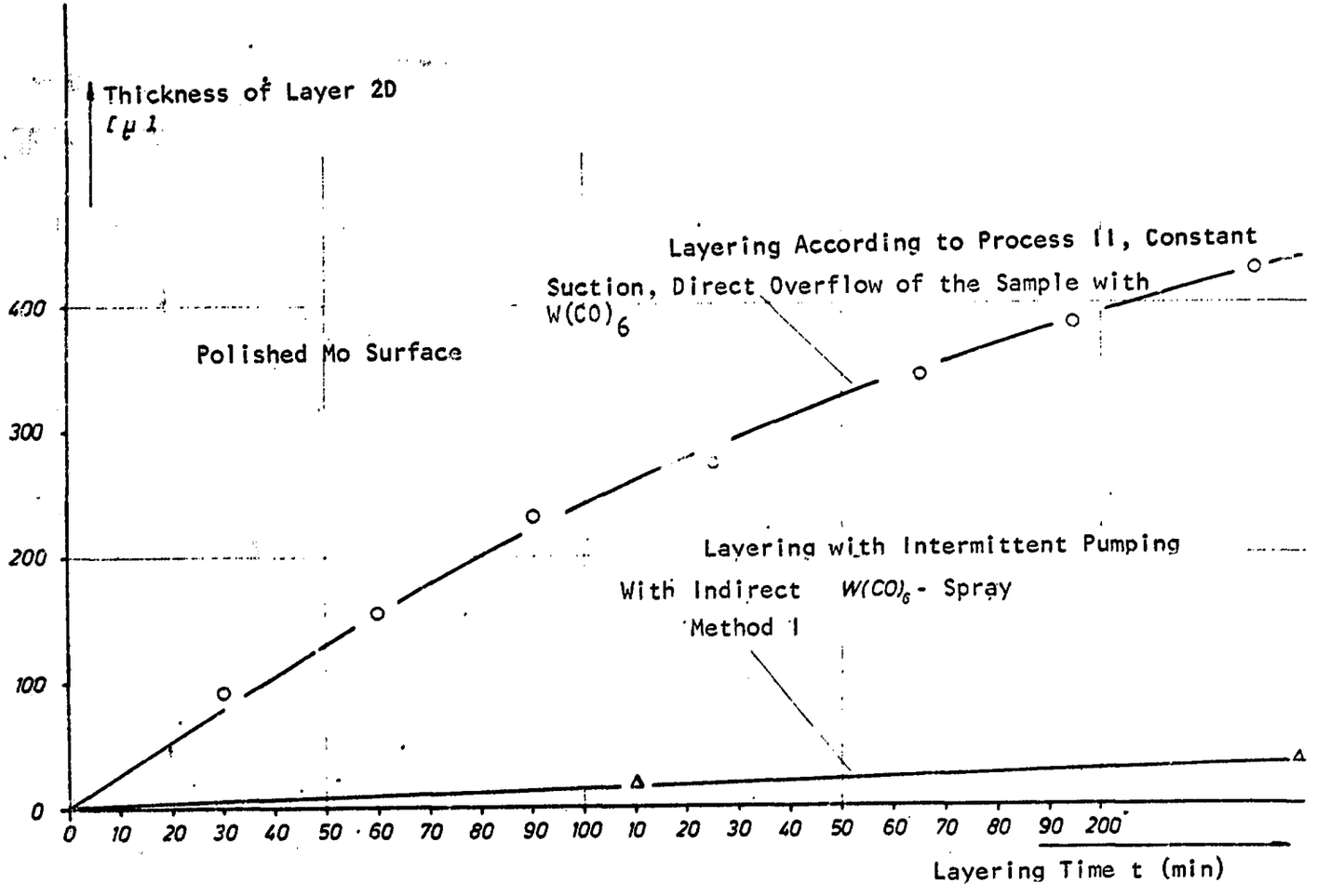

Figure 3.2. Layering with Tungsten by Vapor Planting.

/100

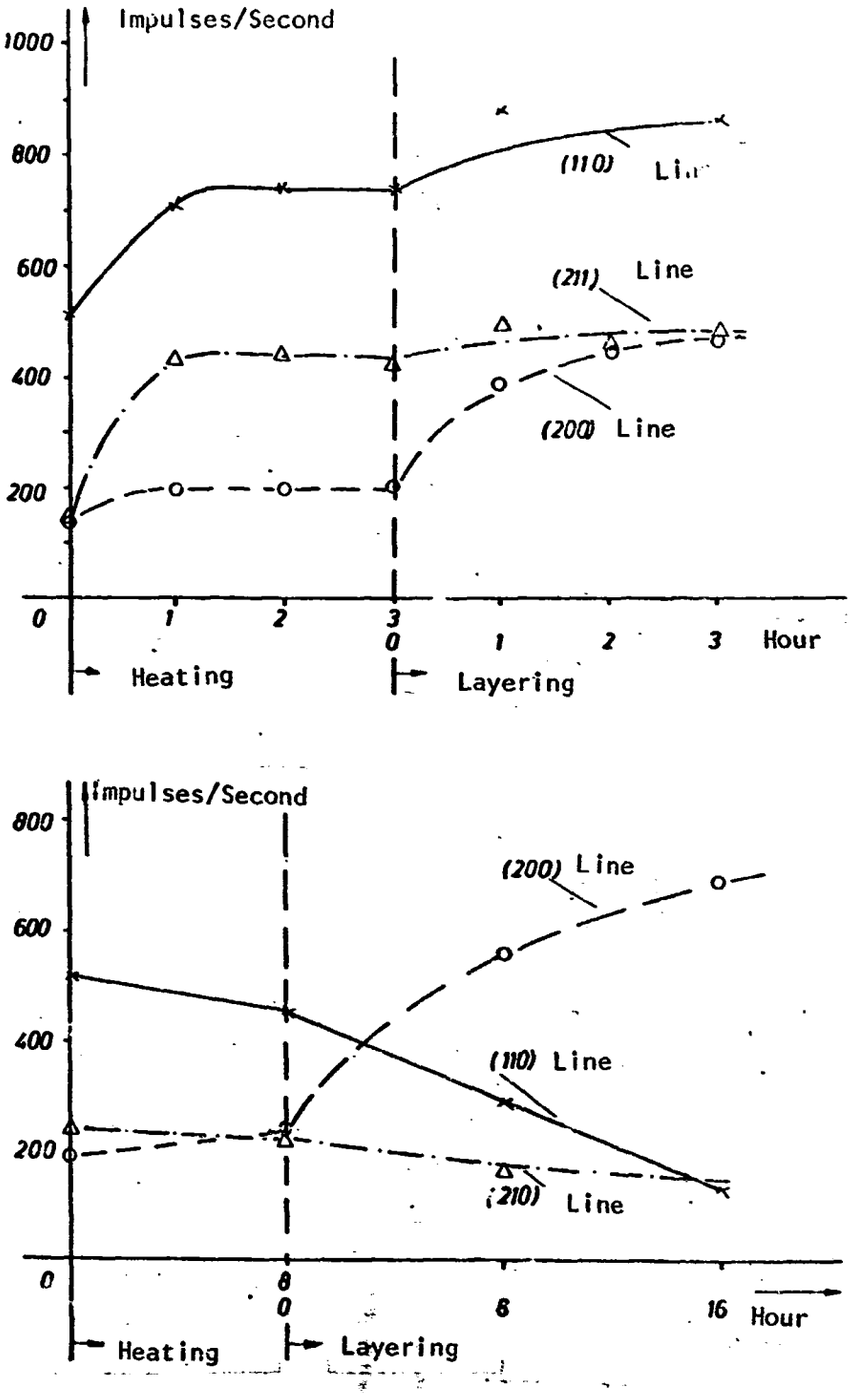

Figure 3.3. Intensity of Individual X-Ray Lines as a Function of Layer Thickness.

The same state of affairs is also noted with respect to the polished sections. The grain boundaries of the molybdenum are taken over by the tungsten when the layering is sufficiently slow.

The grain size distribution in the molybdenum and in the tungsten for various distances from the limiting line are shown in Figure 3.4. The same distributions are found in molybdenum and tungsten in the immediate proximity of the limiting line. The grain size distribution in the tungsten is not changed until the distance from the limiting line increases. The result is even clearer when the average grain diameters are recorded as a function of the distance from the limiting line (Figure 3.5). /49

The epitaxy can be especially well demonstrated when we start with molybdenum samples which have previously been stimulated for recrystallization. In this way we succeed in creating tungsten crystallites of considerable size.

3.1.3.2 The Effect of the Supply of Tungsten Hexacarbonyl

All the effects in section 3.1.3.1 can only be observed when the layering rate does not exceed a certain limiting value. In the case of higher layering rates (direct spraying) the strict epitaxy of the tungsten layer is lost. Simultaneously the structure of the tungsten layers becomes more fine grained.

3.1.3.3 The Effect of Temperature

If the layering is sufficiently slow, no effect of the layering temperature on the grain structure can be detected. If the growth (direct spraying) of the tungsten layer is rapid, completely different conditions will be found.

The grain size distribution in the lower and in the upper layer range of tungsten coatings which were created with a fast layering rate are shown in Figure 3.5. It is recognized immediately that the distribution average values are shifted to higher grain diameters with increasing layering temperature. For purposes of comparison the grain size distribution of an epitatical tungsten layer has also been recorded. The average grain diameters are given over the layering temperature once again in Figure 3.6 to make this clear.

In summary it can be said that the grain structure depends greatly on the layering temperature when the layering rate is rapid. /50

3.1.3.4 The Preferred Orientation of the Deposited Tungsten Layers

It is noted in investigations of the frequency of orientation to prove the epitaxy of the tungsten layers that the (100) orientation provides a tenfold greater contribution to the measurement of the interference line compared to the ASTM value in the layers at hand. Simultaneously, it is found that as the thickness of the layer increases the preferred orientation is more and more pronounced.

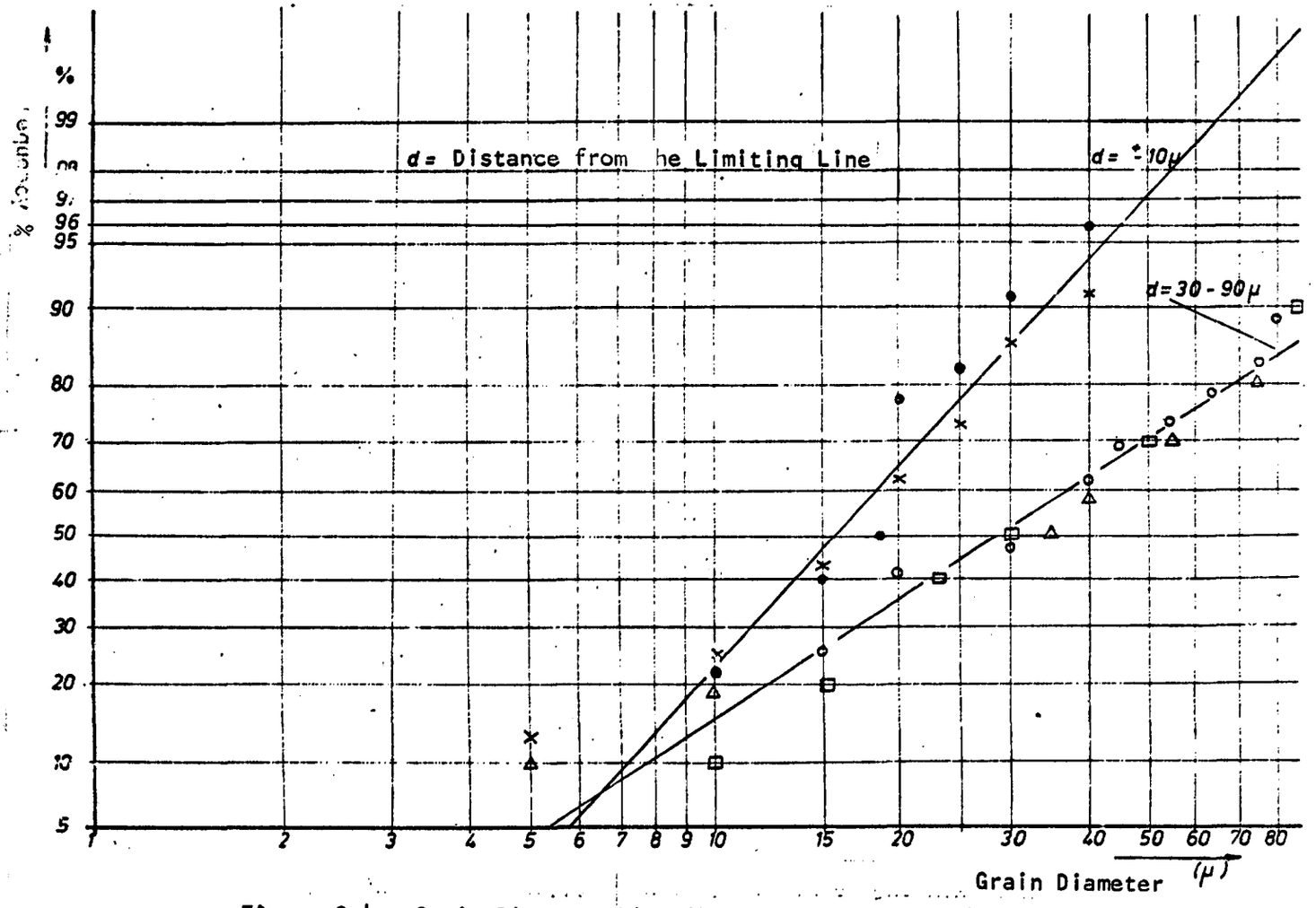

Figure 3.4. Grain Diameter Distribution as a Function of the Layer Thickness when Layering is Slow (1).

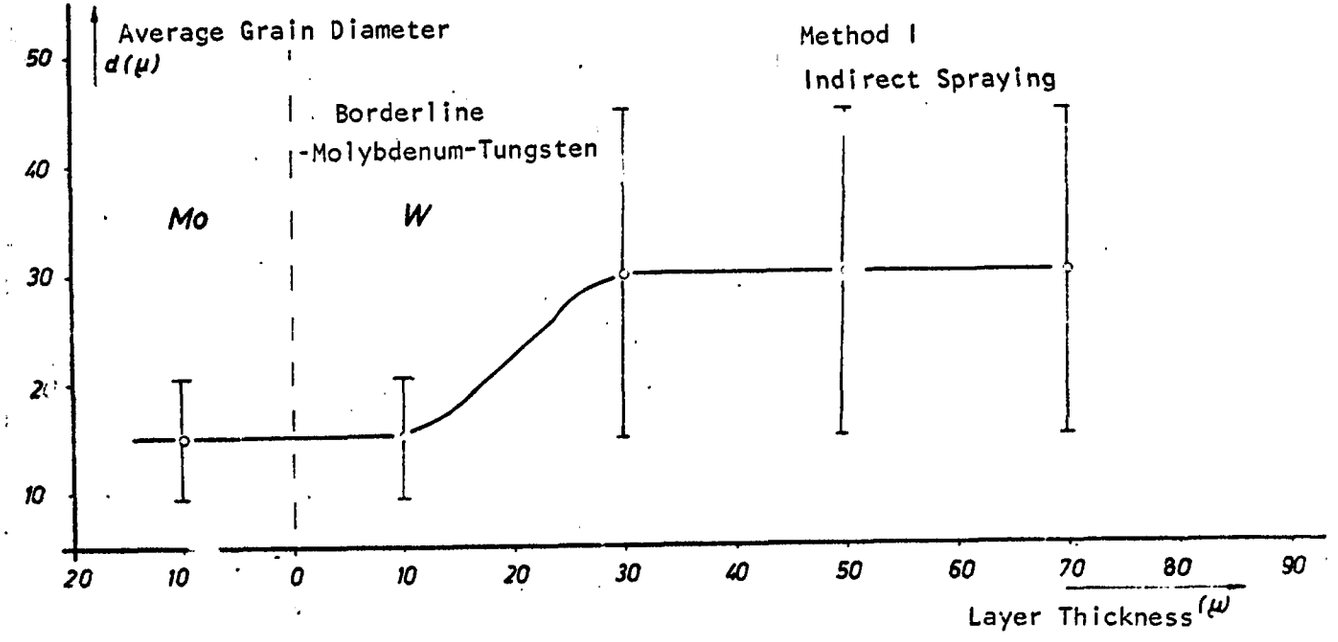

Figure 3.5. Average Grain Diameter in Relation to the Thickness of the Layer.

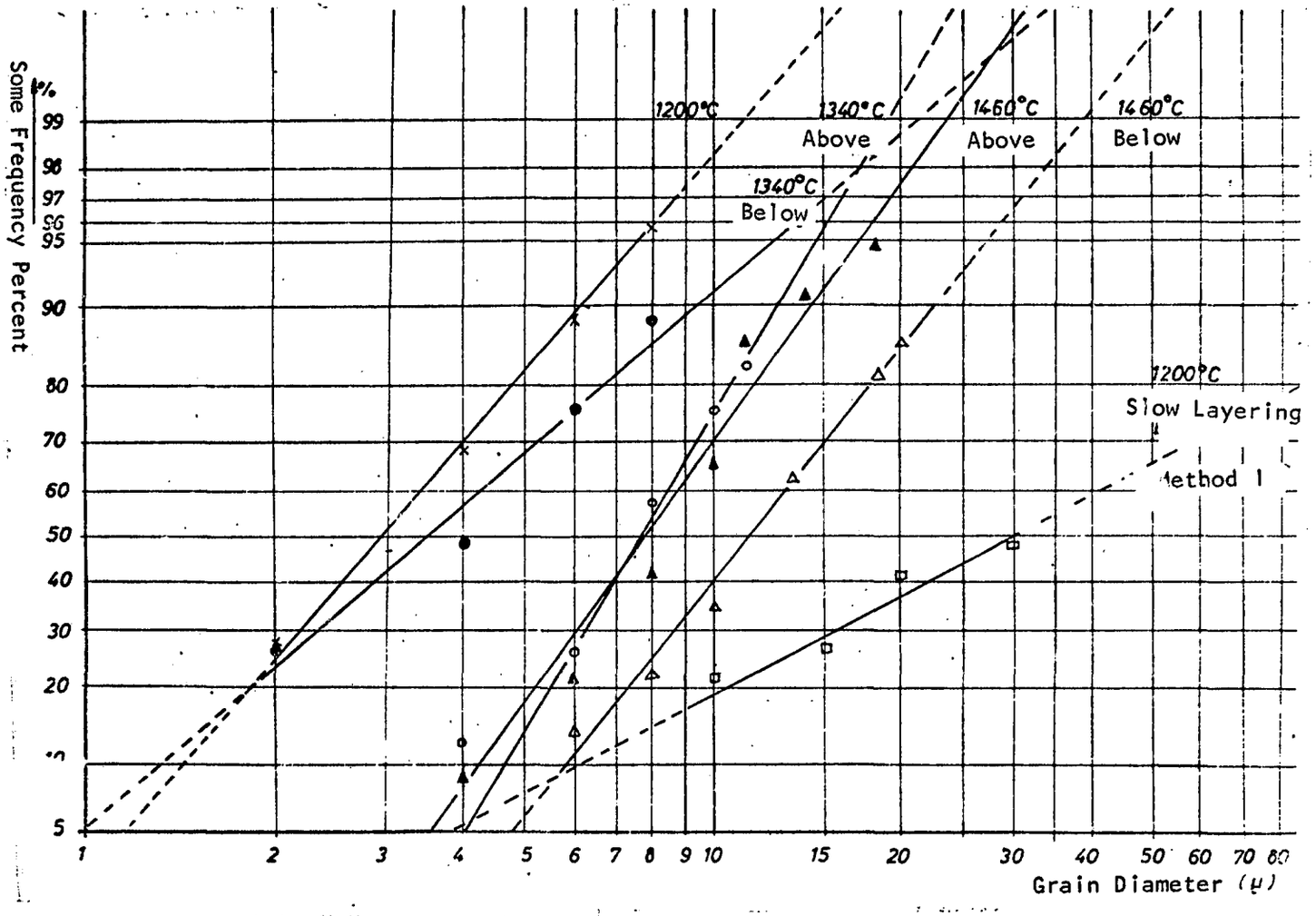

Figure 3.6. Grain Diameter Distribution in Relation to Layering Temperature (Direct Overflow, Constant Suction).

The etching pit method was applied to investigate the preferred orientation and to determine the surface proportion of the (100) crystallite oriented with parallel faces to the surface. A numerical evaluation of the surface proportion is compiled in Table 3.2. The result agrees well with the x-ray measurement. /50

3.1.4 The Physical Process of Layering

3.1.4.1 Model of Crystal Growth

If a tungsten hexacarbonyl molecule strikes the hot metal surface then it is split pyrolytically. The carbon monoxide which is hereby released is volatile while the tungsten atom remains on the surface to be layered. However, it possesses two other degrees of freedom of movement. To be built into the crystal group, the tungsten atom must be accumulated in such a way that the gain in energy is great enough so that the possibility of renewed movement owing to thermal activation of the now built in tungsten atom is slight. This can occur in principle in two ways:

α) The tungsten atom is built in at available growth points of the surface of the metal.

β) The tungston atom loses mobility by combining with a second partner. Simultaneously, the longevity of such a doublet configuration determined by the bonding energy is so large that with sufficient probability a third partner joins in and so forth. In this way, new growth seeds are then formed which then effect the process (α) accordingly. /51

The decision as to whether (α) or (β) is active depends upon the time during which a tungsten atom is free to move on the surface and on the amount of new tungsten atoms joining in per a unit time by means of pyrolysis of tungsten hexacarbonyl.

3.1.4.2 Effect of the Experimental Parameters on the Layer Structure

In the case of indirect spraying, the number of the tungsten hexacarbonyl atoms which are pyrolyzed per a unit time at the surface is relatively small and the movement of the tungsten atoms at 1,200°C is quite high. In this case, only (α) is active. In this way, the available surface structures continue to be formed in this strict manner and also the epitaxy occurring is understood.

In the case of direct spraying and a temperature of about 1200°C, the supply of tungsten in the layering is so high that (β) exclusively is active. If the numbers of growth seeds is formed according to (β) corresponding to the supply of tungsten, then continued growth can proceed in accordance with (α). This explains immediately the observed spiky crystallites. If now in the case of direct spraying the layering temperature is increased, the mobility of the tungsten atoms is higher. The equilibrium concentration of growth points created in accordance with (β), however, decreases and the average

grain diameter of the tungsten crystallites increases as observed (Figure 3.5). Epitaxy as a consequence can also be achieved at higher layering rates in case only the surface mobility of the tungsten atoms depending on the layering temperature is so high that (α) alone is active at the beginning of layering. The (100) preferred orientation forming with increasing thickness of the layer can be explained in the sense of the proposed model by the fact that those crystallites with the greatest probability of inclusion in the structure also continue to be formed the fastest. /52

The problem of controlling the layer structure can as a consequence be solved by following a temperature program during the layering which corresponds to one of the desired structures.

3.2 The Properties of Tungsten Layers Produced in the Vapor Plating Process

3.2.1 Porosity

The electron emitting surface should be free of pores. According to our experimental results, the porosity of the created layers is closely connected with the quality of the initial surface. If we proceed from a dense Mo surface, then the layers are likewise free of pores as has been shown by detailed measurements of density. If we begin with a plasma-sprayed surface, its volume of pores will be largely closed. The covering layer thereby formed is likewise almost closed. If, however, we proceed from a UO_2-Mo cermet surface, then completely different circumstances obtain. At a layering temperature of 1,200°C, the UO_2 accumulated in the surface already evaporates. Simultaneously, thermal stresses occur in the surface caused by the different coefficients of expansion of UO_2 and Mo, and whose relaxation is not excluded. That has as a consequence that the tungsten coating tears up noticeably and the UO_2 evaporates during layering. This can be noted from the often changing proportions in the area of the layer of open and closed pores (Figure 3.8). The total concentration of pores remains almost constant. Microprobe examinations have shown that the evaporating UO_2 precipitates only to a small extent in the cracks of the tungsten layer. The rest evaporates in the containers.

The investigations mentioned in technical literature [20-21] as to uranium losses of thinly layered cermet could accordingly, contrary to the determinations of the authors named, not be explained by diffusion but rather by evaporation. /53

3.2.2 Transpositions, Substructures and Behavior of Recrystallization

As already reported by the author [5], the grain structure of the tungsten layers can be varied in wide ranges--from almost monocrystals to extremely fine-grained layers. Continued investigations have shown that the individual crystallites are largely free from lattice defects, as transpositions

and substructures are. To prove this, an etching pit technique provided by Finke [22] was used. Transposition thicknesses in the order of magnitude of $10^6/cm^2$ were determined for a number of samples. /53

Vapor plating layers are designated as largely stable against recrystallization in technical literature [23]. Our own investigations have largely confirmed this finding for temperatures of 1,600-1,800°C and heating times up to 30 hours. Slight recrystallizations have been observed only with combined plasmas-spray layers with vapor plating covering.

Even if grain boundaries remain uneffected by heat treatments, nevertheless changes in the substructure and transposition net have been observed. The surface of a tungsten layer can be seen in Figure 3.9 enlarged 1,000 times, in which simultaneously etching pits of transposition etchings can be seen before and after a three hour heat treatment at 1,600°C. It can be seen immediately that the transposition thickness has been sharply reduced. A surface which has been treated in a similar fashion shows the same complete healing of a substructure in Figure 3.10. Only a very few etching pits have arisen after heating the washed substructure line which was etched before heating.

In summary it can be said that even if the grain structure of the tungsten layers remains unchanged at the working temperature of thermionic convertors, the transposition net and the substructures, however, are reduced. /54

3.2.3 Chemical Investigations

Spectrographic surface investigations have revealed the following impurities in small amounts:

Al, C, Ca, Fe, Mg, Mo, Si

A quantitative evaluation was not possible since tungsten calibration standards are not available.

Mo and C are specific impurities. The Mo may have arrived at the surface of the sample through diffusion from the base. C likewise stems from the Mo base. Noss-chemical investigations have revealed that the basic material contai. bout 200 ppm C. When the layering is slow, the C is even removed from the basic material by means of the Boudoard reaction. When the layering is rapid, the C concentration remains about the same.

3.3 Diffusion in the Mo W System at the Operating Temperature of the Thermionic Convertor

3.3.1 Statement of the Problem

Essentially two requirements have to be made of the tungsten layer.

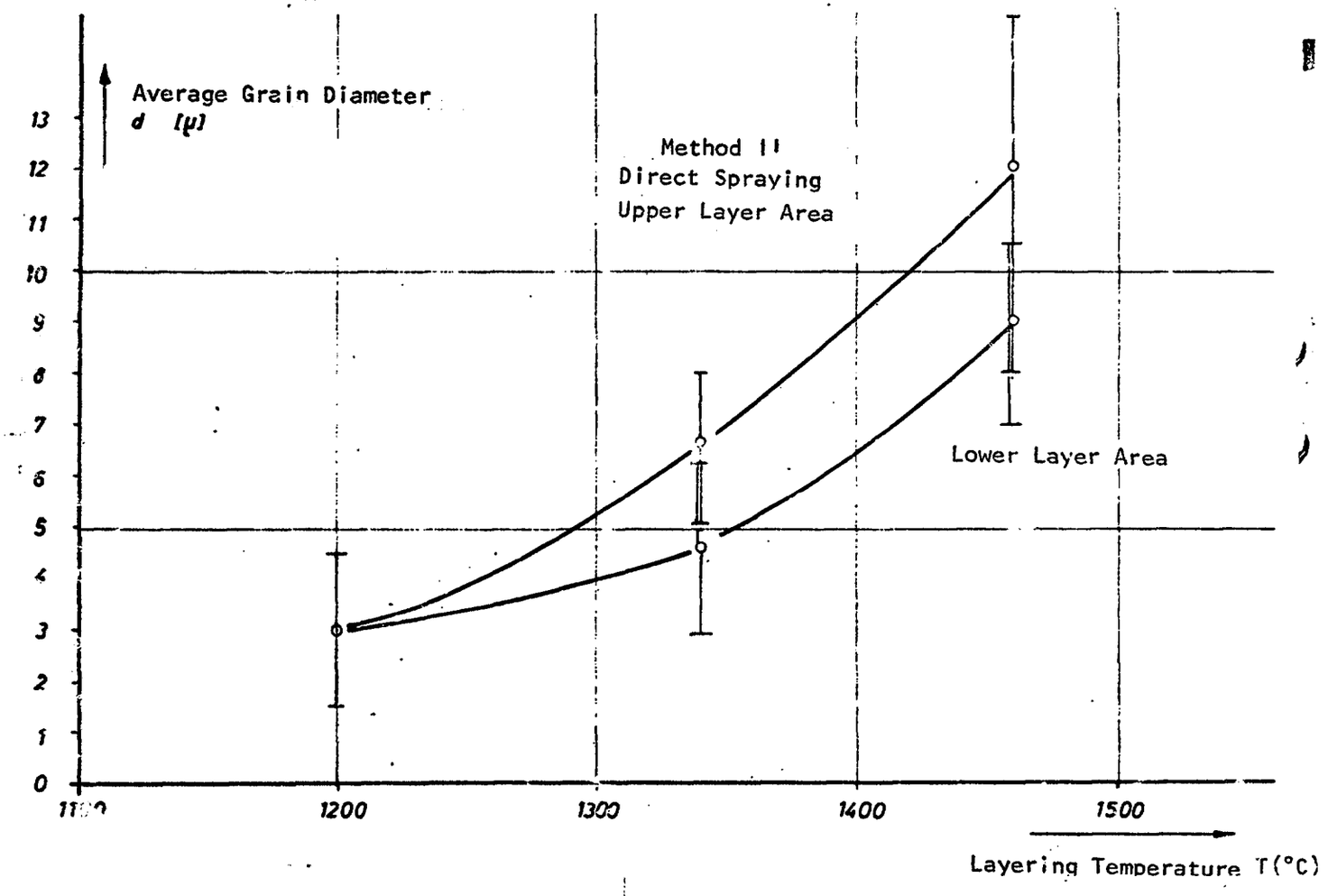

Figure 3.7. Average Grain Diameter in Relation to the Layering Temperature.

/105

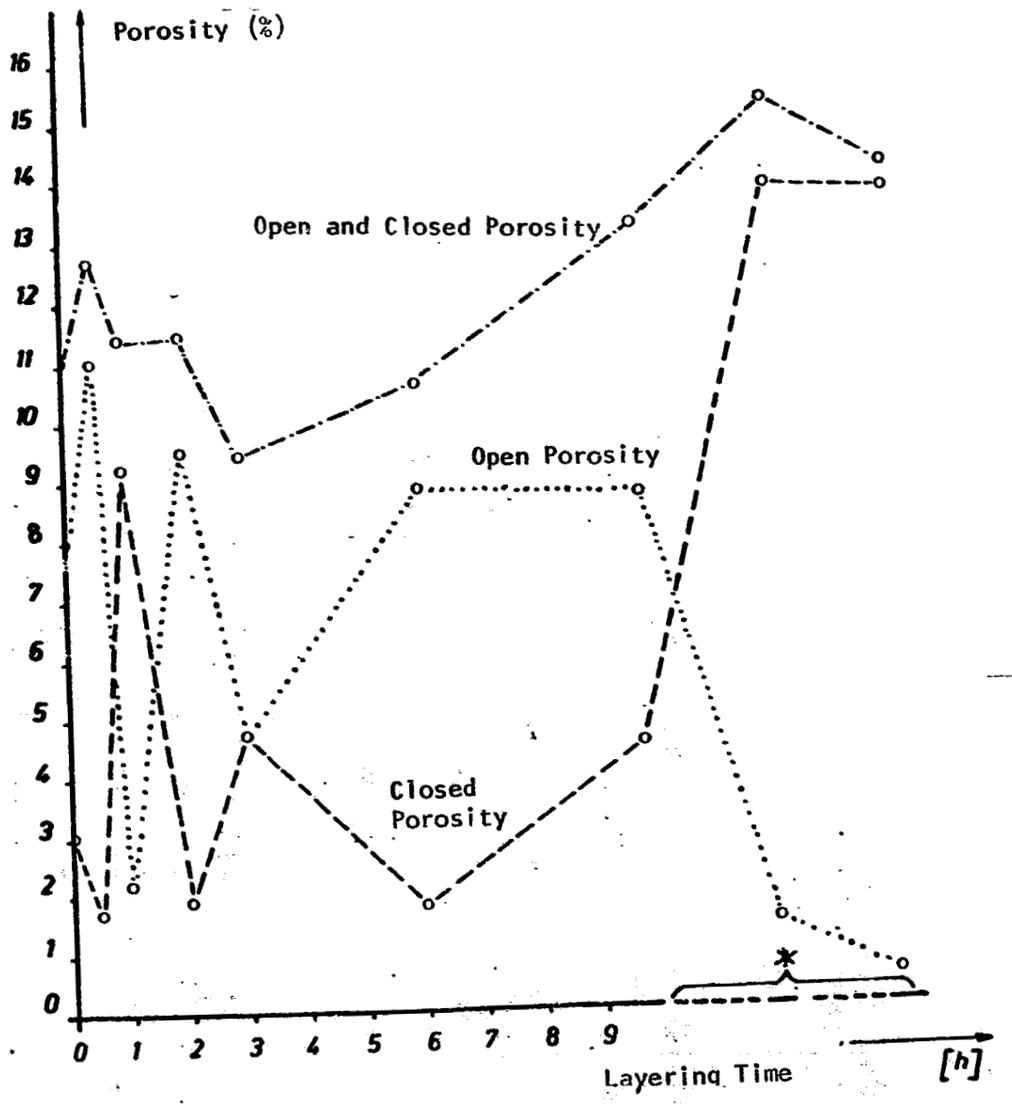

Figure 3.8. Behavior of the Open or Closed Porosity in Layering.

/106

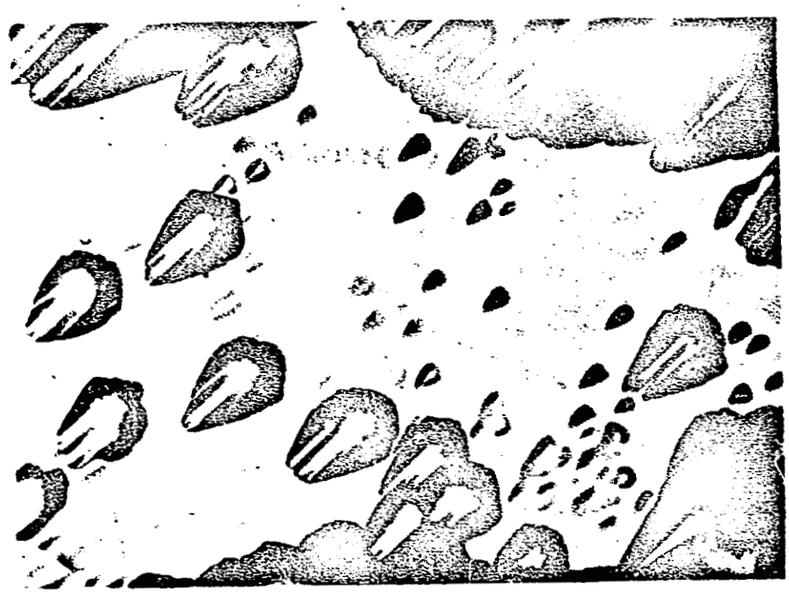

Figure 3.9. W Surface with Etching Pits Enlarged 1,000 Times.

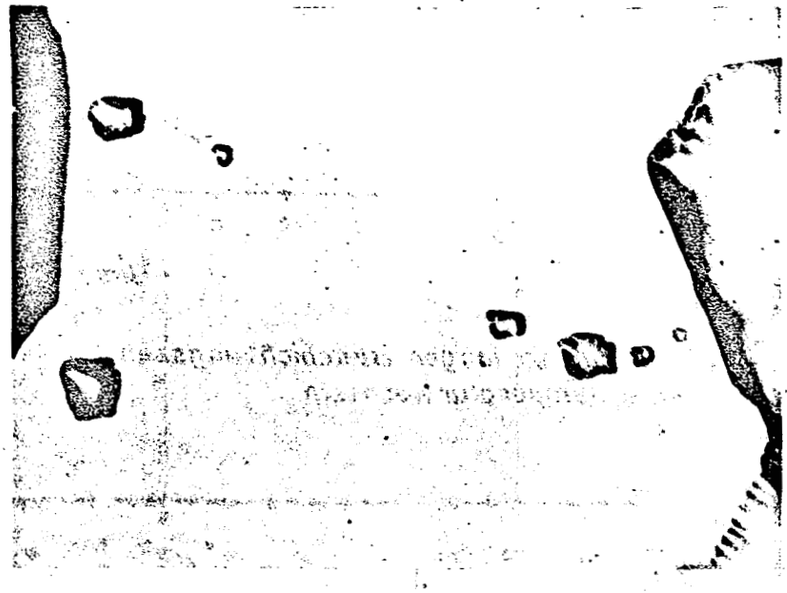

Figure 3.10. W Surface with Etching Pits.

α) The tungsten layer must be so thin that it is not too strongly influenced by the neutron-physical behavior of a combustion cathode. /54

β) The tungsten layer must be so thick that neither uranium from the UO_2 nor the Mo from the base arrive in admissible amounts at the surface of the cathode at an operating temperature of 2,000°K.

To fulfill requirement α), the tungsten layer should not be thicker than 0.2 mm so far as possible. Pure, cohesive tungsten layers are sufficient barriers to diffusion against uranium from UO_2 [24]. The question as to which layer thicknesses are necessary in order to prevent an inadmissible entry of Mo up to the surface of the cathode was the subject of the following written investigation. /55

3.3.2 Experimental

The tungsten layers were placed on Mo according to the "vapor plating" described in 3.2. The ceramic intermediate layers were placed on using the plasma spray method. The protective gas box used for this and the spray parameters are described in detail in section 5.3.

Heating was carried out in a vacuum at 10^{-5} to 10^{-6} mm Hg pressure. The samples were partially brought to temperature hanging in an HF conductor with an Mo wire, and partly heated in a resistance-heated Ta furnace.

The temperatures were measured pyrometrically. The absorption at the glass disks of the container were measured separately and the measured values were corrected accordingly. The spectroemission capability was taken from appropriate tables. The accuracy of the temperature indication should come to ±30°C.

3.3.3 Experimental Results

A survey of the experiments carried can be seen in Table 3.3. The tungsten layer in the experiments 1-5 has grown epitatically on the Mo substratum. The tungsten layer thickness was about 50-60/μ in the initial condition. With progressive heating time at 1,750°C, the layer became increasingly thinner owing to the effects of diffusion as can be seen from Table 3.3. The limiting line Mo-W is shifted clearly in the direction of tungsten. Microhardness measurements show that the limiting line Mo-W which was originally defined so sharply has been expanded to a clearly measurable transition range (Figure 3.11). The microhardness measurements are augmented and confirmed by microprobe measurements for a heating period of eight hours.

In so doing, the microprobe furnishes a narrower transition range than the microhardness measurement. This is understandable when it is considered that the microhardness in general is an essentially finer indicator than the microprobe measurement. /56

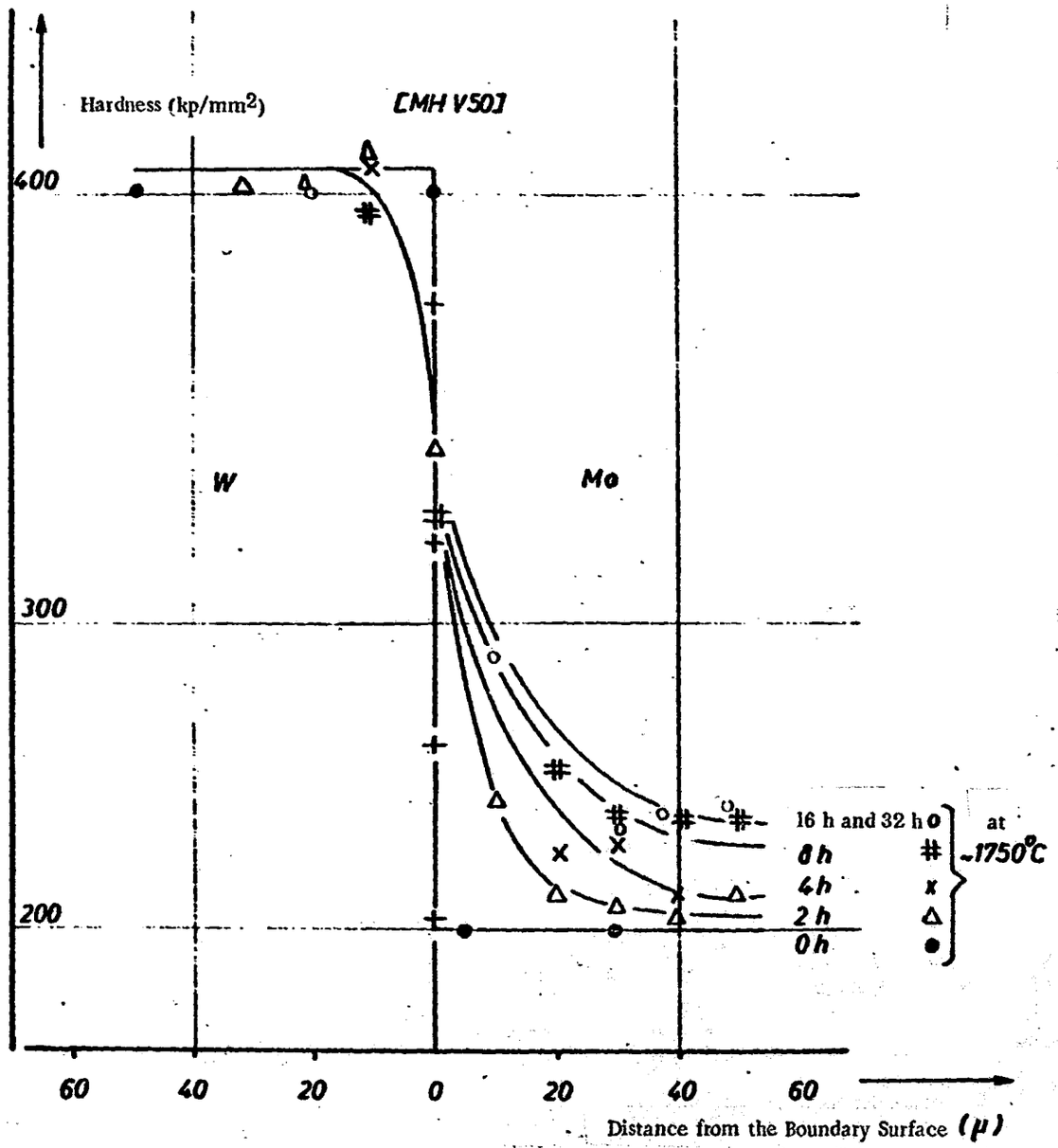

Figure 3.11. Effect of a Heat Treatment on the Curve of the Hardness Profile in the Transition W-Mo.

The study of Mo-W diffusion carried out on samples in which the epitaxy is strongly disturbed or even generally avoided produces completely different results. /56

Sample number 6 was layered relatively quickly so that the tungsten possesses a completely different structure than the molybdenum target (see also section 3.1). As a consequence, the transition Mo-W is considerably distorted and marked by a grain boundary. After 75 hours at 1,830°C, no reduction of the thickness of the layer can be seen in the polished section. Microprobe measurements show that the tungsten and molybdenum diffusion is sharply reduced compared to samples with epitactic transitions. A volume and grain boundary diffusion of the molybdenum is clearly to be distinguished in the tungsten. A grain boundary diffusion reaches into the material at a maximum of 40/μ, and the volume diffusion 15/μ.

Even better results have been provided by sample number 7. The Mo surface in this case was covered by a 30/μ thick and strongly porous Al_2O_3 layer. The remaining pores were filled with tungsten by vapor plating and finally the whole covering layer was coated with tungsten (Figure 3.12). In so doing, the remaining metal canals permeating the Al_2O_3 maintain a satisfactory conductivity, but represent an obstruction for diffusion. Before and after diffusion heating at 1,830°C for 75 hours, visually observed and determined by microhardness, no change of the tungsten layer thickness could be detected. Microprobe investigations revealed that in the case considered no volume diffusion of Mo into W can be found, however, a slight grain boundary diffusion is found. In addition, traces of Mo can be found in the boundary layer W-Al_2O_3. However, a very slight volume diffusion of tungsten appears to be found in the molybdenum.

It can be said in summary that diffusion in the Mo-W system at 1,830°C strongly depends upon the formation of the Mo-W transition. Epitactic transitions permit a massive volume diffusion.

If the transitions are marked by a grain boundary, then the volume diffusion is sharply reduced. Only the grain boundary diffusion is then noticeable. Samples with disturbed Mo-W transitions have a significantly smaller penetration rate even at fairly long heating periods and higher temperatures than those with epitactic border zones. /57

3.3.4 Determination of the Diffusion Coefficients

The diffusion profile of the volume diffusion C = C(x, t) was measured with the microprobe for experiment number 3.. Crank [25] determined from this the diffusion coefficients of the Mo-W system in the following way:

$$D(C_1) = -\frac{1}{2t}\left(\frac{dx}{dC}\right) \Big/ \int_{C_0}^{C_1} (x - x_0)\, dC \qquad (3.1)$$

$C = C_1$

/108

Figure 3.12. W Emitter Layer with Ceramic Intermediate Layer.

The point $x_0 = 0$ can be determined from the curve C = C(x) by the following equation: /57

$$\int_{C=0}^{C=1} (x - x_0)\, dC = 0 \qquad (3.2)$$

To evaluate this, the value dx/dC can be graphically determined after a certain experimental time from the experimentally determined C = C(x). In the present case the tangents were determined with the mirror straightedge. All necessary integrations were carried out numerically with a polar planimeter.

The diffusion profile C = C(x) determined with the microprobe for the heat experiment at t = 8h and at 1,750°C was evaluated in accordance with the manner already described. The result is presented in Figure 3.3.

The diffusion coefficients determined by Kalinowitsch, et al, [27] for several special binary Mo-W alloys in the temperature range observed agree well with the curve of D = D(C) measured by us for Mo and W.

3.3.5 Solution of the Diffusion Equation for Concentration-Dependent Diffusion Coefficients and Time Extrapolation of the Results /58

The result of the previous section 3.3.5 shows that the volume diffusion coefficients of W in Mo and Mo in W depend greatly on their concentration in

one another. An exact solution of the differential equation for the differential equation of two media with concentration-dependent diffusion coefficients which stand in contact in the form of two semi-planes extended to infinity, does not exist.

One can attempt in the first approximation to utilize the solution for the problem with concentration-independent coefficients by using only average values. This approximation gives a very defective reflection of the actual curve C = C(x, t). Compared to the measured profiles, the calculated profiles are too broad.

Fujita-Yamada [26] gives the approximate solution in the form of a polynomial of the third order with respect to local coordinates:

$$C(x,t) = (\alpha\beta - 3/2)\left\{x\sqrt{\frac{\beta}{D_0 t}} - 1\right\}^2 + (\alpha\beta - 5/2)\left\{x\sqrt{\frac{\beta}{D_0 t}} - 1\right\}^3 \qquad (3.3)$$

between: $C = C_{max} = 1$

and: $C = 0$

Thus for D = D(C) the beginning is made:

$$D = D_0 F(C) \qquad (3.4)$$

The concentration dependence is introduced through the constants α and β:

$$\alpha = 30\int_0^1 F(C)\,dC \qquad (3.5)$$

β is determined as a solution of the following quadratic equation

$$24\alpha\beta^2 F(1) + (\alpha - 108 F(1))\beta + 3/2 = 0 \qquad (3.6)$$

The larger of the two roots should be used in this case. /59

This formalism was evaluated for the present case D = D(C) in accordance with Figure 3.13 for Mo in W. All necessary integrations were carried out graphically.

The approximation polynomial is only observed between the points C = 1 and C = 0. Theoretically, C(x, t) is 0 for t only for the case x = ±1 or 0, while the approximation polynomial already achieves these values at infinity. The approximation polynomial as a consequence interpolates the actual curve of

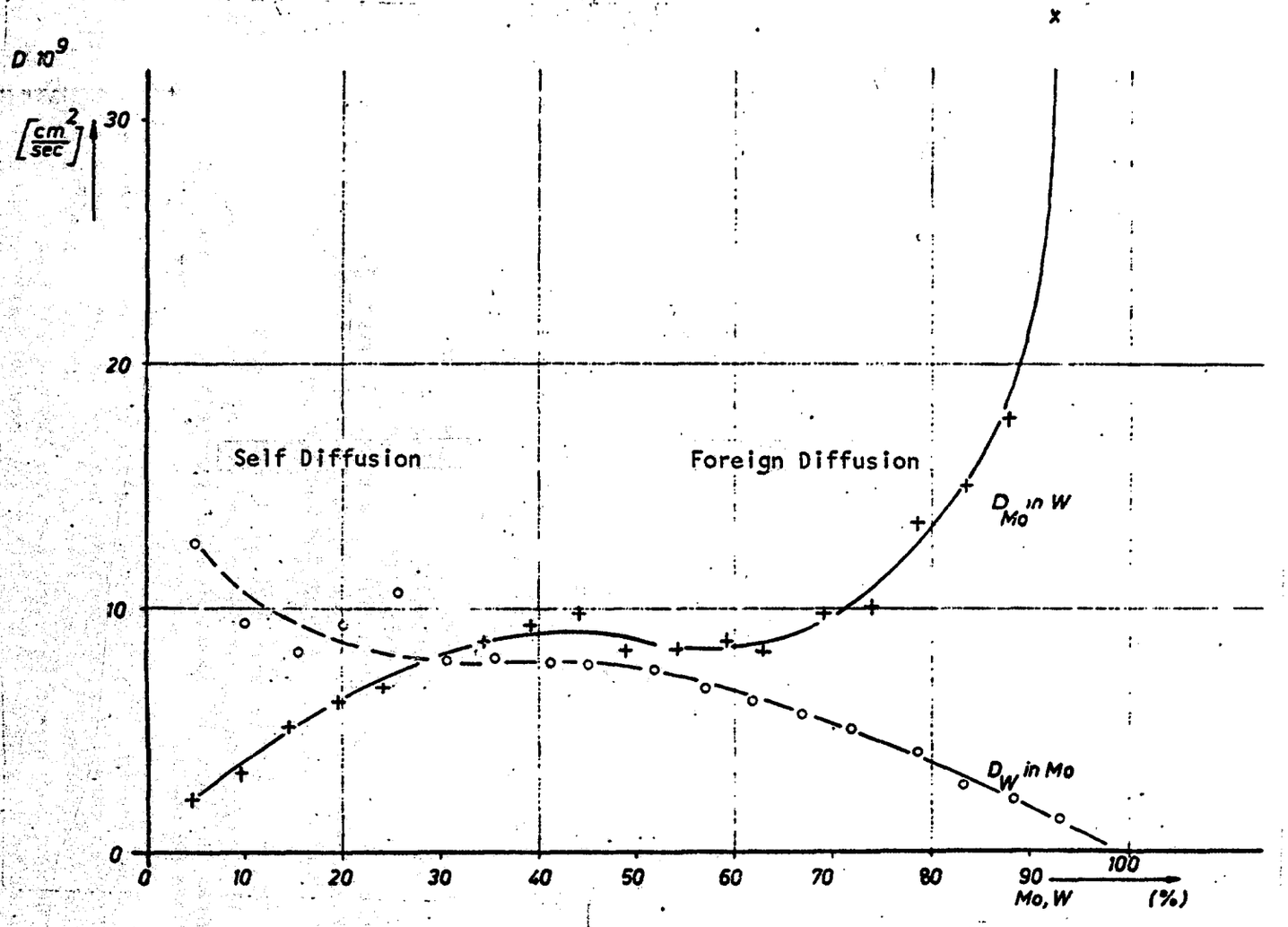

Figure 3.13. Diffusion Coefficient in the MoW System at 1,750°C.

C(x, t) only within a definate range. The points C = 1 and C = 0 of the polynomial should therefore in the present case be interpreted as those places at which the foreign atom concentration reaches noticeable values. The exit potential of the surfaces can for example be an indicator. /59

The diffusion profile widths--in the sense just defined--as they were calculated with the determined diffusion coefficients D = D(C) are given in Table 3.4 by 10^0-10^4h for a heating temperature of 1,750°C.

It is noticeable that even here the calculator profiles are somewhat broader than the measured ones. There are three reasons for this:

α) The present solution is an approximation solution.

β) The microprobe measurement has a detection limit of 1 at%, and as a result only a part of the diffusion profile is detected with it.

δ) The experimental conditions are only a rough approximation for the theoretical case of two semi-planes extended to infinity.

It must be pointed out at this time that these results are only applicable for an epitactic transition Mo-W. In order to describe the diffusion completely one must also consider the effect of the border layer which--as our experiments have shown--is of considerable influence besides taking into account the diffusion coefficients. This may perhaps happen owing to a separated permeability coefficient of the border layer. This can only be neglected in the case of epitactic border zones. /60

3.3.6 Conclusion and Alternative

As the above considerations and measurements have shown, epitactic tungsten layers during the planned utilization time of the thermionic convertors of about two years are only impervious to molybdenum if the layer thickness is of the order of magnitude of centimeters. Schuster [21] came to similar conclusions. However, as was mentioned initially, tungsten layer thicknesses of only about 0.2 mm are desired for neutron-physical reasons.

A diffusion obstacle between Mo and W could be a way out of this problem. Metallic diffusion barriers can first of all be considered for this, e.g. at a layer thickness of about 50/μ irregardless of what material was placed between Mo and W.

Assuming that the diffusion coefficients of Mo are independent of concentration in material X, an estimation as to the magnitude of the necessary diffusion coefficients was made when the layer was to be made impervious for molybdenum for operating times between 10^0 and 10^4 hours. The result of the estimation is that $D.t < 10^{-10}cm^2$. The same values for the diffusioned coefficients of material X in tungsten or molybdenum must also be assumed if no impurity of the emitter is permitted with blocking-layer atoms or so that the

blocking layer does not disappear into the molybdenum by diffusion. Likewise, no formation of brittle, inter-metallic phases can take place.

Metallic materials which meet all these requirements and which additionally can be utilized at ?,000°K are not known. If, for example, Re is placed between Mo and W, then very quickly an inter-metallic phase is formed whose thickness increases quite rapidly.

The problem consequently cannot be solved with metallic diffusion blocks. /61
On the basis of our investigations, however, it is suggested that the problem may be solved by a corresponding disturbance of the border zone Mo-W which leads to a smaller permeability of the transition. This can be achieved by a thin porous ceramic intermediate layer. Layers produced in such a way have offered a substantially more favorable picture at a temperature around 100° higher and a longer heating time than in the case of those with a very high coefficient of permeability in the limiting zone. Continuing experiments in this matter are planned.

4. Combining Technology

/62

4.1 Statement of the Problem

In principle the solution of the series connection of several convertor cells worked out at that time is given in Figure 1.1. The operating temperature of the combination bridge-emitter comes to about 1,730°C. The electrical transition resistance of the bridge-emitter in this case should be as small as possible. The combination bridge-anode possesses a temperature of 700°-800°C and must be vacuum tight in order to avoid the penetration of Cs into the ceramic insulation at the sleeve surface. The combination of the anode parts among one another is necessary in the course of installation, and vacuum tightness is also required here above all. Table 5.1 provides information on the material pairs under discussion.

4.2 Diffusion Bonding

The technique of diffusion bonding has been often mentioned in american technical literature [28-31]. By diffusion bonding we understand the combining of two metals with the application of pressure at high temperature without the appearance of liquid phases. At high temperature, the surfaces are brought into close contact by means of the applied pressure so that then a diffusion can take place along the whole border line and thereby a bonding can take place.

In the experiments described below, all samples were heated to about 1,600°C in a vacuum of about 10^{-5} mm Hg pressure. The applied pressure was about 1-2 kilogram force/cm^2. Heating was effected with a heat inductor and the temperature measurement was carried out with a pyrolyter.

It was determined in a series of pre-experiments that metal surfaces cleaned and polished on the finest paper (grain size 600) led to a good

bonding. Etching of the services does not lead to essentially better results.

Table 5.2 gives a survey of the experiments carried out. All th possible metal pairs which could come about in the thermionic convertor were tested here. /63

Good Nb-Nb connections are obtained without noticeable original line of separation after a bonding time of about two hours. After one hour the separation line is still recognizable, and one-half hour of bonding time leads to an imperfect connection. The area of the original separation line is a volume of high lattice-defect density after joining. After a careful transposition etching it can be seen that many etching pits have formed in the area of the separation line. This knowledge is in principle to be transferred to all diffusion bonding connections.

The connection Nb-Mo takes place essentially more rapidly than Nb-Nb, and even after a half hour the original separation line can no longer be recognized. This is also immediately understandable when it is recognized that not only the self diffusion is active here at the boundary surface--such as in the case of Nb-Nb--but rather a diffusion along the concentration gradient of Nb-Mo. An extension of the bonding time does not show any improvement in the connection.

Essentially the same results are reported for the connection Nb-W as for Nb-Mo. The original separation line is usually only still recognizable by the stage which results during the preparation.

The connection Mo-Mo takes place much more slowly than all the other combinations described so far. After three hours, the original separation line has still not closed. Not until four hours bonding time have passed does a satisfactory combination take place. There are two reasons to be named for this: one is that Mo is much less plastic than Nb so that a close contact of the two surfaces takes place much more slowly, and the other is that here there is no gradient requiring diffusion--similar to the case of Nb-Nb, and as a consequence there is no active self diffusion.

After two hours a satisfactory combination takes place between Mo and W. W-W could not be combined with the bonding technique. The temperatures achieved were too low. /64

In summary it can be said that diffusion bonding led to satisfactory combinations in the case of almost all the interesting pairings. Combining two pieces of the same metal takes place much more slowly than when the pieces are of different metal. Brittle phases do not occur in the diffusion zones since the refractory metals all mix completely.

4.3 Electron Beam Welding[1]

Besides diffusion bonding for combinations in the area of collector-bridge-emitter transition, there is still the technology of e-electron welding. In case Nb bridges are used, collector and bridge are manufactured from a part as described in the present report. There are then four combination tasks which remain:

4.3.1 Welding Mo Bridges of 0.1 and 0.3 mm Thickness to the Collector

4.3.2 Welding Mo Bridges 0.3 mm in Thickness to Mo Emitters Coated with Tungsten

4.3.3 Welding Nb Bridges of 0.24 mm Thickness to UO_2-Mo Cermets

4.3.4 Welding Nb Collector Parts to One Another (1 and 2 mm Wall Thickness)

The proper welding seam types are given in Figure 4.1.

In Reference to 4.3.1: Bridge of 0.3 mm Thickness

The seam type 1 creates a good combination with average welding output and focused e-beam. As a consequence of the surfaced tension, the welding edge is round. The melting zone is of sufficient width. If the combinations are heated at 800° or 1,700°C, the brittleness of the seam is removed. Less recrystallization occurs in the area of the melting zone than in the basic materials. /65

In Reference to 4.3.1: Bridge of 0.1 mm Thickness

If seam 1 is welded here, the Mo sheet of 0.1 mm thickness is bent by the Nb owing to local heating and the thermal tension caused thereby. For these reasons, we went over to seam type 3. In order to avoid heat gradients which are too strong, the piece was fanned with the welding beam. Aside from the brittleness which occurs, a good combination takes place in this way. The brittleness can then be removed by tempering above 1,000°C. The seam surface is spherical. Some pores occur in the welding zone.

In Reference to 4.3.2:

The welding here leads to a good connection only in the case of seam type 4 and with a supreme welding output. The tungsten layer is completely broken through here and the tungsten uniformly distributed in the melted zone, as

---

[1] The experiments were carried out partly in the Institute for Nuclear Energy of the Technical Hochschule in Stuttgart and at this place we expressed our thanks to the Director of the Institute, Professor Doctor Hoecker and colleagues.

micro-hardness measurements show. That means that the tungsten diffusion blocking layer is destroyed after the welding.

In Reference to 4.3.3:

The high proportion of ceramic of 30% by volume of UO_2 in the cermet leads to the fact that the e-beam does not heat the joining point with any uniformity. At the same, the UO_2 evaporates and leaves pores behind. The junction between Mo and cermet only takes place by means of a few metal bridges. The result is totally unsatisfactory.

With Reference to 4.3.4:

After several pre-experiments it was shown that the Nb pipe with walls 1.2 mm thick could be welded together quite well with an easily de-focused e-beam with a medium welding output. If the beam selected is too great, the welding zone will be too wide and the seam sags somewhat. With Nb pipes having a wall thickness of 2 mm, however, the acceleration voltage of 150 kV does not suffice in order to permit the e-beam to completely permeate the material. If the beam current is now increased, the welding depth can be increased to 2 mm. In this case, however, the welding sample during welding is heated red hot. In welding with constant beam, the welding depth is therefore a function of the preheating time. Samples which were not thoroughly welded at the beginning of the welding process therefore show a breakthrough of the seam at the end of the welding. /66

In summary it can be said that actually useable junctions can only be achieved with the welding of 0.1 mm and 0.3 mm thick Mo sheet with the Nb collector and in welding the Nb anodes with 1.2 mm wall thickness. The great disadvantage of the first case is that the melting zones become spherical as a consequence of the surface tension and the knots sometimes have to be redone, in which case difficulties can be expected because of the embrittlement of the molybdenum. The brittleness can, however, be removed by a subsequent heat treatment, which points to a brittleness caused by tensions which arose during welding. The tungsten layer is destroyed when joining Mo bridges with Mo cathodes coated with tungsten. The welding of Mo with cermet is unsatisfactory.

4.4 Argon Arc Welding

The results of the argon arc seam type 1 approximately correspond to those of the e-beam seams 1-3. The outer formation of the seam is about the same. Here, too, melting edges have becomes round as a consequence of surface tension. The welding areas are, however, as can be seen from the polished sections, larger than is the case for e-beam seams. The areas of brittleness which occur are therefore even greater. In contrast to the e-beam seam, the argon arc seams are porous.

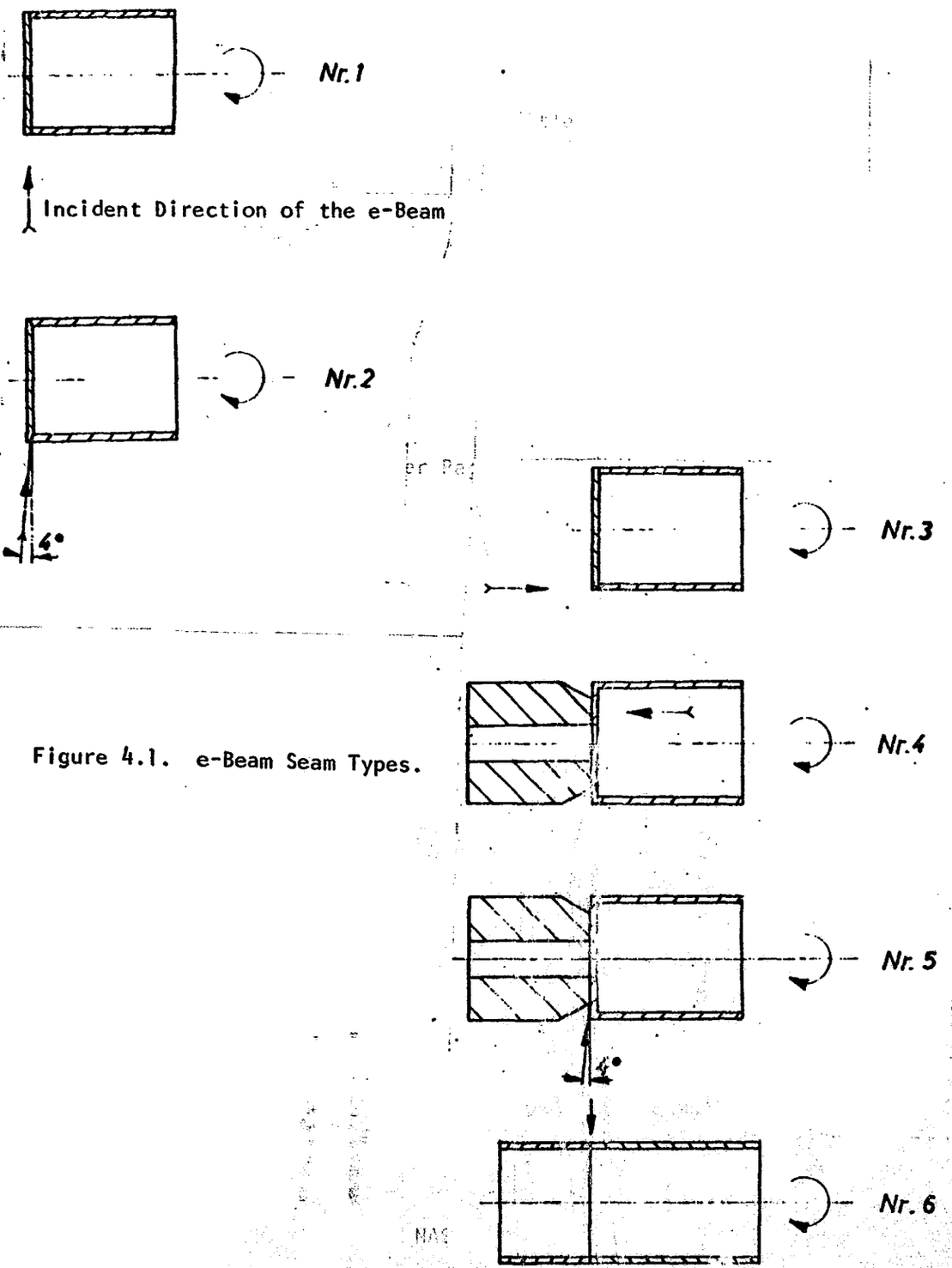

Figure 4.1. e-Beam Seam Types.

/111

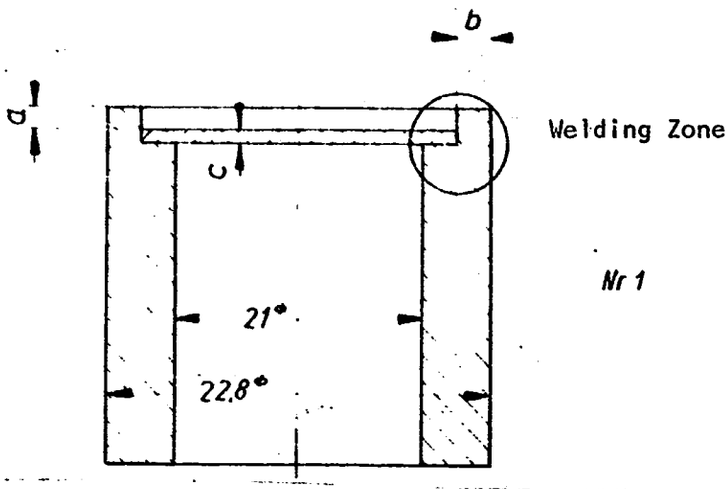

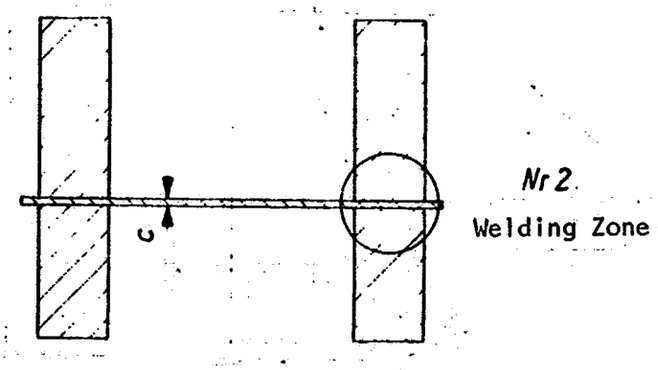

Figure 4.2. Argon-Arc Seam Types.

/112

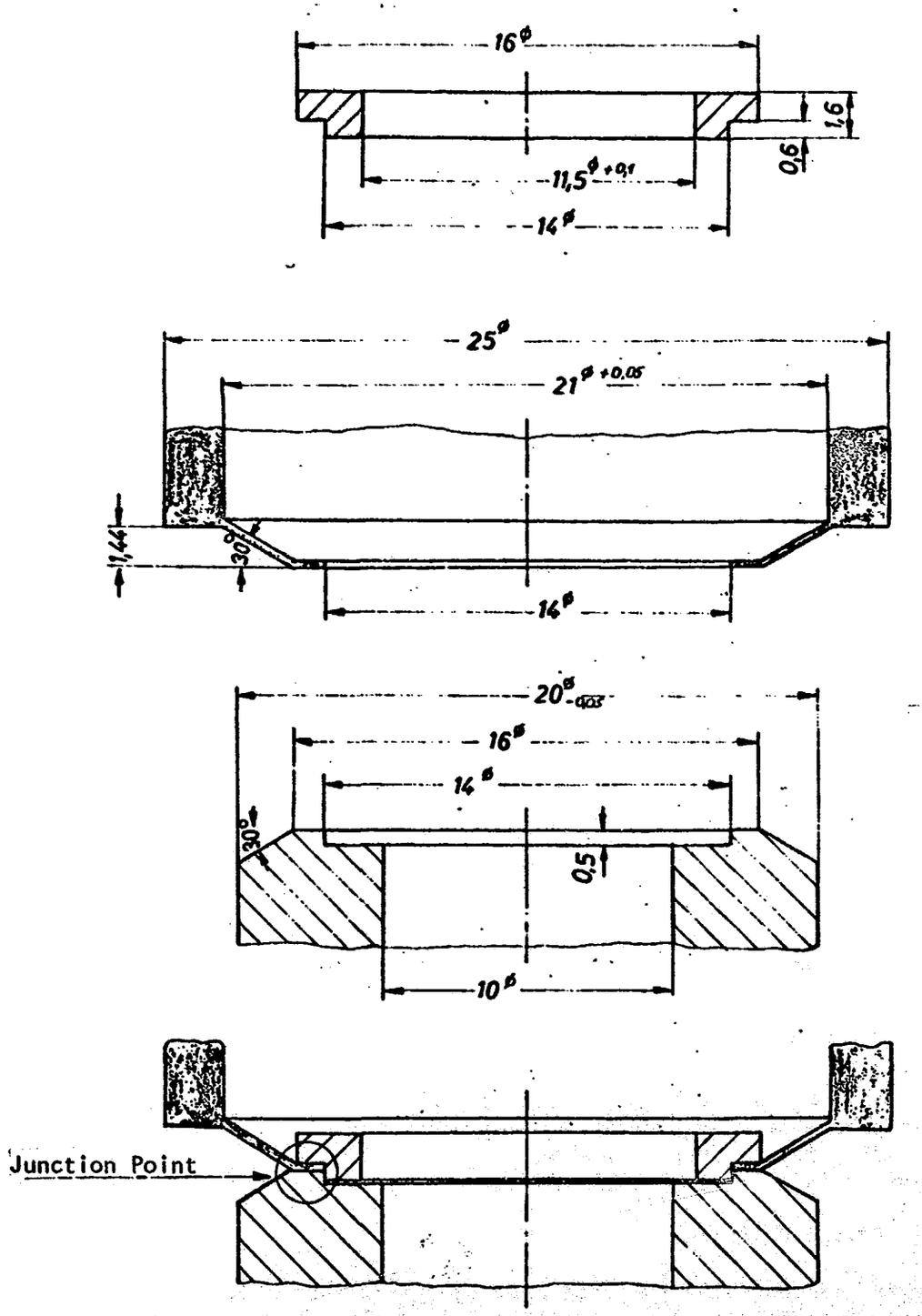

Figure 4.3. Transition Cathode-Bridge.

In planning seam type 2, we proceeded from the experience that the seams are drawn round owing to the surface tension and therefore a subsequent processing is necessary. In order to facilitate this subsequent processing, the membrane between the two pipe sections is welded in. A layer processing of the seam is therefore always possible. With respect to the embrittlement during welding, the same results are found here as in the case of seam type 1. /67
The outer formation of seam 2 is very good, but unfortunately even here pores of considerable size occur.

In summary it can said that seam 2 produces a satisfactory welding when viewed macroscopically. Seen microscopically, the argon arc welding is in any case not satisfactory because of the pores which occur. In addition, during welding problems of the purity of the protective gas occur since all samples showed an oxide coating in the area of the welding zone.

4.5 Selection of the Joining Technologies

From the joining possibilities described in section 3, those which will be applied are selected from two points of view: 1) best possible junctions of the parts one to another; 2) in corporation of the joining process in the assembly of the thermionic combustion element.

4.5.1 Emitter-Bridge

The diffusion bonding method is best suited for joining the thin series-connection bridge with the massive emitter. In a transition from the principle test to the original junction, difficulties were first encountered by centering and uniform transfer of force.

The latter could be avoided by formation of the junction point as shown in Figure 4.3. The centering ring here fulfills three tasks:

α) Centering and holding the bridge.

β) Uniform transfer of force for creation of a uniform applied pressure.

δ) Limitation of the junction surfaces for avoiding forces which are too high in bonding.

With the rupture of junctions produced in such a way, the bridge ruptures /68
either simultaneously with the loosening of the bonding junction or earlier. The tearing forces which can lead to rupture are about 180-200 kg force when the bridge is made of niobium and the emitter surface of molybdenum.

4.5.2 Bridge-Collector

For all practical purposes only the diffusion bonding technique of all the tested technologies is available for joining the bridge to the collector. Since, however, collector and bridge are made of niobium, no attempt was made

to join the components by diffusion bonding and both parts were made of one piece. The manufacture of the collector-bridge part was undertaken as follows (Figure 4.5): /68

The bridge is drawn from the pipe-shaped collector, whereby at first the angle between bridge and pipe axis is 90°. In a second operational stage, the bridge is then ground down to the required wall thickness. There the angle between bridge and axis of the pipe is reduced to 60° by means of a cupping process in a specially prepared tool. The holes required for entry of the Cs are bored in a boring device in a final work process.

4.5.3 Collector-Collector

The collector pieces are welded by an e-beam, where a 100% thorough welding is dispensed with with the thicker anodes (2 mm wall thickness). The welding seam is then arranged in a design so that it must only conduct about 50% of the cell current. This can be achieved simply by having the seam arranged about in the middle of the cell.

5. Manufacture of Three-Layer Pipes (Collector) /69

5.1 Statement of the Problem

The design construction of a thermionic combustion element makes a three-layer pipe necessary, whose inner part serves as collector which must be electrically insulated from the other components. Simultaneously, the waste heat occurring during the operation at the sodium cooling circulator must be dissipated by this system so that additionally a good heat conductivity is promoted.

5.2 Present Experience

The present section describes the manufacture of a three-layer pipe made of Nb-Al_2O_3-Nb which corresponds to the concept of a thermionic in-pile convertor valid in our plant both in its standards of measurement as well as in the working materials and processing methods used.

The method described here for manufacturing a three-layer pipe has already been suggested by us [5] and tested in model tests. It was then shown that a layer of Al_2O_3 placed on steel by plasma spraying shows a toughness and adhesiveness sufficient for the following processing steps.

The resistence to temperature change of sprayed Al_2O_3 layers which also determines the maximum permissible heating rate of a thermionic combustion element is also designated as favorable by Dittrich [32]. Thus Al_2O_3 layers sprayed with flame were quenched in water ten times from 1,000°C without damage.

Reiss [33] describes experiments for determining the permissible heating rate of Al_2O_3 layers. The greatest attainable heating rate without destruction of the layer was measured on the junction of a 0.16 mm Al_2O_3 sprayed layer on a tungsten rod of 1.1 mm Ø and came to (3,000 ± 1,000)°C sec^{-1}. /69

For firm attachment of the outer jacket pipe to the collector sprayed with Al_2O_3, an apparatus suited to the experimental conditions is used as was described earlier [5]. In this way by heating particular zones and simultaneous stretching of a pipe, a controlled reduction of cross section can be achieved which leads to shrinking down to a core introduced into the pipe. /70

5.3 Experimental Construction

5.3.1 Plasma-Spray Device

In the first attempts to place Al_2O_3 on niobium by means of plasma spray, it was found that the metal can assume temperatures up to 1,000°C and more. In order to avoid any oxidation it is therefore necessary to carry out the layering process in an oxygen-free atmosphere of protective gas.

A corresponding apparatus for this was devised (Figure 5.1). This is a vacuum-sealed housing which was pumped out a number of times with an advance vacuum pump and filled with purified argon. On a guide inside the apparatus, the plasma burner moves back and forth in the longitudinal direction by means of a direct current motor with infinitely variable velocity. Between two spring-loaded support points below it is the pipe to be sprayed, whose rate of revolution is also infinitely variable. The interval between the burner and the pipe is variable in wide limits in order to determine the most favorable spraying distances.

5.3.2 Shrinking Apparatus

The apparatus used for the zone-by-zone shrinking of the pipe jacket is shown in Figure 5.2 and its method of functioning can be seen in Figure 5.3: the jacket pipe, surrounded at one place by several windings of a heat inductor is held between two collets in a vacuum chamber. Inside the pipe is the layered and polished collector pipe. If the chamber is now driven by an electric motor along the mechanism, then the pipe system moves relative to the heat inductor and is thereby heated in zones. Simultaneously over an elbow lever which moves with a swing which is adjustable in its steepness, a constant elongation is forced on the jacket pipe according to Poisson's cross contraction which has a reduction of cross section as a consequence. Through corresponding swing positions it is thereby possible to close apertures up to 0.3 mm between the inner and outer core in one movement. /71

/113

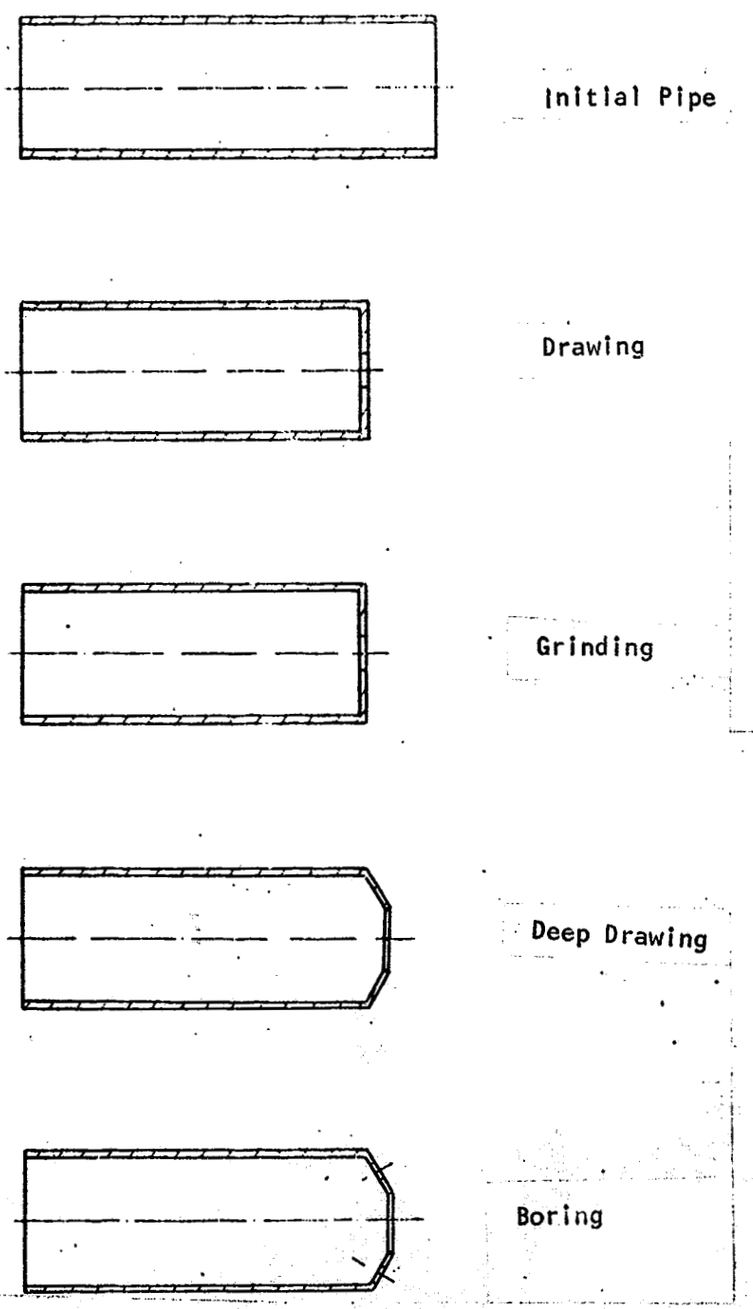

Figure 4.4. Production of an Anode with Drawn-In Bridge.

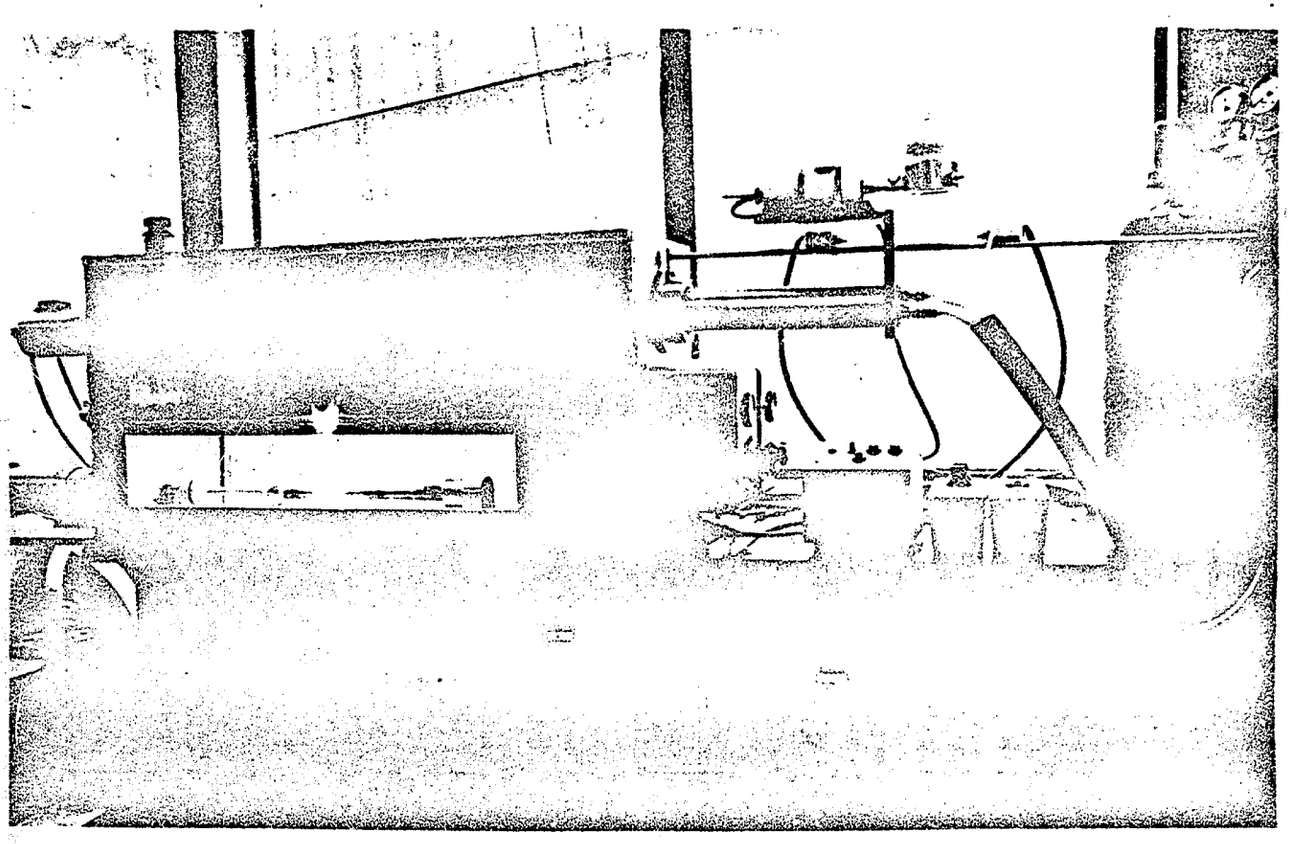

Figure 5.1. Protective Gas Box for Plasma Spraying.

/114

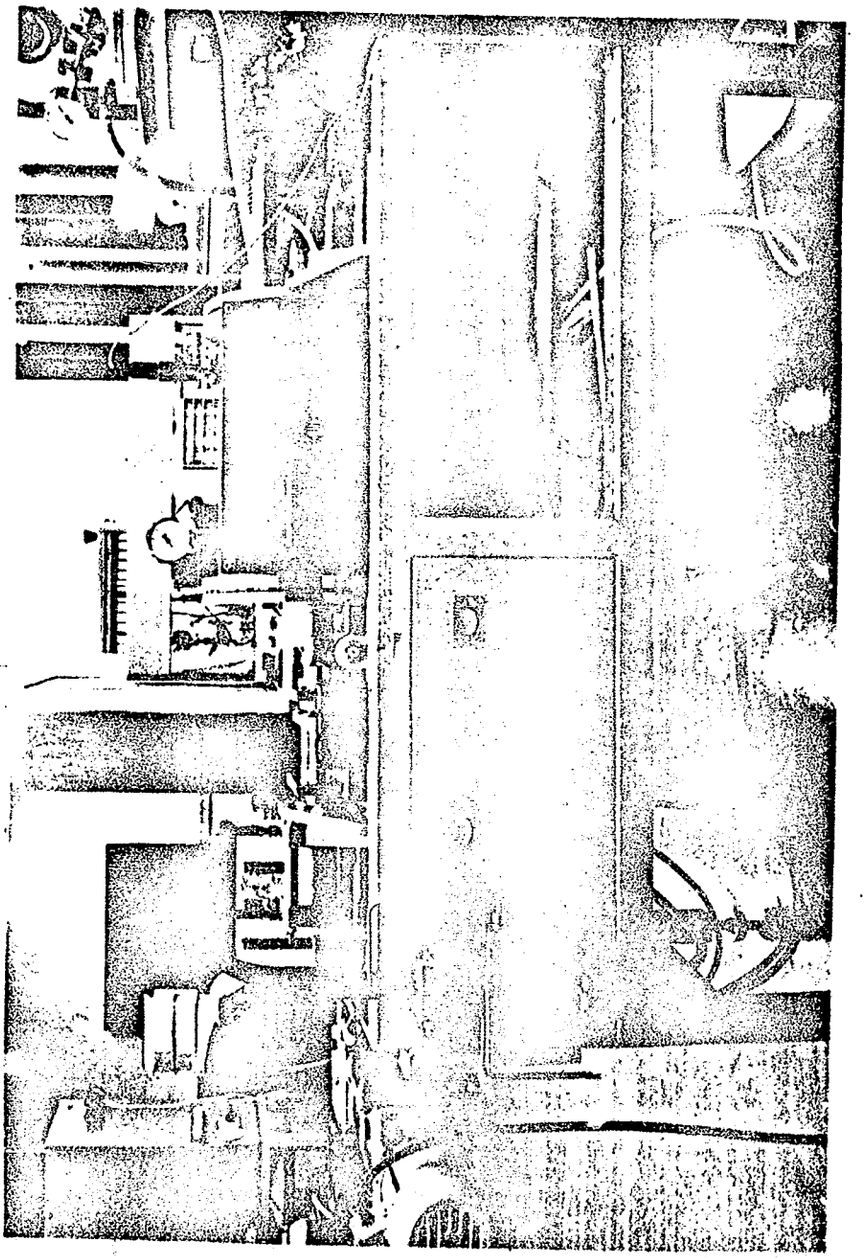

Figure 5.2. Shrinking Apparatus.

/115

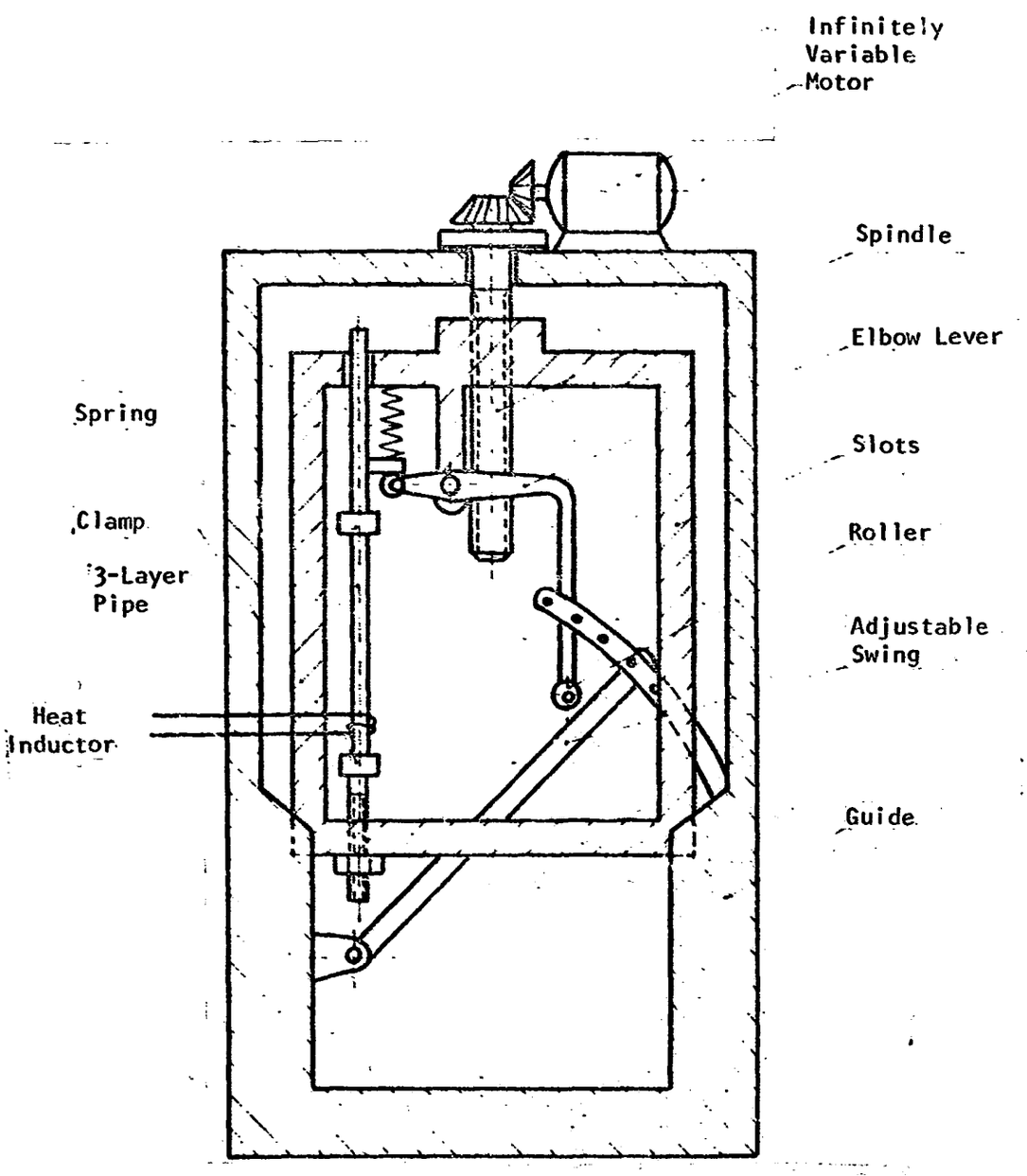

Figure 5.3. Plan of the Zone Shrinking Device.

5.4 Producing a Three-Layer Pipe /71

5.4.1 Layering with Al_2O_3

Since the pipe sections manufactured are to serve chiefly for investigations of the properties of plasma-sprayed Al_2O_3 layers, no axial subdivision of the inner pipe was attempted. Instead, a niobium pipe section was used with 22.75 Ø x 1.0 mm and 150 mm in length. This piece of pipe was placed in a protective gas box described under 5.3.1 and sprayed with plasma after being exhausted to a vacuum three times and filled with argon.

The following conditions determined in the advance experiments were used:

The Al_2O_3 sieve size used had a grain of 25...35/µ. In using a fairly large grain size, the particles could no longer be completely melted because of the limited output of the equipment. The feed rate of the burner came to 60 mm min^{-1}, and the rpm of the niobium pipe 14 revolutions min^{-1}. With a power output of about 14 kW, there is an operating voltage of about 60 V.

The layer thickness achieved with an adjusted spray interval of 115 mm came to 410/µ ± 20/µ with a peak-to-valley depth of about 100/µ.

5.4.2 Subsequent Processing of the Al_2O_3 Layer

Advance experiments have shown that the peak-to-valley depth of the sprayed layer of about 100/µ achieved during spraying is not small enough in order to achieve an adequate surface contact with the sleeve pipe with the subsequent shrinking (Figure 6.4). For this reason tests were successfully /72 carried out to process the surface subsequently by circular grinding with a diamond disk.

In the present case, the sprayed pipe was ground to a diameter of 23.2 mm which corresponds to an Al_2O_3 layer thickness of 225/µ. The stresses occurring during grinding in no case led to a damaging of the oxide layer. A Winter diamond disk of D 100 grain size was used.

5.4.3 Shrinking

In order to shrink by zone down to the anode pipe processed according to 5.4.2, a niobium pipe with 25.6 x 23.6 mm Ø was used. Since the aperture resulting from the pipe combination could not be closed in one working process with the shrinking apparatus, the jacket pipe was then tapered in diameter with the first pass and then shrunk firmly to the inner pipe during the second pass. The elongation adjusted by means of the swing then came to 2.42% in the first pass and 5.0% in the second pass.

The temperature of the heated zone during the two working processes came to about 800°C, and the pressure in the chamber was 10^{-1} mm Hg pressure.

/116

Figure 5.4. Cross Section of a 3-Layer Pipe with Unprocessed $A:_2O_3$ Layer, Enlarged 200 Times.

Figure 5.5. Cross Section of a 3-Layer Pipe with Polished Al_2O_3 Layer, Enlarged 200 Times.

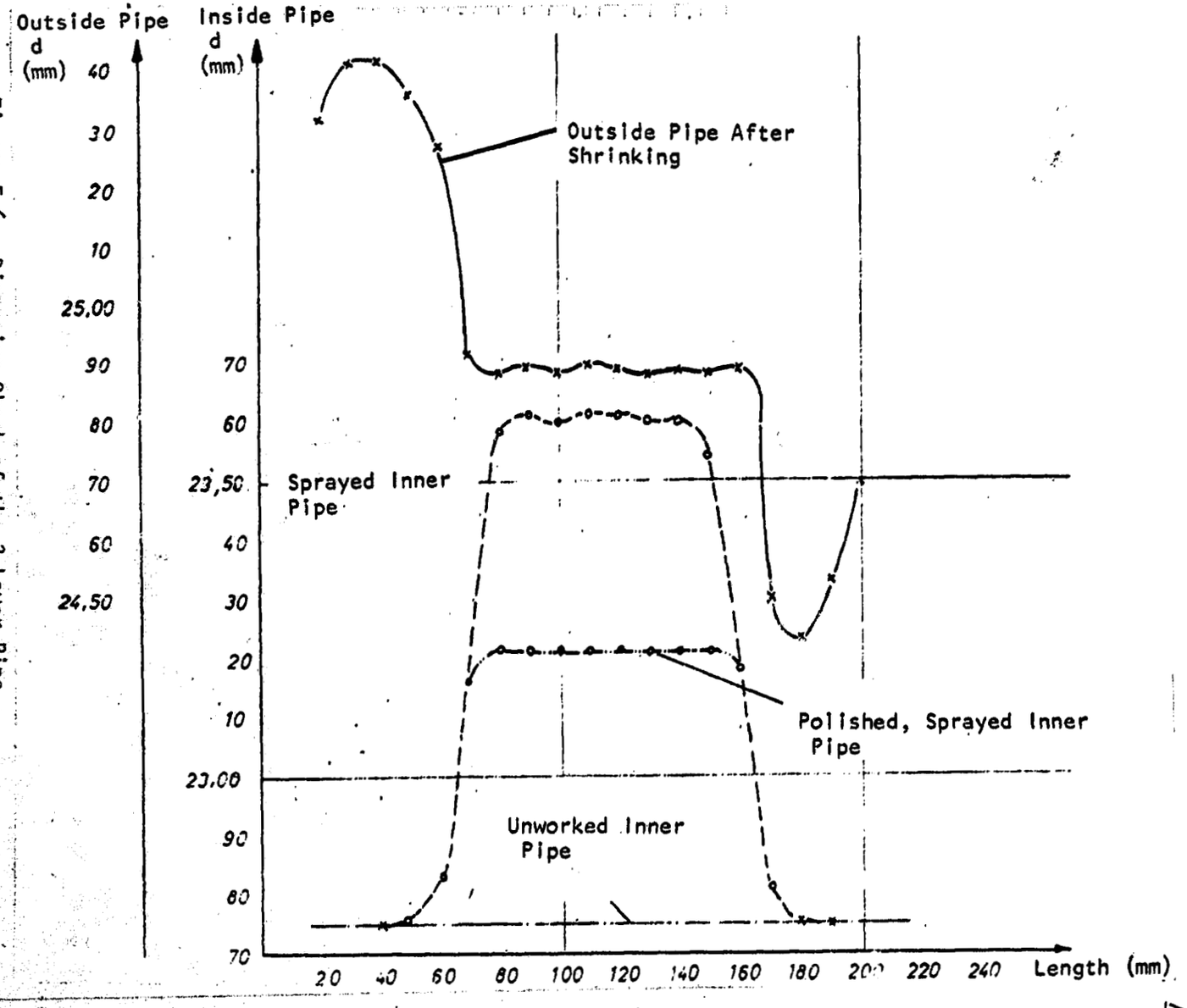

Figure 5.6. Dimension Check of the 3-Layer Pipe.

/117

A size check of the finished pipe shows that the jacket pipe after shrinking shows a light corrugated profile (Figure 5.6). The cost for this can be found in the fact that the power transmitted by the heat inductor is not sufficient in order to let the drawing process run continuously. Instead it must be interrupted each time after a drawing length of about 20 mm until the next zone has been heated to operating temperature. /72

This deficiency will be eliminated with the use of an MF generator planned for future experiments.

5.5 Characteristics of the Three-Layer Pipe /73

The investigations carried out so far permit qualitative evaluations of the properties achieved. As shown in Figure 5.5 a good surface contact of the oxide layer can also be achieved with the jacket pipe by means of grinding the Al_2O_3 layer.

The layer, however, still shows a large proportion of pores so that it will be the goal of future experiments to increase the density of the sprayed layer.

Experiments so far have also shown that the oxide layer is adequately insulated electrically, and accurate measurements will still be carried out.

No reliable data can be provided for the heat conductivity of the three-layer pipe. Experiments in this regard will also be carried out at our plant next year. It is expected that the results found there will provide information about the development cost which is still necessary.

5.6 Observation in Conclusion

The production of a cylindrical three-layer system of niobium-Al_2O_3-niobium is possible according to the method described.

The plasma-spray method especially permits the production of Al_2O_3 layers with consideration of proper protective measures. Its structure, however, can still be improved. The layers are both adhesive enough as well as sufficiently resistent to fracture in order to permit further processing stages to follow.

The zone shrinking is suitable for application and permits the controlled shrinking of a jacket pipe onto the anode pipe sprayed with Al_2O_3 without damaging the oxide layer in so doing.

Both the mechanical as well as the electrical and thermal properties of the compound system achieved are being studied and improved at the present time.

TABLE 2.1. HEATING TABLE INVESTIGATIONS OF COATED PARTICLES.

	Type			Temperature	Program	Time or Number of Cycles
1	Ø = 150 /u/5-6 /u	Coating		2000°K	Long-term heating	5 h
2	Ø = 70-120 /u/5 /u	"		2000°K	"	5 h
3	Ø = 70-120 /u/2-3 /u	"		2000°K	"	4 h 10'
4	Ø = 150 /u/5-6 /u	"		2000°K	Cycle	6
5	Ø = 70-120 /u/5 /u	"		2000°K	"	16
6	Ø = 70-120 /u/2-3 /u	"		2000°K	"	7

TABLE 2.2. LONG-TERM HEATING EXPERIMENTS.

	Type				Temperature	Time
1	Ø	=	150/u/5-6/u	Coating	2100°K	75 h
2	Ø	=	150/u/5-6/u	"	2100°K	239 h
3	Ø	=	70-120/u/5/u	"	2100°K	239 h
4	Ø	=	70-120/u/2-3/u	"	2100°K	239 h

TABLE. 2.3. RESULTS OF THE ACTIVATION-ANALYTICAL INVESTIGATIONS.

Elements	75 h/2100°K	8 h/2100°K
Ta	0,2 /ug 0 %	0,2 /ug 0 %
Mo	70 /ug = 99,4 %	70 /ug = 99,0 %
W	0,46 /ug = 0,6 %	0,46 /ug = 0.6 %
U	0,005 /ug ≈ 0 %	0,18 /ug = 0,4 %

Coated Particles: Ø = 150 /u, Coating Thickness 5-6 /u (Art 1)

Tr. Note: Commas indicate decimal points.

/80

TABLE 3.1.

hkl	I/I_{110} W	ASTM % Mo	I/I_{110} Tungsten Surface	Measured Molybdenum Base
110	100	100	100	100
200	15	21	107	86
211	23	39	2	12

TABLE 3.2.

Sample	Surface Proportion of the	(100) Planes	(111) Planes	(110) Planes
a		43,5	18,0	2
b		54,0	4,0	-

The remainder of the surface could not be determined.

Tr. Note: Commas indicate decimal points.

TABLE 3.3. EXPERIMENTS CARRIED OUT, OPTICALLY MEASURED LAYER THICKNESS BEFORE AND AFTER HEATING, STRUCTURE OF THE TRANSITION.

	Heating Time	Heating Temperature	Tungsten Layer Thickness Before and	After the Heating	Structure of the Transition
1	2 h	1750°C	60 µ	54 µ	Epitactically
2	4 h	1750°C	60 µ	25 µ	"
3	8 h	1750°C	60 µ	18 µ	"
4	16 h	1750°C	60 µ	?	"
5	32 h	1750°C	60 µ	8 µ	"
6	75 h	1830°C	200 µ	200 µ	Not "
7	75 h	1830°C	200 µ	200 µ	Al_2O_3 Intermediate Layer

TABLE 3.4. CALCULATED WIDTH OF DIFFUSION ZONE AT 1,750°C FOR VARIOUS HEATING TIMES. /82

Time	Profile Width
10^0 h	137 /u
8 h	387 /u
10^1 h	435 /u
10^2 h	1370 /u
10^3 h	4350 /u
10^4 h	13700 /u

TABLE 5.1. POSSIBLE MATERIALS.

Cathode Surface	Mo, W, UO_2-Mo-Cermet
Bridge	Nb, W on Nb, Mo
Anode	Nb

TABLE 5.2. SURVEY OF THE DIFFUSION BONDING EXPERIMENTS.

Pairings	Experimental Times			
Nb-Nb	0,5 h	1,0 h	2,0 h	
Nb-Mo	2 min.	0,5 h	1,0 h	2,0 h
Nb-W	0,5 h	1,0 h	2,0 h	
Mo-Mo	3 h	4 h		
Mo-W	2 h			

Temperature 1600°C

Pressure 1-2 kp/cm^2

Tr. Note: Commas indicate decimal points.

REFERENCES

1. Siemens Firm, "Continuation of a Study on the Energy Production for Purposes of Space Travel Using Nuclear-Technical Methods", *1963 Annual Report for the Federal Ministry for Scientific Research.* /74
2. Budnick, D. and Janner, K., "Power Supply Reactors for Purposes of Space Travel", *1964 Annual Report of the Siemens-Schuckert Werke AG, for the Federal Ministry for Scientific Research.*
3. Budnick, D., Janner, K., Jung, W., Oldekop, W. and Peehs, M., *Thermionische Kernreaktorenergieversorgungsanlagen fur einen Leistungsbereich von 5 bis 50 kWe. D.G.R.R.* [Thermionic Nuclear Reactor Power Supply Equipments for a Power Range of 5 to 50 kWe, D.G.R.R], Technical Book Series, Vol. 2, 1966.
4. Jung, W., "Thermionic Convertors for the Power Supply of Space Vehicles", *1964 Annual Report of the Siemens-Schuckertwerks Ag for the Federal Ministry for Scientific Research.*
5. Boehm, H., Jung, W. and Peehs M., "Development of Thermionic Reactor Combustion Elements and the Construction of Experimental Cells", *1965 Annual Report for the Federal Ministry for Scientific Research.*
6. Budnick, D. and Janner, K., "Power Supply Reactors for Space Travel (Continuation of the Study)", *1965 Annual Report of the Siemens AG for the Federal Ministry for Scientific Research.*
7. Budnick, D. and Janner, K., *Projektierung des Thermionikeinsatzes fur einen Thermionik-Kernreaktor zur Energieversorgung von Raumflugkorpern* [Planning the Use of Thermionics for a Thermionic Nuclear Reactor for the Power Supply of Space Vehicles], BMwF, RV1, 624, 12, 1966.
8. Schoeck, G., "Creep and Recovery", *Seminary of the American Society for Metallurgy*, New York, 1965. /75
9. General Electric, GEMP-270A, 1964.
10. Biersack, J., *Nukleonik* [Nucleonics], Vol. 8, No. 8, 1966.
11. Winkenbach, *Umaschau*, No. 24, 1966.
12. Stahl, *Personliche Mitteilung* [Personal Report], 1966.
13. Ackermann, et al, *f. Chem. Phys.* [Chemistry and Physics], Vol. 25, No. 6, p. 1089, 1956.
14. Rom, *2 AGARD/NATO Lecture Series on Nuclear and Electrical Rocket Propulsion*, Brussels, 1964.
15. IAEA, *Report of the Panel on Thermodynamics and Transport Properties of* UO_2, p. 40, Vienna, 1964.
16. Schmidt, *BBC-Nachrichten* [BBC-News], September, 1964.
17. Huberman-Hoelzl, *Thermionic Specialist Conference Gatlinburg/Term*, October, 1963.
18. Flaherty-Panisko, HW 76303, September, 1963.
19. Weinburg, et al, *Thermionic Specialist Conference*, London, 1965.
20. West, *J. of Less Com. Mat.*, Vol. 9, p. 40, 1965.
21. Schuster, *DGLR Conference*, Stuttgart, December 1965.
22. Finke, *Praktische Metallographie*, Vol. 2, No. 4, 1965.
23. Weinberg, et al, *Trans. Am. Nucl. Soc.* [Transactions of the American Nuclear Society], Vol. 7, No. 2, November, 1964.

24. Kaznoff-Sanderson, *Thermionic Specialist Conference*, London, September, 1965.
25. Crank, *Mathematics of Diffusion*, Oxford Clarendon Press, 1956.
26. Fujita-Yamada, see Crank, p. 177.
27. Kalinowitsch, et al, (Russian), *Pulver Met* [Powder Metallurgy], C28, 1965.
28. Albom, *Welding Journal*, p. 491, 1964.
29. Annessa, *Welding Research Supplement*, 1965.
30. Goetsch, *Reactor Material*, Vol. 7, No. 1, 1964.
31. Tarr, U.S. Patent Number 3-170-234, February, 1964.
32. Dittrich, F. J., *American Ceramic Society Bulletin*, Vol. 4, No. 6, p. 492, 1965.
33. Riess, F., *KFZ Karlsruhe*, Report Number 4, JNR-3/66, June, 1966.

/76

Translated for the National Aeronautics and Space Administration under Contract No. NASw-1695 by Techtran Corporation, PO Box 729, Glen Burnie, Md. 21061